SOCIEDADE BRASILEIRA DE MATEMÁTICA

ENSAIOS MATEMÁTICOS
2013, Volume **24**, 1–91
https://doi.org/10.21711/217504322013/em241

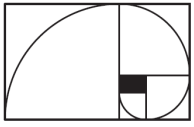

Isometric embeddings of the square flat torus in ambient space

Vincent Borrelli
Saïd Jabrane
Francis Lazarus
Boris Thibert

Abstract. This memoir is concerned with isometric embeddings of a square flat torus in the three dimensional Euclidean space. The existence of such embeddings was proved by John Nash and Nicolaas Kuiper in the mid 50s. However, the geometry of these embeddings could barely be conceived from their original papers. Here we provide an explicit construction based on the convex integration theory introduced by Mikhail Gromov in the 70s. We then turn this construction into a computer implementation leading us to the visualisation of an isometrically embedded flat torus. The pictures reveal a geometric object in-between fractals and ordinary surfaces. We call this object a C^1 fractal.

2010 Mathematics Subject Classification: 35-04, 53C21, 53C42.

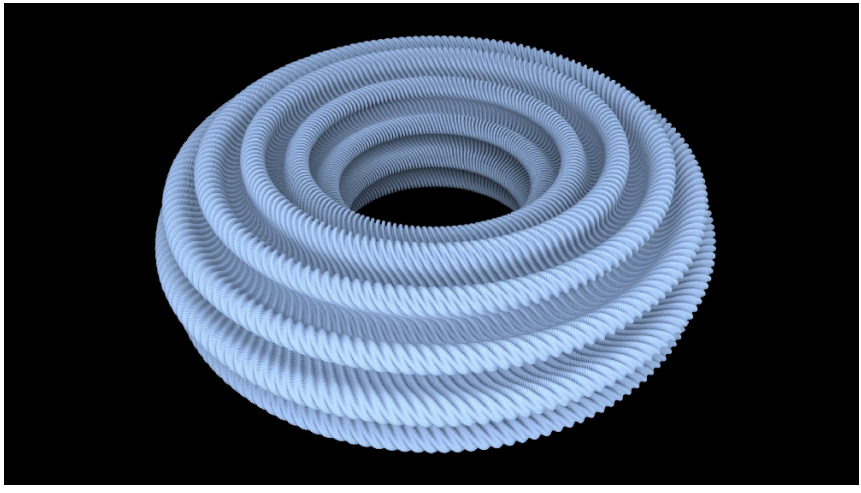

Image of an embedding of a flat torus in the 3D Euclidean space

Contents

Chapter 1

General introduction and historical background

Isometric embeddings: from Schlaefli to Nash

A map f from a Riemannian manifold (M^n, g) into a Euclidean space $\mathbb{E}^q = (\mathbb{R}^q, \langle ., . \rangle)$ is an isometry if the pullback of the inner product is the initial metric: $f^* \langle ., . \rangle = g$. This implies that f preserves length, that is the length of every C^1 curve $\gamma : [a, b] \to M^n$ is equal to the length of its image $f \circ \gamma$. Suppose that, in some local coordinate system, the metric is given by

$$g = \sum_{i,j}^{n} g_{ij} \mathrm{d}x_i \mathrm{d}x_j,$$

then the isometric condition $f^* \langle ., . \rangle = g$ is equivalent to a non linear PDE system

$$\langle \frac{\partial f}{\partial x_i}, \frac{\partial f}{\partial x_j} \rangle = g_{ij}, \quad 1 \leq i \leq j \leq n$$

of $s_n = \frac{n(n+1)}{2}$ equations. It was conjectured by Schlaefli [45] in 1873 that any n-dimensional Riemannian manifold can be locally isometrically embedded in $\mathbb{E}^{s_n}$.

In the years 1926-1927, Janet and Cartan proved that the above PDE system has a solution if the dimension of the ambient space is at least s_n and (M^n, g) is an analytic Riemannian manifold. The number s_n is thus called the *Janet dimension.* In this case, every point of M^n has a neighborhood which admits an isometric embedding into $\mathbb{E}^q$ [31, 10]. Their proof relies on the Cauchy-Kowalevski Theorem and thus cannot be extended to the non analytic case. In the smooth case, the best known general result is due

to Gromov and Rokhlin [22] and also Greene [19]. By using a Nash-Moser iteration they proved that local isometric embeddings exist if $q \geq s_n + n$. A better result is known for $n = 2$: any smooth riemannian surface admits local isometric embeddings into $\mathbb{E}^4$ [44]. For the smooth case, Schlaefli's conjecture is still open even for $n = 2$ (see [26] for a general reference on smooth isometric embeddings, see [54] for an essay in french on the history of isometric immersions).

In 1954, Nash surprised the mathematical community by breaking down the barrier of the Janet dimension, considering maps with only C^1 regularity [39]. Precisely, he proved that any *strictly short* global embedding $f_0 : (M^n, g) \longrightarrow \mathbb{E}^q$, i.e., an embedding that strictly shortens distances: $f_0^*\langle ., . \rangle < g$, can be deformed into a true C^1 global isometric embedding f provided that $q \geq n+2$. Moreover, the embedding f can be required to be arbitrarily C^0 close to the initial map f_0. But its C^1 regularity cannot be improved to C^2 in general since the curvature tensor would then provide obstructions to the existence of isometric maps. Shortly after, the theorem of Nash was extended by Kuiper to the codimension 1 [34].

The result of Nash and Kuiper has many counterintuitive corollaries. We mention here three examples, each dealing with one of the three Gaussian curvature cases, $K > 0$, $K < 0$ and $K \equiv 0$ for surfaces.

A celebrated theorem of Alexandrov, Weyl, Nirenberg and Pogorelov states that any abstract smooth Riemannian sphere $(\mathbb{S}^2, g)$ admits a smooth isometric embedding in $\mathbb{E}^3$. Moreover, two smooth convex embeddings of the sphere are congruent [5, 11, 40, 43]. A consequence of the Nash-Kuiper theorem is that this rigidity no longer remains in the C^1 setting. For instance, there exists a C^1 isometric embedding of the unit round sphere into any ball of arbitrary small radius!

The Efimov-Hilbert theorem shows that there is no C^2 isometric immersion in the three-dimensional Euclidean space of a complete surface of Gaussian curvature bounded from above by a negative constant [13], see also [38]. In contrast, a direct consequence of the Nash-Kuiper theorem is the existence of C^1 isometric embedding of the hyperbolic plane into $\mathbb{E}^3$ and of any complete orientable surface with negative Gaussian curvature.

A flat torus $\mathbb{E}^2/\Lambda$ is a quotient of the Euclidean 2-plane by a lattice $\Lambda = \mathbb{Z}e_1 + \mathbb{Z}e_2$, (e_1, e_2) being a basis of $\mathbb{E}^2$. Obviously, the Gaussian curvature of a flat torus is identically zero. A classical argument shows that any C^2 complete compact surface in $\mathbb{E}^3$ has a point with positive Gaussian curvature. From the Theorema Egregium it ensues that there is no C^2 isometric embedding of any flat torus. In fact, Hartmann and Nirenberg showed that a C^2 complete surface of $\mathbb{E}^3$ with zero Gaussian curvature has to be a plane or a cylinder [28]. They also provide a local geometrical description: every C^2 surface with zero Gaussian curvature is ruled, that

is there is a straight-line (contained in the surface) passing through every point of the surface. In the flat torus case, since strictly short embeddings can be easily constructed, the Nash-Kuiper theorem implies that any flat torus admits a C^1 isometric embedding into $\mathbb{E}^3$.

It should be stressed that a C^1 isometric map which is not C^2 has no defined Gaussian curvature but has a defined Gauss map: the image of any C^1 isometric embedding admits a tangent space at any of its points. The unusual regularity of the Nash-Kuiper embeddings puzzles the imagination. Although the proof is constructive, it is not sufficiently explicit to allow for visualization.

The Gromov Convex Integration Theory

The Nash-Kuiper result has long appeared as a curiousity; a separate and isolated result in Riemannian geometry. Obviously, it seems to have no relevance to the subsequent achievements of differential topology: the discovery of the eversion of the sphere by Smale in 1958 [46, 47], the classification of immersions by Hirsch (1959, [29, 30]), the classification of piecewise-linear immersions Haefliger and Poénaru (1964, [24]), the Folding Theorem of Poénaru (1966, [42]), the classification of submersions of open manifolds by Phillips (1967, [41]), the classification of non-degenerate immersed circles by Feldman (1968, [17]) and the classification of k-mersions by Feit (1969, [16]). Nevertheless, there exists a deep but invisible link that unifies all those results with the one of Nash-Kuiper. This link had to be put into light by Gromov in the 70-80's.

In his thesis (1969, see [23]), Gromov revisits the work of Smale and proves a general theorem including some of the above results as corollaries. More precisely, he first reformulates problems in differential topology in a general sheaf-theoretic language. For instance, the immersion condition for a map $f : \mathbb{R}^n \longrightarrow \mathbb{R}^q$, $n \leq q$, requires that the Jacobian matrix for df_x has maximal rank at each point x of $\mathbb{R}^n$. This defines a subset $\mathcal{R}$ inside the one-jet space of maps between $\mathbb{R}^n$ and $\mathbb{R}^q$:

$$J^1(\mathbb{R}^n, \mathbb{R}^q) = \{(x, y, L) \text{ with } x \in \mathbb{R}^n, y \in \mathbb{R}^q \text{ and } L : \mathbb{R}^n \longrightarrow \mathbb{R}^q \text{ is linear } \}$$

by

$$\mathcal{R} = \{(x, y, L) \in J^1(\mathbb{R}^n, \mathbb{R}^q) \mid rank\ L = n\}.$$

This subset has a natural bundle structure induced by the projection on the first factor $\mathcal{R} \longrightarrow \mathbb{R}^n$ and any section $x \longmapsto (x, y(x), L_x)$ of

that bundle is called a *formal solution* of the *differential relation* $\mathcal{R}$. A map f is a *solution* of $\mathcal{R}$ –that is an immersion– if and only if its 1-jet $x \mapsto j^1 f(x) = (x, f(x), df_x)$ is a section of $\mathcal{R}$.

Gromov turns the Smale method –the so called Covering Homotopy Theorem– into a general procedure to solve a large class of differential relations $\mathcal{R} \subset J^1(M^n, N^q)$. Precisely, if the manifold M^n is open and if $\mathcal{R}$ is both open and invariant by the action of the diffeomorphism group $Diff(M^n)$, he proves that every formal solution, that is every section of $\mathcal{R}$, can be deformed into a true solution by a sequence of "internal" twistings. Even more, the space of sections of $\mathcal{R}$ is then weakly homotopy equivalent to the space of solutions of $\mathcal{R}$. He calls such a property, a *h-principle* (h stands for homotopy). The differential relations of immersions is open and $Diff(M^n)$-invariant and thus satisfies the h-principle. Hence, the classification of immersions reduces to a topological task: the homotopic classification of sections of $\mathcal{R}$. This is, in essence, the Smale-Hirsch theorem. But the Nash-Kuiper theorem remains beyond the scope of this first approach since the isometric differential relation is not $Diff(M^n)$-invariant.

The fundamental step of the Nash-Kuiper proof is to construct from a strictly short embedding f_1 another embedding f_2 which is still strictly short but closer to an isometry, i.e.:

$$g - f_2^* \langle ., . \rangle < g - f_1^* \langle ., . \rangle.$$

To this end, curves are lengthened in the normal neighborhood of the embedding f_1 by turning them into spirals (Nash) or into oscillating curves (Kuiper). This fundamental step is then iteratively repeated to obtain an isometric embedding in the limit.

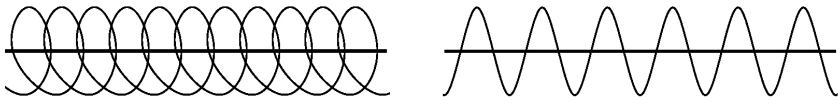

Figure 1.1: The Nash spiraling process and the Kuiper oscillations

Four years after his thesis, Gromov extracts the basic idea of the Nash-Kuiper fundamental step and converts it into a powerful tool to solve partial differential relations: the Convex Integration Theory ([20], see also [21, 49, 14]). The main ingredient of this theory is a barycentric formula which captures the spirit of both the Nash spiraling and the Kuiper oscilating processes (see the formula 2.1 in Chapter 2). This formula plays a

role that is similar to the Covering Homotopy Theorem in Smale's method. However it is quite different in nature and allows to solve differential relations which were, until then, out of reach. Indeed, the theorem obtained by Gromov is of great generality: if the differential relation $\mathcal{R}$ is open as a subset of $J^1(M^n, N^q)$ and if it satisfies a mild convexity condition called *ampleness* then the h-principle holds for $\mathcal{R}$.

As a consequence Gromov recovers the Smale-Hirsch classification of immersions as well as the Nash-Kuiper Theorem. Nevertheless, this last theorem requires extra work since the isometric differential relation is neither ample nor open. The lack of ampleness forces to start with a strictly short initial map while the non openess is circumvented through an iterative use of the Gromov theorem to obtain in the limit the desired C^1 isometric embedding.

The Convex Integration Theory gives a unified vision of a number of key results in differential topology but it also provides new and unexpected results. For instance, it shows that the differential relation of isometric maps satisfies the h-principle. As a consequence, the space $I(M^n, \mathbb{E}^q)$ of immersions of a Riemannian manifold M^n inside a Euclidean space is weakly homotopy equivalent to the space of C^1 isometric immersions $I_{iso}(M^n, \mathbb{E}^q)$. In particular, the eversion of the sphere can be performed among C^1 isometric immersions. The interested reader will find a good reference on the history of Immersion Theory in [50] (see also [48]).

Thurston Corrugations

The h-principle in general, and the Convex Integration Theory in particular have long been ignored because they contradict mathematical intuition. As quoted from [6]: "analysis experts [did] not believe in [them] and as a result prove from time to time parts of what was already in [Gromov's work]". In addition, the high degree of abstraction was a discouraging obstacle which seems to confine the whole theory to a conceptual level.

For instance, although the Convex Integration Theory gives the deep reason of the existence of an eversion of the sphere, it played no role in the whole history of its visualization. Albeit constructive, Smale's proof was far from practical and did not allow for visualization or for a simple mental picture. Finding explicit regular homotopies that turn the sphere inside out had been a natural and significant challenge. The successful response to this challenge is certainly one of the best known pages of the history of differential topology (accounts of which can be found in [18, 36, 51]).

One of the most convincing visual eversions was invented by Thurston and displayed in a computer graphics video in 1994 [37]. The basic idea was to start with a mere homotopy and to modify it by introducing ondulations in order to remove singular points. These oscillations, called *corrugations*, soon proved to be a powerful tool to generate regular homotopies between two given immersions. They also offered, in Thurston's own words, a "clear, compelling and coherent method to see, prove and understand" ([36], chapter "Making waves: The Theory of Corrugations").

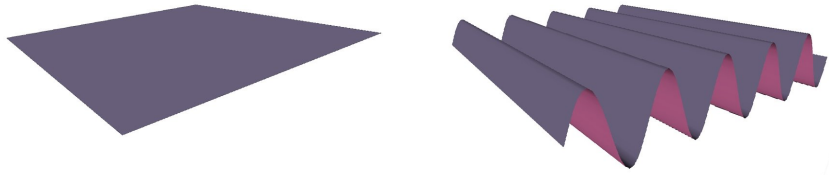

Figure 1.2: Thurston corrugations on a plane

Thurston corrugations are quite similar to the oscillations introduced by Kuiper to build C^1 isometric maps. The whole Theory of Corrugations can be seen as a simplified version of the Convex Integration Theory where all quantitative aspects are ignored. The effectiveness of the corrugations method was certainly a first evidence of the practicable nature of convex integration. However, it is likely that this evidence went unnoticed at the time, especially as convex integration was still widely unknown (despite Gromov's book [21]).

In constrast, it was clear that the rapid advance of computer capabilities was opening a new era in mathematics. Computers helped to prove theorems (as in the Appel and Haken proof of the 4-color map theorem), to renew the interest in exotic concepts (as fractals, a term coined by Mandelbrot in 1975) or to understand barely conceivable results (as the Smale sphere eversion). Simultaneously, the development of the computer led to an interesting philosophical questioning about mathematical visualization and more generally, about the essence of mathematical activity [27, 52].

Back to Nash-Kuiper C^1 isometric embeddings

The first book entirely devoted to the Convex Integration Theory appears in 1998 [49]. In this book, Spring provides a meticulous and comprehensive exposition of what is presented in the Gromov's treatise [21].

He also fills some gaps. For instance, the iterated convex hull extension for non ample relations is discussed in great detail. The technique is then applied to prove the h-principle version of the Nash-Kuiper theorem. This book was followed four years later by the work of Eliashberg and Mishachev which goes one step further in the understanding of the h-principle. The authors realize that the h-principle stems from a more general phenomenon: the Holonomic Approximation Theorem (see [14]). The fourth chapter of the book broaches the Convex Integration Theory with a viewpoint slightly different to that of Spring. It ends with a (relatively) short proof of the Nash-Kuiper theorem. Without doubt, these two books have helped greatly to popularize Convex Integration Theory. Eliahberg and Mishachev also make apparent that the theory does not only yield the existence of solutions, it can also provide effective constructions.

This was used recently by Conti, De Lellis and Székelyhidi to explore the Hölder regularity of isometric immersions [12]. They showed that any strictly short immersion $f_0 : (M^n, g) \longrightarrow \mathbb{E}^q$ can be deformed into a $C^{1,\alpha}$ isometric immersion where α is any number such that

$$\alpha < \frac{1}{1 + 2(n+1)s_n}.$$

Borisov has conjectured that the optimal upper bound is $\frac{1}{2}$ if $n = 2$ [7]. De Lellis and Székelyhidi also discovered a stunning analogy between isometric immersions and the incompressible Euler equations. Just as the Convex Integration Theory generates low regular solutions to the isometric differential relation, an adapted version of convex integration produces highly irregular weak solutions to the Euler equations. Moreover, a weak form of the h-principle holds [35], see also [53].

In a recent article [8], we take advantage of the constructive nature of Convex Integration Theory to convert the Nash-Kuiper process into an algorithm that generates C^1 isometric embeddings of the square flat torus $\mathbb{E}^2/\mathbb{Z}^2$ into $\mathbb{E}^3$. The implementation led us to the first images of such an embedding. These pictures reveal a geometric structure made up of an infinite stack of corrugations with decreasing amplitudes and increasing frequencies. The resulting object lies in-between a fractal and smooth surface, we have called it a C^1 *fractal*.

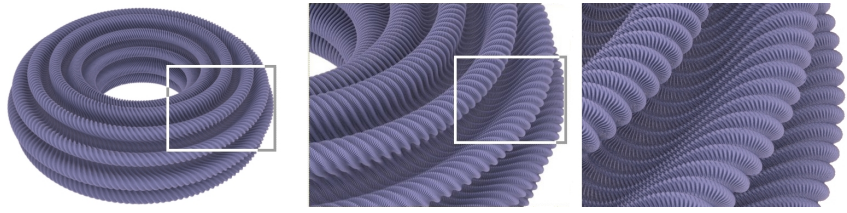

Figure 1.3: The C^1 fractal structure of the square flat torus $\mathbb{E}^2/\mathbb{Z}^2$ into $\mathbb{E}^3$.

Content of the paper

This paper contains a full version of the short article [8]. It provides all the details to implement the algorithm and to generate computer images of an isometric embedding. It also gives complete proofs of the theorems describing the geometric structure of the embedded square flat torus (see Theorems 21 and 23).

It is divided into four parts: in Chapter 2, we present the Convex Integration process in the case of isometric embeddings. The convex integration takes as input a map f and a positive integer N and outputs a corrugated map F with N oscillations. The shape of the corrugations depends on the choice of a family of loops (see Section 2.2). This family of loops is a free parameter of the theory. We propose a family of loops whose effect on the curvature is the simplest one: it adds a single term of frequency N to the curvature measure. We then consider the problem of periodicity: in general, even if the map f is defined over a torus, the map F fails to be doubly periodic. We overcome this problem by spreading out the periodicity gap smoothly over the whole torus. Chapter 3 describes how to reduce the isometric default of an initial embedding using only three convex integrations. We then iteratively apply this reduction to obtain a sequence of embeddings converging toward an isometric embedding of the square flat torus. In Chapter 4 we present the details of the implementation as well as computer images. Chapter 5 is devoted to the description of the geometric structure of the Gauss map $\mathbf{n}_\infty$ of the limit isometric embedding. This Gauss map is obtained as an infinite product of rotations applied to the Gauss map $\mathbf{n}_0$ of the input embedding. The analytic expression of these rotations is quite involved but their asymptotic expression is fairly simple. This remarkable fact is the purpose of the Corrugation Theorem 21. The asymptotic expression also reveals a formal resemblance of the normal map with a Riesz product. Theorem 23 puts into light the Riesz-like behaviour of the normal map.

Chapter 2

Convex Integration

In this chapter we provide the necessary details of the convex integration process applied to the isometric immersion of a torus. In the first two sections we show how to apply convex integration to the isometric immersion of a curve. In Section 2.3.1 this one-dimensional procedure is generalised to cylinders. Section 2.3.2 explains how to tackle the torus from the cylinder case and settle the main result for this chapter: the One Step Theorem.

2.1 One-dimensional Convex Integration

Suppose that for each $x \in I := [0,1]$ we are given a subset $\mathcal{R}_x$ of vectors in $\mathbb{R}^n$. The disjoint union $\mathcal{R} = \cup_{x\in I}\mathcal{R}_x$ is called a *differential relation*. A *solution* of $\mathcal{R}$ is a C^1 curve $f : I \to \mathbb{R}^n$ such that $f'(x) \in \mathcal{R}_x$, for all $x \in I$. In other words, a differential relation expresses a condition on the derivative of a curve that depends on the considered parameter. (In a more general setting, the differential relation depends on the parameter *and* the image point on the curve [14].)

Given a C^1 curve $f : I \to \mathbb{R}^n$, Convex Integration often allows us to construct a solution of $\mathcal{R}$ that is C^0-close to f. The first step of the process is to define a C^1 one-parameter family of loops $h(x,\cdot) : \mathbb{R}/\mathbb{Z} \to \mathcal{R}_x$ so that $f'(x)$ is the average of $h(x,\cdot)$:

$$\forall x \in I, \quad f'(x) = \int_0^1 h(x,u)\mathrm{d}u. \tag{2.1}$$

In practice, we first choose a path whose average is $f'(x)$. The loop $h(x,\cdot)$ is then obtained by travelling along this path in both directions (see Fig. 2.1).

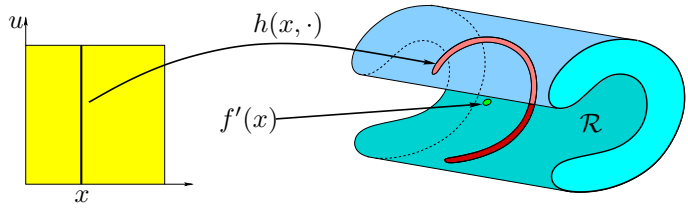

Figure 2.1: The loop $h(x,\cdot)$ is shown as a (red) thick curve contained in the differential relation $\mathcal{R}$ (in blue) and surrounding $f'(x)$. In this figure the sections $\mathcal{R}_x$ are all translates of a single section of the cylindrical relation $\mathcal{R}$.

The curve f is said to be strictly *short* if $f'(x)$ is interior to the convex hull of $\mathcal{R}_x$ for all $x \in I$. When $\mathcal{R}$ is open and path connected, this is a necessary and sufficient condition for h to exist [49, 14]. Our choice for h is discussed in the next section. In the second step of the process we simply define $F : I \to \mathbb{R}^n$ by

$$F(t) := f(0) + \int_{u=0}^{t} h(x, \{Nx\})\mathrm{d}x, \tag{2.2}$$

where N is a positive integer and $\{Nx\}$ is the fractional part of Nx. Intuitively, F is obtained by integrating h along a periodic curve with period $1/N$ (see Fig. 2.2). When N is large enough, the restriction of h to each period is close to a single loop $h(x,\cdot)$ and its integral is close to $f'(x)$. Summing over the N periods, we see that F is roughly equal to a Riemann sum of f', hence to f. This is formally stated in the following lemma.

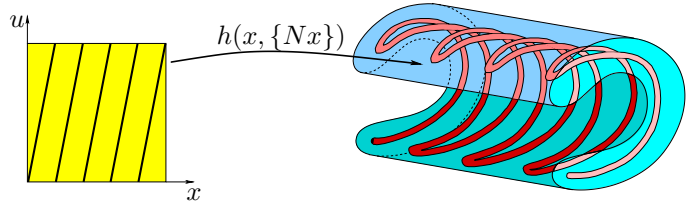

Figure 2.2: Because the parameter u belongs to $S^1 = \mathbb{R}/\mathbb{Z}$, the horizontal edges of the left square domain must be glued to produce a cylindrical domain. The path $x \mapsto (x, \{Nx\})$ winds N times around that cylinder.

Lemma 1 (C^0-density)**.** *Let f, h, N, and F be defined as above. Then F is a solution of $\mathcal{R}$ and*

$$\|F - f\|_\infty \leq \frac{K(h)}{N},$$

where $K(h)$ only depends on the C^1-norm[1] of h.

Proof. Since $h(t, \{Nt\}) \in \mathcal{R}_t$, it follows from the derivation of (2.2) that F is a solution of $\mathcal{R}$. By (2.1), we have

$$f(t) = f(0) + \int_{x=0}^{t} \int_{u=0}^{1} h(x, u) \mathrm{d}u\mathrm{d}x.$$

Put $n = \lfloor Nt \rfloor$, $I_j = [\frac{j}{N}, \frac{j+1}{N}]$ for $0 \leq j \leq n-1$, $I_n = [\frac{n}{N}, t]$ and $R_k = I_k \times [0, 1]$ for $0 \leq k \leq n$. We write

$$F(t) - f(0) = \sum_{k=0}^{n} F_k \quad \text{and} \quad f(t) - f(0) = \sum_{k=0}^{n} f_k$$

with $F_k = \int_{I_k} h(s, \{Ns\}) \mathrm{d}s$ and $f_k = \int_{R_k} h(x, u) \mathrm{d}u\mathrm{d}x$. We consider $j \in [0, n-1]$. By the change of variables $u = Ns - j$, we get

$$F_j = \int_0^1 \frac{1}{N} h(\frac{u+j}{N}, u) \mathrm{d}u.$$

We now define $H_j : R_j \to \mathbb{R}^n, (x, u) \mapsto h(\frac{u+j}{N}, u)$. In particular, H_j is constant over each horizontal segment in R_j. It ensues that

$$F_j = \int_{R_j} H_j(x, u) \mathrm{d}u\mathrm{d}x,$$

implying

$$\begin{aligned} \|F_j - f_j\| &\leq \int_{R_j} \|H_j - h\| \mathrm{d}u\mathrm{d}x \\ &\leq \frac{1}{N^2} \|\frac{\partial h}{\partial x}\|_\infty. \end{aligned}$$

The last inequality follows from the mean value theorem and the fact that the area of R_j is $1/N$. For $j = n$, a simpler upper bound holds:

$$\|F_n - f_n\| \leq \|F_n\| + \|f_n\| \leq \frac{2}{N} \|h\|_\infty.$$

[1]Here and in the sequel, $\|.\|$ is the Euclidean norm and $\|g\|_\infty := \sup_{p \in D} \|g(p)\|$ denotes the C^0-norm of any function g with domain D. We recall that for $k \geq 1$, the C^k-norm of the n-variate function g is given by $\sum_{\substack{i_1 + \cdots + i_n \leq k \\ 0 \leq i_1, \ldots, i_n \leq k}} \|\frac{\partial^{i_1 + \cdots + i_n}}{\partial x_1^{i_1} \ldots \partial x_n^{i_n}} g\|_\infty$.

We finally obtain

$$\begin{aligned}\|F(t) - f(t)\| &\leq \sum_{j=0}^{n-1} \|F_j - f_j\| + \|F_n - f_n\| \\ &\leq \frac{1}{N}\|\frac{\partial h}{\partial x}\|_\infty + \frac{2}{N}\|h\|_\infty.\end{aligned}$$

□

2.2 The choice of the loops $h(s,\cdot)$

As far as the isometric embedding problem is concerned, we deal with closed differential relations for which $\mathcal{R}_s$ is a sphere of radius $r(s)$ in $\mathbb{R}^n$, for some strictly positive function $r : I \to \mathbb{R}_+^*$. In other words, the relation $\mathcal{R}$ constrains the norm of the derivative. In this case, a curve f is short if and only if $\|f'(s)\| \leq r(s)$, for all $s \in I$. Suppose that f' is never zero and let $\mathbf{n} : I \to \mathbb{R}^n$ be a vector field normal to f. We choose the loop $h(s,\cdot)$ with image in the circle of radius $r(s)$, intersection of $\mathcal{R}_s$ with the plane spanned by $\mathbf{t}(s) := f'(s)/\|f'(s)\|$ and $\mathbf{n}(s)$, and set

$$h(s,u) = r(s)(\cos(\alpha_s \cos(2\pi u))\mathbf{t}(s) + \sin(\alpha_s \cos(2\pi u))\mathbf{n}(s)) \qquad (2.3)$$

with $\alpha_s := J_0^{-1}(\|f'(s)\|/r(s))$ (see Fig. 2.3). Here J_0 is the Bessel function of 0 order restricted to the interval $[0, z]$, where $z \approx 2.4$ is the smallest positive root of J_0. With this choice, the identity (2.1) easily follows from the integral formula

$$J_0(x) = \int_0^1 \cos(x \cos 2\pi u)\mathrm{d}u.$$

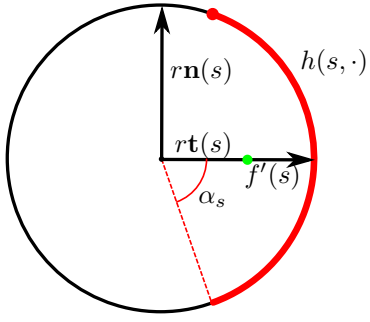

Figure 2.3: The loop $h(s,\cdot)$ starts from the top of the (red) thick arc, sweeps the arc and comes back to its starting point.

As noted in [8], our convex integration formula (2.3) captures the natural geometric notion of a corrugation. Indeed, in the planar case $n = 2$ the signed curvature measure

$$\mu := k\mathrm{d}s = k(t)\|F'(t)\|\mathrm{d}t$$

of the resulting curve F given by (2.2) is connected to the signed curvature measure $\mu_0 := k_0\mathrm{d}s$ of the initial curve f by the following simple formula

$$\mu := \mu_0 + (\alpha' \cos(2\pi N t) - 2\pi N \alpha \sin(2\pi N t))\,\mathrm{d}t.$$

Our corrugation thus modifies the curvature in the simplest way by sine and cosine terms with frequency N. As an example, when $r \equiv 1$ is the constant unitary function, formula (2.3) provides a plane curve F isometric to the segment I (with the usual metric in $\mathbb{R}$) that oscillates N times about f. A more in-depth analysis of the one-dimensional convex integration process based on formula (2.3) can be found in [9].

2.3 Two-dimensional Convex Integration: the primitive case

Given a Riemannian metric μ on the torus $\mathbb{T}^2 = \mathbb{R}^2/\mathbb{Z}^2$, our objective is to find an isometric embedding of $(\mathbb{T}^2, \mu)$ in the 3-dimensional Euclidean space. This is an embedding $f_{iso} : (\mathbb{T}^2, \mu) \to (\mathbb{R}^3, \langle\cdot,\cdot\rangle_{\mathbb{R}^3})$ satisfying $f_{iso}^*\langle\cdot,\cdot\rangle_{\mathbb{R}^3} = \mu$. As described in the original methods [39, 34], we shall start with an initial smooth[2] embedding $f : (\mathbb{T}^2, \mu) \to (\mathbb{R}^3, \langle\cdot,\cdot\rangle_{\mathbb{R}^3})$ that is not isometric. The general strategy is to view the torus as a family of curves and to apply one-dimensional convex integration along each curve. Intuitively, though, the one-dimensional process can only deal with one-dimensional constraints. Following [39, 34, 14], we thus assume in this first chapter (see Chapter 3 for the general case) that μ differs from $f^*\langle\cdot,\cdot\rangle_{\mathbb{R}^3}$ by a *primitive* metric. In other words, we suppose that

$$\mu = f^*\langle\cdot,\cdot\rangle_{\mathbb{R}^3} + \rho\ell \otimes \ell \tag{2.4}$$

for some positive function $\rho : \mathbb{T}^2 \to \mathbb{R}_+^*$ and some non zero linear form ℓ on $\mathbb{R}^2$, identifying each tangent plane of $\mathbb{T}^2$ with $\mathbb{R}^2$. We further assume that $\ker\ell$ contains a non trivial vector with integer coordinates. This is a rather weak assumption, as the set of integral vectors is dense in the set of directions of the plane. We choose $V \in \ker\ell$, with relatively prime integer coordinates. As a consequence, the curve $\gamma : [0,1] \to \mathbb{T}^2$, $t \mapsto [O + tV]$ is a simple closed curve in $\mathbb{T}^2$. Henceforth, we shall denote by $\mathcal{C}yl$ the cylinder obtained by cutting $\mathbb{T}^2$ along γ. We also consider the vector U such that

[2] We use the term *smooth* as a synonym of C^∞.

(U, V) is a direct orthogonal basis and $\|U\|\|V\| = 1$ (See Fig. 2.4). In particular, the rectangle determined by the origin O of $\mathbb{R}^2$ and the points $O + U$ and $O + V$ is a fundamental domain of $\mathbb{T}^2$ under the action of $\mathbb{Z}^2$ on $\mathbb{R}^2$, and the cylinder $\mathcal{C}yl$ can be viewed as the set of points of the form $O + tV + sU$ for $t \in \mathbb{R}/\mathbb{Z}$ and $s \in I$. For convenience, we shall assume that

$$\ell(U) = \|U\|,$$

should we rescale ℓ and ρ accordingly.

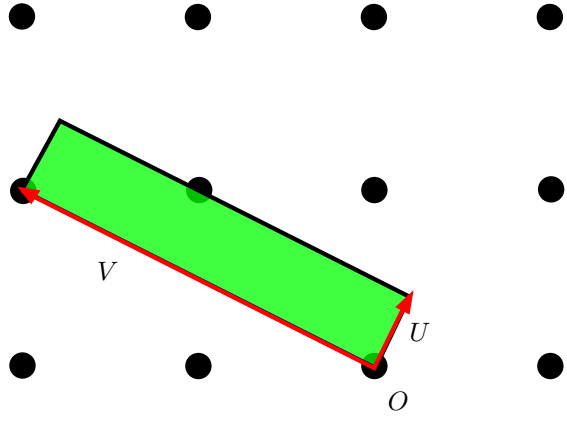

Figure 2.4: The integral lattice of $\mathbb{R}^2$. The (green) rectangle is a fundamental domain of the action of $\mathbb{Z}^2$ on $\mathbb{R}^2$.

2.3.1 Convex integration on the cylinder $\mathcal{C}yl$

In a first step we extend the one-dimensional convex integration process to the cylinder $\mathcal{C}yl$ in order to get an almost isometric embedding of $(\mathcal{C}yl, \mu)$ in the three dimensional Euclidean space. We show that the naive approach that consists in applying the one-dimensional convex integration along the generating lines of $\mathcal{C}yl$ generally fails. In Section 2.3.1, we correct the naive approach and provide bounds on the isometric quality of the obtained immersion.

A first attempt toward an isometry

The function f trivially induces a function on $\mathcal{C}yl$ that we still denote by f. Likewise the metric μ induces a metric on $\mathcal{C}yl$. We may consider $\mathcal{C}yl$ as a collection of curves $\phi_t : I \to \mathcal{C}yl$, $s \mapsto O + tV + sU$ with $t \in \mathbb{R}/\mathbb{Z}$ (See Fig. 2.5). In order to get an isometric embedding out of $f : (\mathcal{C}yl, \mu) \to (\mathbb{R}^3, \langle \cdot, \cdot \rangle_{\mathbb{R}^3})$ we could apply to each curve $f \circ \phi_t$ the one-dimensional convex

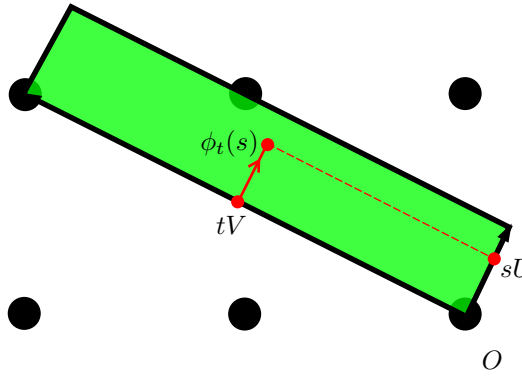

Figure 2.5: The point $\phi_t(s)$ has coordinates (s,t) in the frame (O,U,V).

integration process described in the previous sections. Let us push this strategy a little forward. The isometry condition applied to a mapping defined on the image of ϕ_t amounts to constrain the norm of its derivative to be equal to $\sqrt{\mu(U,U)}$. This leads us to define a parametrised version $h(t,s,u)$ of (2.3) with

$$\begin{aligned} h(t,s,u) &= \bar{h}(\phi_t(s),\cos(2\pi u)), \qquad \text{where} \\ \bar{h}(p,c) &= r(p)\big(\cos(\alpha(p)c)\mathbf{t}(p)+\sin(\alpha(p)c)\mathbf{n}(p)\big), \end{aligned}$$

and

$$r := \sqrt{\mu(U,U)}, \quad \mathbf{t} := U{\cdot}f/\|U{\cdot}f\|, \quad \alpha := J_0^{-1}(\|U{\cdot}f\|/r).$$

As usual $X{\cdot}f = df(X)$ denotes the derivation of f along the vector field X. A natural choice for $\mathbf{n}$ is given by the normal to the embedding, namely

$$\mathbf{n} := U{\cdot}f \wedge V{\cdot}f/\|U{\cdot}f \wedge V{\cdot}f\|.$$

Equation (2.1) becomes

$$\frac{\partial(f\circ\phi_t)}{\partial s}(s) = \int_0^1 h(t,s,u)\mathrm{d}u$$

and by (2.2), we obtain a smooth mapping $F : (\mathcal{C}yl,\mu) \to (\mathbb{R}^3,\langle\cdot,\cdot\rangle_{\mathbb{R}^3})$ satisfying

$$F\circ\phi_t(s) := f(O+tV) + \int_{u=0}^{s} h(t,u,\{Nu\})\mathrm{d}u. \tag{2.5}$$

How far is F from being an isometry? To get an answer we just need to evaluate and compare the two metrics $F^*\langle\cdot,\cdot\rangle_{\mathbb{R}^3}$ and μ at (V,V), (U,U),

and (U, V). On the one hand, noting that $\frac{\partial \phi_t}{\partial s} = U$, we have[3]

$$\langle U{\cdot}F, U{\cdot}F\rangle_{\mathbb{R}^3} = \left\langle \frac{\partial F \circ \phi_t(s)}{\partial s}, \frac{\partial F \circ \phi_t(s)}{\partial s} \right\rangle_{\mathbb{R}^3} = \|h(t, s, \{Ns\})\|^2$$

and

$$\|h(t, s, \{Ns\})\|^2 = r^2 = \mu(U, U),$$

whence

$$F^*\langle \cdot, \cdot \rangle_{\mathbb{R}^3}(U, U) = \mu(U, U).$$

On the other hand, by differentiating (2.5) with respect to t, we see that $\frac{\partial F \circ \phi_t(s)}{\partial t}$ can be obtained by a convex integration process from $\frac{\partial f \circ \phi_t(s)}{\partial t}$. We can thus apply Lemma 1 to show that $\|\frac{\partial F \circ \phi_t(s)}{\partial t} - \frac{\partial f \circ \phi_t(s)}{\partial t}\| = O(1/N)$. Noting that $\frac{\partial \phi_t}{\partial t} = V$, this is expressed by:

$$V{\cdot}F \approx_N V{\cdot}f,$$

where $u \approx_N v$ means $u = v + O(\frac{1}{N})$. From the primitive condition (2.4) together with $V \in \ker \ell$, we deduce that

$$\left\langle \frac{\partial f \circ \phi_t(s)}{\partial t}, \frac{\partial f \circ \phi_t(s)}{\partial t} \right\rangle_{\mathbb{R}^3} = \langle V{\cdot}f, V{\cdot}f\rangle_{\mathbb{R}^3} = \mu(V, V),$$

whence

$$F^*\langle \cdot, \cdot \rangle_{\mathbb{R}^3}(V, V) \approx_N \mu(V, V).$$

Whether or not F is close to an isometry eventually rests on the proximity between $\mu(U, V)$ and $\langle U{\cdot}F, V{\cdot}F\rangle_{\mathbb{R}^3}$. We have

$$\langle U{\cdot}F, V{\cdot}F\rangle_{\mathbb{R}^3} = \langle h(t, s, \{Ns\}), V{\cdot}F\rangle_{\mathbb{R}^3} \approx_N \langle h(t, s, \{Ns\}), V{\cdot}f\rangle_{\mathbb{R}^3}$$

and, omitting some parameters,

$$\begin{aligned}
\langle h(t, s, \{Ns\}), V{\cdot}f\rangle_{\mathbb{R}^3} &= \langle r(\cos(\alpha\cos(2\pi Ns))\mathbf{t}, V{\cdot}f\rangle_{\mathbb{R}^3} \\
&= \left\langle r\frac{\cos(\alpha\cos(2\pi Ns))}{\|U{\cdot}f\|}U{\cdot}f, V{\cdot}f \right\rangle_{\mathbb{R}^3} \\
&= r\frac{\cos(\alpha\cos(2\pi Ns))}{\|U{\cdot}f\|}\langle U{\cdot}f, V{\cdot}f\rangle_{\mathbb{R}^3} \\
&= r\frac{\cos(\alpha\cos(2\pi Ns))}{\|U{\cdot}f\|}\mu(U, V).
\end{aligned}$$

The first equality follows from the orthogonality between $\mathbf{n}(s)$ and $V{\cdot}f$, while the last equality results from $V \in \ker \ell$. We conclude that

$$F^*\langle \cdot, \cdot \rangle_{\mathbb{R}^3}(U, V) \approx_N r\frac{\cos(\alpha\cos(2\pi Ns))}{\|U{\cdot}f\|}\mu(U, V).$$

[3]In the following, we sometimes omit the parameter $p = \phi_t(s)$.

Therefore, unless $\mu(U,V)$ is null, this definition of F does not converge to an isometry, no matter how large is N. We now correct this first attempt by replacing U with a vector field W that is μ-orthogonal to V.

A second attempt toward an isometry

We shall again consider the cylinder $\mathcal{C}yl$ as a collection of curves. This time, we replace U by

$$W = U + \zeta V \quad \text{with} \quad \zeta = -\frac{\mu(U,V)}{\mu(V,V)} = -\frac{\langle U{\cdot}f, V{\cdot}f\rangle_{\mathbb{R}^3}}{\langle V{\cdot}f, V{\cdot}f\rangle_{\mathbb{R}^3}},$$

chosen so that $\mu(W,V) = 0$. And we replace ϕ_t by the integral curve $\varphi(t,\cdot) : I \to \mathcal{C}yl$ of W with initial condition $O + tV$ (see Fig. 2.6), so that

$$\varphi(t,0) = O + tV \quad \text{and} \quad \frac{\partial\varphi}{\partial s}(t,s) = W(\varphi(t,s)).$$

If we write this differential equation in the coordinate system of (U,V), we observe that

$$\varphi(t,s) = 0 + sU + \psi(t,s)V \tag{2.6}$$

for some function $\psi : \mathbb{R}/\mathbb{Z} \times I \to \mathbb{R}$ such that $\psi(t,0) = t$. In particular, the

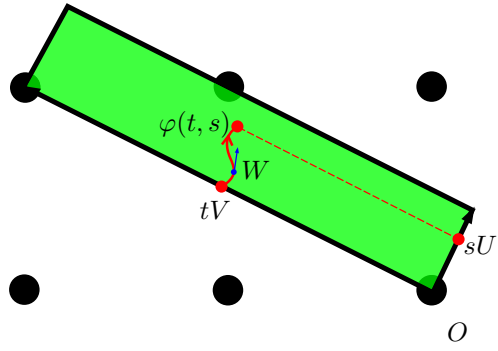

Figure 2.6: The integral curve $s \mapsto \varphi(t,s)$ of the (non constant) vector field W.

curve $\varphi(t,\cdot)$ joins the point $O + tV$ on one boundary of $\mathcal{C}yl$ to the point $O + U + \psi(t,1)V$ on the other boundary of $\mathcal{C}yl$, and $\varphi : \mathbb{R}/\mathbb{Z} \times I \to \mathcal{C}yl$ is indeed a diffeomorphism. We also observe by differentiating 2.6 that $\frac{\partial\varphi}{\partial t}(s,t)$ is proportional to V, so that

$$\ell(\frac{\partial\varphi}{\partial t}) = 0 \qquad \text{and} \qquad \mu(\frac{\partial\varphi}{\partial t}, W) = 0. \tag{2.7}$$

We mimic the previous strategy and apply the convex integration to each curve $f \circ \varphi(t, \cdot)$. For this, we redefine the parametrised version $h(t, s, u)$ of (2.3) by

$$\begin{aligned} h(t,s,u) &= \bar{h}(\varphi(t,s), \cos(2\pi u)), \quad \text{where} \\ \bar{h}(p,c) &= r(p)\big(\cos(\alpha(p)c)\mathbf{t}(p) + \sin(\alpha(p)c)\mathbf{n}(p)\big), \end{aligned} \tag{2.8}$$

and, omitting the parameter p,

$$r := \sqrt{\mu(W,W)}, \quad \mathbf{t} := W{\cdot}f/\|W{\cdot}f\|,$$
$$\mathbf{n} := W{\cdot}f \wedge V{\cdot}f/\|W{\cdot}f \wedge V{\cdot}f\|, \quad \alpha := J_0^{-1}(\|W{\cdot}f\|/r).$$

We can now write

$$(W{\cdot}f)(\varphi(t,s)) = \frac{\partial(f\circ\varphi)}{\partial s}(t,s) = \int_0^1 h(t,s,u)\mathrm{d}u$$

and we obtain a smooth mapping $F : (\mathcal{C}yl, \mu) \to (\mathbb{R}^3, \langle\cdot,\cdot\rangle_{\mathbb{R}^3})$ by setting

$$F \circ \varphi(t,s) := f(O + tV) + \int_{u=0}^{s} h(t,u,\{Nu\})\mathrm{d}u. \tag{2.9}$$

We shall first compare the mappings F and f, as well as some of their derivatives.

Lemma 2 (C^0-density)**.** *With the previously defined quantities f, h, N and F, we have*

$$\|F - f\|_\infty \le \frac{K(h)}{N},$$

where $K(h)$ only depends on the C^1-norm of h.

Proof. We first remark that φ being a diffeomorphism, $\|F - f\|_\infty = \|F\circ\varphi - f\circ\varphi\|_\infty$. The lemma then follows from the C^0-density lemma 1 applied to $f \circ \varphi(t, \cdot)$. □

Lemma 3. *With the previously defined quantities f, h, N, and F, we have*

$$\|\frac{\partial(F\circ\varphi)}{\partial t} - \frac{\partial(f\circ\varphi)}{\partial t}\|_\infty \le \frac{K(h)}{N},$$

where $K(h)$ only depends on the C^2-norm of h.

Proof. By differentiating (2.9) with respect to t we observe that $\frac{\partial(F\circ\varphi)}{\partial t}(t,\cdot)$ is obtained from $\frac{\partial(f\circ\varphi)}{\partial t}(t,\cdot)$ by a convex integration process. We can thus apply the C^0-density lemma to $\frac{\partial(f\circ\varphi)}{\partial t}(t,\cdot)$ instead of f to conclude that

$$\|\frac{\partial(F\circ\varphi)}{\partial t} - \frac{\partial(f\circ\varphi)}{\partial t}\|_\infty \le \frac{1}{N}(2\|\frac{\partial h}{\partial x_1}\|_\infty + \|\frac{\partial^2 h}{\partial x_1 \partial x_2}\|_\infty),$$

where $\frac{\partial h}{\partial x_1}$ and $\frac{\partial^2 h}{\partial x_1 \partial x_2}$ are the derivatives of h with respect to the first parameter x_1 and the second parameter x_2. □

Lemma 4. *With the previously defined quantities f and F, including $\mu = f^*\langle \cdot, \cdot \rangle_{\mathbb{R}^3} + \rho \ell \otimes \ell$, we have*

$$\|W{\cdot}F - W{\cdot}f\|_\infty \leq \sqrt{7}.\|U\|.\|\rho\|_\infty^{\frac{1}{2}}.$$

We need the following preliminary sublemma for our proof.

Sublemma 5. *The inequality*

$$1 + J_0^2(\alpha) - 2J_0(\alpha)\cos(\alpha) \leq 7(1 - J_0^2(\alpha))$$

holds for every $\alpha \in [0, z]$ (recall that z is the first positive root of J_0).

Proof. Subtracting the right hand side from the left hand side, we rewrite this inequality as

$$4J_0^2(\alpha) - J_0(\alpha)\cos(\alpha) - 3 \leq 0.$$

By considering the alternating Taylor series of J_0 and cos, we get

$$J_0(\alpha) \leq 1 - \frac{\alpha^2}{4} + \frac{\alpha^4}{64} \quad \text{and} \quad \cos(\alpha) \geq 1 - \frac{\alpha^2}{2}.$$

Whence

$$0 \leq 4J_0(\alpha) - \cos(\alpha) \leq 3 - \frac{\alpha^2}{2} + \frac{\alpha^4}{16} \leq 3 + \frac{\alpha^2}{2},$$

where the last inequality follows from $-\frac{\alpha^2}{2} + \frac{\alpha^4}{16} \leq \frac{\alpha^2}{2}$ for all $\alpha \in [0, z]$. We can now write

$$\begin{aligned} 4J_0^2(\alpha) - J_0(\alpha)\cos(\alpha) - 3 &= J_0(\alpha)(4J_0(\alpha) - \cos(\alpha)) - 3 \\ &\leq (1 - \frac{\alpha^2}{4} + \frac{\alpha^4}{64})(3 + \frac{\alpha^2}{2}) - 3. \end{aligned}$$

Putting $x = \alpha^2/4$, this last polynomial can be rewritten

$$(1 - x + \frac{x^2}{4})(3 + 2x) - 3 = \frac{x}{2}(x - x_1)(x - x_2),$$

where $x_1 < 0 < z^2/4 < x_2$. It ensues that this polynomial is negative for $\alpha \in [0, z]$. □

Proof of Lemma 4. By definition of φ, we have

$$\frac{\partial F \circ \varphi}{\partial s}(t, s) = dF(\frac{\partial \varphi}{\partial s}(t, s)) = W{\cdot}F.$$

It now follows from (2.9) that

$$W{\cdot}F = h(t,s,\{Ns\}) = r\big(\cos(\alpha\cos(2\pi Ns))\mathbf{t} + \sin(\alpha\cos(2\pi Ns))\mathbf{n}\big)$$

where $r, \alpha, \mathbf{t}, \mathbf{n}$ should be considered at the point $\varphi(t,s)$.
Since $W{\cdot}f = \|W{\cdot}f\|\mathbf{t}$ and $J_0(\alpha) = \|W{\cdot}f\|/r$, we obtain

$$\begin{aligned}\|W{\cdot}F - W{\cdot}f\|^2 &= r^2 + \|W{\cdot}f\|^2 - 2r\|W{\cdot}f\|\cos(\alpha\cos(2\pi Ns)) \\ &= r^2(1 + J_0(\alpha)^2 - 2J_0(\alpha)\cos(\alpha\cos(2\pi Ns))).\end{aligned}$$

We also have $\cos(\alpha\cos(2\pi Ns)) \geq \cos(\alpha)$ for every $\alpha \in [0,z] \subset [0,\pi]$. By application of the sublemma, we get

$$\begin{aligned}\|W{\cdot}F - W{\cdot}f\|^2 &\leq r^2(1 + J_0(\alpha)^2 - 2J_0(\alpha)\cos(\alpha)) \\ &\leq 7r^2(1 - J_0(\alpha)^2) = 7(r^2 - \|W{\cdot}f\|^2).\end{aligned}$$

By (2.4) we have

$$r^2 = \mu(W,W) = \|W{\cdot}f\|^2 + \rho\ell(W)^2 = \|W{\cdot}f\|^2 + \rho\|U\|^2$$

since $\ell(W) = \ell(U + \zeta V) = \ell(U) = \|U\|$. Putting all this together, we finally get

$$\|W{\cdot}F - W{\cdot}f\|^2 \leq 7\|U\|^2\rho.$$

□

We are now ready to compare the respective differential maps df and dF of f and F. We use the induced norm $\|L\| = \sup_{v\neq 0}\|Lv\|/\|v\|$ for a linear operator L. The notation $\|df\|_\infty$ thus designates the supremum of the induced norm of $df(p)$ over all $p \in \mathcal{C}yl$.

Lemma 6.

$$\|dF - df\|_\infty \leq \sqrt{7}\|\rho\|_\infty^{\frac{1}{2}} + \frac{K(\zeta,\psi,h)}{N},$$

where $K(\zeta,\psi,h)$ only depends on the C^0-norm of ζ and $(\frac{\partial\psi}{\partial t})^{-1}$, and on the C^2-norm of h.

Proof. Since (U,V) is an orthogonal basis with respect to the Euclidean metric, we have

$$\|dF - df\| \leq \frac{\|U{\cdot}F - U{\cdot}f\|}{\|U\|} + \frac{\|V{\cdot}F - V{\cdot}f\|}{\|V\|}. \tag{2.10}$$

On the one hand, we have by (2.6):

$$\frac{\partial\varphi}{\partial t} = \frac{\partial\psi}{\partial t}V,$$

whence

$$\|V{\cdot}F - V{\cdot}f\| = |\frac{\partial\psi}{\partial t}|^{-1}.\|\frac{\partial(F\circ\varphi)}{\partial t} - \frac{\partial(f\circ\varphi)}{\partial t}\|. \tag{2.11}$$

We remark that $|\frac{\partial\psi}{\partial t}|$ is the Jacobian of the diffeomorphism φ, so it never vanishes. On the other hand, we get from $W = U + \zeta V$ that

$$\|U{\cdot}F - U{\cdot}f\| \leq \|W{\cdot}F - W{\cdot}f\| + |\zeta|.\|V{\cdot}F - V{\cdot}f\|. \tag{2.12}$$

Inserting (2.11) and (2.12) into (2.10), and recalling that $\|U\|\|V\| = 1$, we obtain

$$\|dF - df\| \leq \frac{\|W{\cdot}F - W{\cdot}f\|}{\|U\|} + \frac{|\zeta|\|V\|^2 + 1}{\|V\|}.|\frac{\partial\psi}{\partial t}|^{-1}.\|\frac{\partial(F\circ\varphi)}{\partial t} - \frac{\partial(f\circ\varphi)}{\partial t}\|.$$

We can now apply the lemmas 3 and 4 to conclude. □

We end this section with a comparison between the pullback metric $F^*\langle\cdot,\cdot\rangle_{\mathbb{R}^3}$ and the target metric μ. We measure the difference of two scalar products by the Frobenius norm of the difference of their matrices expressed in the canonical basis of $\mathbb{R}^2$. We recall that the Frobenius norm of a matrix is the square root of the sum of its squared coefficients.

Lemma 7.

$$\|\mu - F^*\langle\cdot,\cdot\rangle_{\mathbb{R}^3}\|_\infty \leq \frac{K(f\circ\varphi, h)}{N}\|d\varphi^{-1}\|_\infty^2,$$

where $K(f\circ\varphi, h)$ only depends on the C^0-norm of $\frac{\partial f\circ\phi}{\partial t}$ and on the C^2-norm of h.

Proof. We shall first measure the difference between $\varphi^*\mu$ and $\varphi^*F^*\langle\cdot,\cdot\rangle_{\mathbb{R}^3} = (F\circ\varphi)^*\langle\cdot,\cdot\rangle_{\mathbb{R}^3}$. We have

$$\begin{aligned}(F\circ\varphi)^*\langle\cdot,\cdot\rangle_{\mathbb{R}^3}(\partial_s,\partial_s) &= \|\frac{\partial F\circ\varphi}{\partial s}\|^2\\ &= \|h(t,s,\{Ns\})\|^2\\ &= \mu(W,W)\\ &= \varphi^*\mu(\partial_s,\partial_s),\end{aligned}$$

where we used $W = \frac{\partial\varphi}{\partial s}$ for the last equality. We remark from (2.7) that $\mu(\frac{\partial\varphi}{\partial t},\frac{\partial\varphi}{\partial t}) = f^*\langle\cdot,\cdot\rangle_{\mathbb{R}^3}(\frac{\partial\varphi}{\partial t},\frac{\partial\varphi}{\partial t})$. Whence

$$\begin{aligned}|((F\circ\varphi)^*\langle\cdot,\cdot\rangle_{\mathbb{R}^3} - \varphi^*\mu)(\partial_t,\partial_t)| &= \Big|\|\frac{\partial F\circ\varphi}{\partial t}\|^2 - \|\frac{\partial f\circ\varphi}{\partial t}\|^2\Big|\\ &\leq \|\frac{\partial F\circ\varphi}{\partial t} - \frac{\partial f\circ\varphi}{\partial t}\|\|\frac{\partial F\circ\varphi}{\partial t} + \frac{\partial f\circ\varphi}{\partial t}\|\\ &\leq \|\frac{\partial F\circ\varphi}{\partial t} - \frac{\partial f\circ\varphi}{\partial t}\|\Big(2\|\frac{\partial f\circ\varphi}{\partial t}\|\\ &\quad +\|\frac{\partial F\circ\varphi}{\partial t} - \frac{\partial f\circ\varphi}{\partial t}\|\Big).\end{aligned}$$

This shows with the help of Lemma 3 that

$$|((F\circ\varphi)^*\langle\cdot,\cdot\rangle_{\mathbb{R}^3}-\varphi^*\mu)(\partial_t,\partial_t)|\leq\frac{K_1(f\circ\varphi,h)}{N}$$

for some number $K_1(f\circ\varphi,h)$ that only depends on the C^0-norm of $\frac{\partial f\circ\varphi}{\partial t}$ and on the C^2-norm h. We also remark from (2.7) and (2.4) that

$$f^*\langle\cdot,\cdot\rangle_{\mathbb{R}^3}(\frac{\partial\varphi}{\partial t},\frac{\partial\varphi}{\partial s})=\mu(\frac{\partial\varphi}{\partial t},\frac{\partial\varphi}{\partial s})=\mu(\frac{\partial\varphi}{\partial t},W)=0,$$

where the last equality follows from the collinearity of $\frac{\partial\varphi}{\partial t}$ and V. Since $h(t,s,\{Ns\})$ is in the span of $\mathbf{t}$ and $\mathbf{n}$, that is also the span of $\frac{\partial f\circ\varphi}{\partial s}$ and $\mathbf{n}$, we infer from the previous equation that

$$\left\langle\frac{\partial(f\circ\varphi)}{\partial t},h(t,s,\{Ns\})\right\rangle_{\mathbb{R}^3}=0.$$

So

$$\begin{aligned}|((F\circ\varphi)^*\langle\cdot,\cdot\rangle_{\mathbb{R}^3}-\varphi^*\mu)(\partial_t,\partial_s)| &= |(F\circ\varphi)^*\langle\cdot,\cdot\rangle_{\mathbb{R}^3}(\partial_t,\partial_s)|\\ &= \left|\left\langle\frac{\partial(F\circ\varphi)}{\partial t},h(t,s,\{Ns\})\right\rangle_{\mathbb{R}^3}\right|\\ &= \left|\left\langle\frac{\partial(F\circ\varphi)}{\partial t}-\frac{\partial(f\circ\varphi)}{\partial t},h(t,s,\{Ns\})\right\rangle_{\mathbb{R}^3}\right|\\ &\leq \|\frac{\partial(F\circ\varphi)}{\partial t}-\frac{\partial(f\circ\varphi)}{\partial t}\|.\|h(t,s,\{Ns\})\|.\end{aligned}$$

This shows again with the help of Lemma 3 that

$$|(F\circ\varphi)^*\langle\cdot,\cdot\rangle_{\mathbb{R}^3}(\partial_t,\partial_s)|=|((F\circ\varphi)^*\langle\cdot,\cdot\rangle_{\mathbb{R}^3}-\varphi^*\mu)(\partial_t,\partial_s)|\leq\frac{K_2(h)}{N}\quad(2.13)$$

for some number $K_2(h)$ that only depends on the C^2-norm of h. To summarise, we have obtained

$$\|\varphi^*\mu-\varphi^*F^*\langle\cdot,\cdot\rangle_{\mathbb{R}^3}\|\leq\frac{K_1(f\circ\varphi,h)+2K_2(h)}{N}.$$

We finally conclude noting that

$$\|\mu-F^*\langle\cdot,\cdot\rangle_{\mathbb{R}^3}\|\leq\|\varphi^*\mu-\varphi^*F^*\langle\cdot,\cdot\rangle_{\mathbb{R}^3}\|.\|d\varphi^{-1}\|^2_\infty.$$

□

Henceforth, we denote by $\Phi:\mathbb{R}^2\times\mathbb{R}\to\mathbb{R}^2$ the flow of W, considered as a vector field in $\mathbb{R}^2$. In particular, $\varphi(t,s)=\Phi(O+tV,s)$.

A note on $d\varphi^{-1}$. From (2.6), we know that $s = \ell(\varphi(t,s) - O)/\|U\|$. From the group action of the flow Φ, together with $\varphi(t,0) = O + tV$, we see that (Figure 2.6)

$$\varphi^{-1}(p) = \Big(\Big\langle \Phi\left(p, -\frac{\ell(p-O)}{\|U\|}\right) - O, \frac{V}{\|V\|^2}\Big\rangle_{\mathbb{R}^2}, \frac{\ell(p-O)}{\|U\|}\Big).$$

This shows that any reasonable bound on the derivatives of the flow essentially holds for the derivatives of φ^{-1}.

2.3.2 Convex integration on the torus $\mathbb{T}^2$

In the previous section 2.3.1, we have constructed an almost isometric map $F : (\mathcal{C}yl, \mu) \to (\mathbb{R}^3, \langle\cdot,\cdot\rangle_{\mathbb{R}^3})$ that is C^0-close to the map induced on $\mathcal{C}yl$ by $f : (\mathbb{T}^2, \mu) \to (\mathbb{R}^3, \langle\cdot,\cdot\rangle_{\mathbb{R}^3})$. In general, the map F will not coincide on the two boundaries of $\mathcal{C}yl$. This forbids to quotient F into a map on $\mathbb{T}^2$. We therefore define a new map $\bar{F}$ out of F by setting

$$\bar{F} \circ \varphi(t,s) = F \circ \varphi(t,s) - w(s)(F \circ \varphi(t,1) - f \circ \varphi(t,1)), \qquad (2.14)$$

where $w : I \to I$ is a smooth S-shaped function satisfying

$$w(0) = 0, \quad w(1) = 1, \quad \text{and} \quad \forall k \in \mathbb{N}^* : w^{(k)}(0) = w^{(k)}(1) = 0.$$

Lemma 8. *If $f : \mathbb{T}^2 \to \mathbb{R}^3$ and $w : I \to I$ are smooth maps, then $\bar{F}$ descends to the quotient as a smooth map on $\mathbb{T}^2$.*

We need a preliminary lemma.

Lemma 9. *If $f : \mathbb{T}^2 \to \mathbb{R}^3$ is a smooth map, then $W{\cdot}F$ descends to the quotient as a smooth map on $\mathbb{T}^2$.*

Proof. Recall from the proof of Lemma 4 that

$$(W{\cdot}F)(\varphi(t,s)) = h(t,s,\{Ns\}) = \bar{h}(\varphi(t,s), \cos(2\pi Ns)),$$

where $\bar{h}$ was defined by Equation (2.8). Since $s = l(\varphi(t,s) - O)/\|U\|$, we can now write

$$(W{\cdot}F)(p) = \bar{h}(p, \cos(2\pi N \frac{\ell(p-O)}{\|U\|})).$$

But $\frac{\ell(p-O)}{\|U\|}$ is either 0 or 1 on the boundary $\partial\mathcal{C}yl$ of $\mathcal{C}yl$. It follows from the periodicity of the cosine function that $p \mapsto (p, \cos(2\pi N \frac{\ell(p-O)}{\|U\|}))$ defines a smooth map on $\mathbb{T}^2$. We can conclude by noting that $\bar{h} : \mathbb{T}^2 \times \mathbb{R} \to \mathbb{R}^3$ is smooth. □

Proof of Lemma 8. Setting $s = 0$ and $s = 1$ in (2.14) and noting from (2.9) that $F \circ \varphi(t,0) = f \circ \varphi(t,0)$, we get

$$\forall t \in \mathbb{R}/\mathbb{Z}: \quad \bar{F} \circ \varphi(t,0) = f \circ \varphi(t,0) \ \text{ and } \ \bar{F} \circ \varphi(t,1) = f \circ \varphi(t,1). \quad (2.15)$$

It follows that the restrictions of $\bar{F}$ and f to the boundary $\partial \mathcal{C}yl$ of $\mathcal{C}yl$ are identical. Hence, the map $\bar{F}$ descends to the quotient on $\mathbb{T}^2$. Let us show that this quotient map is C^1. By differentiating the restrictions of $\bar{F}$ and f to $\partial \mathcal{C}yl$ we obtain for all $p \in \partial \mathcal{C}yl$:

$$d\bar{F}_p(V) = df_p(V). \quad (2.16)$$

By further derivations of (2.16) and a simple induction, we obtain that the equality

$$\bar{F}^{(k)} \underbrace{(V, \ldots, V)}_{k\times} = f^{(k)} \underbrace{(V, \ldots, V)}_{k\times}$$

holds on $\partial \mathcal{C}yl$. It ensues that $F^{(k)}(V, \ldots, V)$ descends to the quotient on $\mathbb{T}^2$. Furthermore, by differentiating (2.14) with respect to s we obtain for all $(t,s) \in \mathbb{R}/\mathbb{Z} \times I$:

$$W \cdot \bar{F}(\varphi(t,s)) = W \cdot F(\varphi(t,s)) - w'(s)(F \circ \varphi(t,1) - f \circ \varphi(t,1)).$$

Or equivalently, recalling that Φ is the flow of W:

$$W \cdot \bar{F}(p) = W \cdot F(p) - w'(s(p))\big(F \circ \Phi(p, 1-s(p)) - f \circ \Phi(p, 1-s(p))\big), \quad (2.17)$$

where $s(p) = \frac{\ell(p-O)}{\|U\|}$. We know from the preliminary lemma 9 that the first term in this sum descends to the quotient. On the other hand, since all derivatives of the second term involve non-trivial derivatives of w, they vanish on $\partial \mathcal{C}yl$. It follows that $\bar{F}^{(k)}(W, V_2 \ldots, V_k)$ descends to the quotient for $V_i \in \{V, W\}$, $2 \le i \le k$. We conclude that $\bar{F}^{(k)}$ descends to the quotient on $\mathbb{T}^2$. $\square$

We close this chapter with its main result.

Theorem 10 (One Step Theorem)**.** *Let $f : (\mathbb{T}^2, \mu) \to (\mathbb{R}^3, \langle \cdot, \cdot \rangle_{\mathbb{R}^3})$ be a smooth embedding satisfying equation (2.4). Let $\bar{F}$ be given by (2.14). Then*

1. $\|\bar{F} - f\|_\infty \le \frac{K_1(h)}{N}$ *and* $\|\bar{F} - f\|_\infty \le 2\sqrt{7}\|U\| \ \|\rho\|_\infty^{\frac{1}{2}}$,
2. $\|d\bar{F} - df\|_\infty \le \frac{K_2(h,\zeta,\psi,w')}{N} + \sqrt{7}\|\rho\|_\infty^{\frac{1}{2}}$,
3. $\|V \cdot \bar{F} - V \cdot f\| \le \frac{K_3(h,\psi)}{N}$,
4. $\|W \cdot \bar{F} - W \cdot f\| \le \sqrt{7}.\|U\|.(1 + \|w'\|_\infty).\|\rho\|_\infty^{\frac{1}{2}}$, *and*

5. $\|\mu - \bar{F}^*\langle\cdot,\cdot\rangle_{\mathbb{R}^3}\|_\infty \leq \frac{K_4(f\circ\varphi,r,h,w',\phi^{-1})}{N}$,

where

- $K_1(h)$ *only depends on the* C^1*-norm of* h,
- $K_2(h,\zeta,\psi,w')$ *only depends on the* C^2*-norm of* h *and on the* C^0*-norm of* w', ζ, *and* $(\frac{\partial\psi}{\partial t})^{-1}$,
- $K_3(h,\psi)$ *only depends on the* C^0*-norm of* $(\frac{\partial\psi}{\partial t})^{-1}$ *and on the* C^2*-norm of* h,
- $K_4(f\circ\varphi,r,h,w',\varphi^{-1})$ *only depends on the* C^0*-norm of* $\frac{\partial f\circ\phi}{\partial t}$, r, w', $d\varphi^{-1}$ *and on the* C^2*-norm of* h.

Notation. The map $\bar{F}$ resulting from our convex integration process depends on the initial map f, the primitive metric μ and the oscillation number N. We denote this map by $IC(f,\mu,N)$, *i.e.*

$$IC(f,\mu,N) := \bar{F}. \tag{2.18}$$

Proof. from (2.14) we derive for all $p \in \mathcal{C}yl$:

$$\|\bar{F}(p) - f(p)\| \leq \|F(p) - f(p)\| + \|w\|_\infty\|F - f\|_\infty \leq 2\|F - f\|_\infty.$$

It remains to apply Lemma 2 to conclude the first inequality of Point 1 in the theorem. Furthermore, $\|F - f\|_\infty$ is bounded by $\|W{\cdot}F - W{\cdot}f\|_\infty$ as shown below:

$$\begin{aligned}\|F\circ\varphi(t,s) - f\circ\varphi(t,s)\| &= \|\int_0^s (\frac{\partial F\circ\varphi}{\partial s}(t,u) - \frac{\partial f\circ\varphi}{\partial s}(t,u))\mathrm{d}u\| \\ &\leq \int_0^s \|(W{\cdot}F)(\varphi(t,u)) - (W{\cdot}f)(\varphi(t,u))\|\mathrm{d}u \\ &\leq \|W{\cdot}F - W{\cdot}f\|_\infty.\end{aligned}$$

The second inequality of the first item then directly follows from Lemma 4. We now prove the second item of the theorem. Following the proof of Lemma 6, we can obtain

$$\|d\bar{F} - df\| \leq \frac{\|W{\cdot}\bar{F} - W{\cdot}f\|}{\|U\|} + \frac{|\zeta|\|V\|^2+1}{\|V\|}\cdot|\frac{\partial\psi}{\partial t}|^{-1}\cdot\|\frac{\partial(\bar{F}\circ\varphi)}{\partial t} - \frac{\partial(f\circ\varphi)}{\partial t}\|.$$

On the one hand, differentiating (2.14) we respect to s, we easily get

$$\|W{\cdot}\bar{F} - W{\cdot}f\| \leq \|W{\cdot}F - W{\cdot}f\|_\infty + \|w'\|_\infty\|F - f\|_\infty. \tag{2.19}$$

On the other hand, differentiating (2.14) with respect to t, we easily deduce

$$\|\frac{\partial(\bar{F}\circ\varphi)}{\partial t} - \frac{\partial(f\circ\varphi)}{\partial t}\| \leq 2\|\frac{\partial(F\circ\varphi)}{\partial t} - \frac{\partial(f\circ\varphi)}{\partial t}\|_\infty.$$

We can plug these last two inequalities into the previous one and apply Lemmas 2, 3, and 4 to conclude the second item. The previous inequality together with (2.11) give the third item of the theorem. Likewise, the item 4 in the theorem follows from the inequality (2.19) together with Lemma 4, noting as above that $\|F - f\|_\infty \leq \|W{\cdot}F - W{\cdot}f\|_\infty$.

We now consider Item 5 of the theorem. We follow the proof of Lemma 7 and first bound the difference between $\varphi^*\mu$ and $(F \circ \varphi)^*\langle\cdot,\cdot\rangle_{\mathbb{R}^3}$. We have from (2.14):

$$(\bar{F}\circ\varphi)^*\langle\cdot,\cdot\rangle_{\mathbb{R}^3}(\partial_s,\partial_s) = \|\frac{\partial \bar{F}\circ\varphi}{\partial s}\|^2 = \|W{\cdot}F - w'(s)(F\circ\varphi(t,1) - f\circ\varphi(t,1))\|^2.$$

Using that $\varphi^*\mu(\partial_s,\partial_s) = \mu(W,W) = r^2 = \|W{\cdot}F\|^2$, we easily obtain

$$\begin{aligned} |(\bar{F}\circ\varphi)^*\langle\cdot,\cdot\rangle_{\mathbb{R}^3}(\partial_s,\partial_s) - \varphi^*\mu(\partial_s,\partial_s)| \quad &\leq \quad |w'|_{C^0}\|F-f\|_\infty(2\|r\|_\infty \\ &\quad +\|w'\|_\infty\|F-f\|_\infty). \end{aligned}$$

We deduce from Lemma 2 that

$$|(\bar{F}\circ\varphi)^*\langle\cdot,\cdot\rangle_{\mathbb{R}^3}(\partial_s,\partial_s) - \varphi^*\mu(\partial_s,\partial_s)| \leq \frac{X(w',r,h)}{N}, \tag{2.20}$$

where $X(w',r,h)$ only depends on the C^0-norm of w' and r and on the C^2-norm of h. We also have from (2.14) and the fact that $\varphi^*\mu(\partial_t,\partial_t) = \|\frac{\partial f\circ\varphi}{\partial t}\|^2$:

$$\begin{aligned} \left|(\bar{F}\circ\varphi)^*\langle\cdot,\cdot\rangle_{\mathbb{R}^3}(\partial_t,\partial_t) - \varphi^*\mu(\partial_t,\partial_t)\right| = \Big|\|\frac{\partial F\circ\varphi}{\partial t} - w(s)(\frac{\partial F\circ\varphi}{\partial t}(t,1) - \frac{\partial f\circ\varphi}{\partial t}(t,1))\|^2 \\ -\|\frac{\partial f\circ\varphi}{\partial t}\|^2\Big|. \end{aligned}$$

We put $A := \frac{\partial F\circ\varphi}{\partial t}$, $B := \frac{\partial F\circ\varphi}{\partial t}(t,1) - \frac{\partial f\circ\varphi}{\partial t}(t,1)$, and $C := \frac{\partial f\circ\varphi}{\partial t}$. Hence,

$$\begin{aligned} \left|(\bar{F}\circ\varphi)^*\langle\cdot,\cdot\rangle_{\mathbb{R}^3}(\partial_t,\partial_t) - \varphi^*\mu(\partial_t,\partial_t)\right| \quad &= \quad \left|\|A - w(s)B\|^2 - \|C\|^2\right| \\ &\leq \quad \|A - w(s)B - C\|\ \|A - w(s)B + C\| \\ &\leq \quad (\|A-C\| + \|B\|)(\|A-C\| \\ &\quad +2\|C\| + \|B\|), \end{aligned}$$

so that

$$\begin{aligned} \left|(\bar{F}\circ\varphi)^*\langle\cdot,\cdot\rangle_{\mathbb{R}^3}(\partial_t,\partial_t) - \varphi^*\mu(\partial_t,\partial_t)\right| \leq 4\|\frac{\partial F\circ\varphi}{\partial t} - \frac{\partial f\circ\varphi}{\partial t}\|_\infty(\|\frac{\partial F\circ\varphi}{\partial t} - \frac{\partial f\circ\varphi}{\partial t}\|_\infty \\ +\|\frac{\partial f\circ\varphi}{\partial t}\|_\infty). \end{aligned}$$

We now deduce from Lemma 3 that

$$\left|(\bar{F}\circ\varphi)^*\langle\cdot,\cdot\rangle_{\mathbb{R}^3}(\partial_t,\partial_t) - \varphi^*\mu(\partial_t,\partial_t)\right| \leq \frac{Y(f\circ\varphi,h)}{N} \tag{2.21}$$

for some function $Y(f\circ\varphi,h)$ that only depends on the C^0-norm of $\frac{\partial f\circ\varphi}{\partial t}$ and on the C^2-norm of h. Recall from (2.7) that $\varphi^*\mu(\partial_t,\partial_s)=\mu(\frac{\partial\varphi}{\partial t},W)=0$. Whence

$$\left|(\bar F\circ\varphi)^*\langle\cdot,\cdot\rangle_{\mathbb{R}^3}(\partial_t,\partial_s)-\varphi^*\mu(\partial_t,\partial_s)\right|=\left|(\bar F\circ\varphi)^*\langle\cdot,\cdot\rangle_{\mathbb{R}^3}(\partial_t,\partial_s)\right|.$$

We put $D=\frac{\partial F\circ\varphi}{\partial s}$ and $E=F\circ\varphi(t,1)-f\circ\varphi(t,1)$. Together with the previous notations, we get

$$\begin{aligned}\left|(\bar F\circ\varphi)^*\langle\cdot,\cdot\rangle_{\mathbb{R}^3}(\partial_t,\partial_s)\right| &= |\langle A-wB,D-w'E\rangle_{\mathbb{R}^3}|\\ &\leq |\langle A,D\rangle_{\mathbb{R}^3}|+|w'|\|E\|(\|A\|+\|B\|)+\|B\|\|D\|.\end{aligned}$$

We note that $\langle A,D\rangle_{\mathbb{R}^3}=(F\circ\varphi)^*\langle\cdot,\cdot\rangle_{\mathbb{R}^3}(\partial_t,\partial_s)$, whence by (2.13): $|\langle A,D\rangle_{\mathbb{R}^3}|\leq\frac{Z_1(h)}{N}$, for some function $Z_1(h)$ of the C^2-norm of h. By Lemma 2, we have $\|E\|\leq\frac{Z_2(h)}{N}$, for some function $Z_2(h)$ of the C^1-norm of h. By Lemma 3, we also have $\|B\|\leq\|A-C\|_\infty\leq\frac{Z_3(h)}{N}$, for some function $Z_3(h)$ of the C^2-norm of h. Noting that $\|A\|\leq\|A-C\|+\|C\|$, we get $\|A\|\leq\frac{Z_3(h)}{N}+\|C\|$. We finally note that $\|D\|=\|W\cdot F\|=r$. Putting all this together we obtain

$$\left|(\bar F\circ\varphi)^*\langle\cdot,\cdot\rangle_{\mathbb{R}^3}(\partial_t,\partial_s)-\varphi^*\mu(\partial_t,\partial_s)\right|\leq\frac{Z(f\circ\phi,w',r,h)}{N},\qquad(2.22)$$

where

$$Z(f\circ\phi,w',r,h)=Z_1(h)+\|w'\|_\infty Z_2(h)\left(\|\frac{\partial f\circ\varphi}{\partial t}\|_\infty+2\frac{Z_3(h)}{N}\right)+Z_3(h)r.$$

As in the proof of Lemma 7, we write

$$\|\mu-\bar F^*\langle\cdot,\cdot\rangle_{\mathbb{R}^3}\|\leq\|\varphi^*\mu-\varphi^*\bar F^*\langle\cdot,\cdot\rangle_{\mathbb{R}^3}\|.\|d\varphi^{-1}\|^2_\infty.$$

This last inequality, together with (2.20), (2.21), and (2.22) allows to complete the proof of the third point of the theorem with

$$K_4(f\circ\varphi,r,h,w',\varphi^{-1})=(X(w',r,h)+Y(f\circ\varphi,h)+2Z(f\circ\phi,w',r,h))\|d\varphi^{-1}\|^2_{C^0}.$$

□

Chapter 3

Isometric immersions of the square flat torus

3.1 Our convex integration process

In the previous chapter, we saw how to build a quasi-isometry $\overline{f} : (\mathbb{T}^2, g) \to \mathbb{E}^3$ from an immersion $f : \mathbb{T}^2 \to \mathbb{R}^3$ in the primitive case where

$$g - f^*\langle \cdot, \cdot \rangle_{\mathbb{R}^3} \;=\; \rho\, \ell \otimes \ell \quad \text{where} \quad \rho > 0.$$

The aim of this chapter is to build an isometry in the more general case where the *isometric default*

$$D := g - f^*\langle \cdot, \cdot \rangle_{\mathbb{R}^3}$$

is a metric, i.e., when $f : (\mathbb{T}^2, g) \to \mathbb{E}^3$ is *strictly short*. Following Nash [39, 34, 14] we shall decompose D into a sum of primitive metrics. For this, we first observe that the set of inner products in $\mathbb{R}^2$ is a convex cone

$$Q_+ = \big\{E\mathrm{d}x\otimes\mathrm{d}x+F(\mathrm{d}x\otimes\mathrm{d}y+\mathrm{d}y\otimes\mathrm{d}x)+G\mathrm{d}y\otimes\mathrm{d}y,\ EG-F^2>0,\ F>0,\ G>0\big\},$$

whose boundary is composed of squares of linear forms $\ell' \otimes \ell'$. In the previously cited works, the decomposition is obtained by sampling Q_+ with an infinite number of metrics q_i with the property that any metric q is a convex combination of a finite subset of the q_i. The coefficients of this combination have local support and can be defined to change smoothly with q. Each q_i is further decomposed into a sum of two squares of linear forms. This leads to a decomposition of the form

$$D = \sum_{j=1}^{N} \rho_j(D) \ell_j \otimes \ell_j \quad \text{with} \quad \rho_j(D) > 0,$$

where the integer N and the linear forms ℓ_1, ..., ℓ_N are defined locally. In our approach, we manage to make a uniform choice and to reduce this number to $N = 3$ by assuming that f is such that the image of its isometric default D belongs to the open cone

$$\mathcal{C} := \{\rho_1\ell_1 \otimes \ell_1 + \rho_2\ell_2 \otimes \ell_2 + \rho_3\ell_3 \otimes \ell_3 \mid \rho_1 > 0, \rho_2 > 0, \rho_3 > 0\},$$

where ℓ_1, ℓ_2 and ℓ_3 are the three linear forms over $\mathbb{R}^2$ given by:

$$\ell_1 := \mathrm{d}x \ , \ \ell_2 := \frac{1}{\sqrt{5}}(\mathrm{d}x + 2\mathrm{d}y) \ , \ \ell_3 := \frac{1}{\sqrt{5}}(\mathrm{d}x - 2\mathrm{d}y).$$

In order to reduce the value of the three coefficients of the isometric default D, we proceed by three successive convex integrations as in the primitive case. More precisely, we first set

$$\mu_1 := f^*\langle\cdot,\cdot\rangle_{\mathbb{R}^3} + \rho_1(D_1)\ell_1 \otimes \ell_1 \quad \text{with} \quad D_1 := D,$$

and build the quasi isometry $f_1 := IC(f, \mu_1, N_1)$ (see notation (2.18)). We shall prove that for N_1 large enough, the new isometric default

$$D_2 := g - f_1^*\langle\cdot,\cdot\rangle_{\mathbb{R}^3} = \rho_1(D_2)\ \ell_1 \otimes \ell_1 \ + \ \rho_2(D_2)\ \ell_2 \otimes \ell_2 \ + \ \rho_3(D_2)\ \ell_3 \otimes \ell_3$$

satisfies

$$D_2 \in \mathcal{C}, \quad \rho_1(D_2) \approx 0, \quad \rho_2(D_2) \approx \rho_2(D_1) \quad \text{and} \quad \rho_3(D_2) \approx \rho_3(D_1).$$

In particular $\rho_2(D_2) > 0$. We next set

$$\mu_2 := f_1^*\langle\cdot,\cdot\rangle_{\mathbb{R}^3} + \rho_2(D_2)\ell_2 \otimes \ell_2,$$

and build the quasi isometry $f_2 := IC(f_1, \mu_2, N_2)$. For N_2 large enough, the new isometric default

$$D_3 := g - f_2^*\langle .,.\rangle$$

satisfies

$$D_3 \in \mathcal{C}, \quad \rho_1(D_3) \approx 0, \quad \rho_2(D_3) \approx 0 \quad \text{and} \quad \rho_3(D_3) \approx \rho_3(D_2).$$

In particular $\rho_3(D_3) > 0$, and we finally set $f_3 := IC(f_2, \mu_3, N_3)$ with

$$\mu_3 := f_2^*\langle\cdot,\cdot\rangle_{\mathbb{R}^3} + \rho_3(D_3)\ell_3 \otimes \ell_3.$$

For N_3 large enough, f_3 is almost an isometry for the metric g. We denote this last immersion

$$IC(f, g, N_1, N_2, N_3). \tag{3.1}$$

If we make N_1, N_2 and N_3 tend to infinity, the C^0 proximity property of the One Step Theorem (Point 1) implies that the limit immersion is the initial $f : (\mathbb{T}^2, g) \to \mathbb{E}^3$, thus is not an isometry. Because finite values of the N_i only provide an approximation of an isometry, the whole process must be repeated indefinitely in order to get closer and closer to an isometry. To ensure that each constructed embedding is strictly short, we consider, as in the Nash process, an increasing sequence g_k that converges to the flat metric $\mathrm{d}x \otimes \mathrm{d}x + \mathrm{d}y \otimes \mathrm{d}y$. In our process, the sequence $\mathcal{F}_k$ defined recursively by

$$\mathcal{F}_k := IC(\mathcal{F}_{k-1}, g_k, N_{k,1}, N_{k,2}, N_{k,3}),$$

will converge to an isometry. In order to iterate the process, we also need to ensure that the isometric default $D_k := g_{k+1} - \mathcal{F}_k^* \langle \cdot, \cdot \rangle_{\mathbb{R}^3}$ lies in the cone $\mathcal{C}$ (*cf.* point *ii)* below). Our construction eventually relies on the following result.

Theorem 11 (Stage Theorem)**.** *Let g and $\overline{g}$ be two Riemannian metrics on $\mathbb{T}^2$ and let*

$$f : (\mathbb{T}^2, g) \longrightarrow \mathbb{E}^3$$

be an immersion, such that

1. $\overline{g} - g \in C^\infty(\mathbb{T}^2, \mathcal{C})$
2. $g - f^* \langle \cdot, \cdot \rangle_{\mathbb{R}^3} \in C^\infty(\mathbb{T}^2, \mathcal{C})$

There exist integers N_1, N_2 and N_3 such that the immersion

$$\overline{f} := IC(f, g, N_1, N_2, N_3)$$

satisfies

i) $\overline{f}(0,0) = f(0,0)$

ii) $\overline{g} - \overline{f}^* \langle \cdot, \cdot \rangle_{\mathbb{R}^3} \in C^\infty(\mathbb{T}^2, \mathcal{C})$

iii) $\left\| g - \overline{f}^* \langle \cdot, \cdot \rangle_{\mathbb{R}^3} \right\|_\infty \leq \|\overline{g} - g\|_\infty$

iv) $\|d\overline{f} - df\|_\infty \leq 11 \ \|g - f^* \langle \cdot, \cdot \rangle_{\mathbb{R}^3}\|_\infty^{\frac{1}{2}}$.

Remark 1. The important point in the above assumptions 1 and 2 is that $\overline{g} - g$ and $g - f^* \langle \cdot, \cdot \rangle_{\mathbb{R}^3}$ lie in $\mathcal{C}$ at every point of $\mathbb{T}^2$.

Remark 2. We recall that for a linear operator L, $\|L\| = \sup_{X \neq 0} \frac{\|L(X)\|}{\|X\|}$ designates its induced Euclidean norm and that for a bilinear form B over $\mathbb{R}^2$, $\|B\| = \sqrt{\sum_{1 \leq i,j \leq 2} B_{ij}^2}$ designates the Frobenius norm of its matrix in the canonical basis. For metrics or differentials defined over $\mathbb{T}^2$, $\|.\|_\infty$ designates the supremum of the appropriate norm over all $p \in \mathbb{T}^2$.

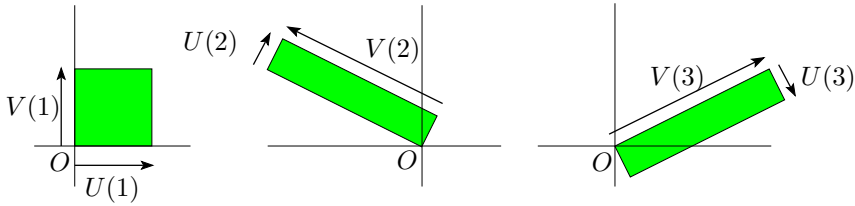

Figure 3.1: The fundamental domains for $\mathbb{E}^2/\mathbb{Z}^2$ spanned by the $(U(i), V(i))$'s.

The next section is devoted to the proof of the Stage Theorem. In Section 3.3, we will build a sequence of maps converging towards a C^1 isometric immersion of the square flat torus into the three dimensional Euclidean space.

3.2 Proof of the Stage Theorem

We build the required map $\overline{f}$ by applying to f three corrugations (that is three convex integrations) in directions depending on the ℓ_i's. We put

$$U(1) := \partial_x, \quad U(2) := \frac{1}{5}(\partial_x + 2\partial_y), \quad U(3) := \frac{1}{5}(\partial_x - 2\partial_y)$$

and

$$V(1) := \partial_y, \quad V(2) := -2\partial_x + \partial_y, \quad V(3) := 2\partial_x + \partial_y.$$

For every $i \in \{1, 2, 3\}$, the rectangle spanned by $V(i)$ and $U(i)$ is a fundamental domain for $\mathbb{R}^2/\mathbb{Z}^2$.

3.2.1 A Preliminary lemma

We will need the following lemma.

Lemma 12 (Preliminary lemma)**.** *Let $B := \rho_1\ell_1\otimes\ell_1 + \rho_2\ell_2\otimes\ell_2 + \rho_3\ell_3\otimes\ell_3$ be any symmetric bilinear form, then*

$$\begin{aligned} |\rho_1| &\leq \frac{\sqrt{17}}{4}\,\|B\| \\ |\rho_2| &\leq \frac{5\sqrt{3}}{8}\,\|B\| \\ |\rho_3| &\leq \frac{5\sqrt{3}}{8}\,\|B\|\,. \end{aligned}$$

In particular,

$$\max\{|\rho_1|, |\rho_2|, |\rho_3|\} \leq \frac{5\sqrt{3}}{8}\,\|B\|\,.$$

PROOF. The bilinear form B can be decomposed into

$$B = B_{xx}\mathrm{d}x \otimes \mathrm{d}x + B_{xy}(\mathrm{d}x \otimes \mathrm{d}y + \mathrm{d}y \otimes \mathrm{d}x) + B_{yy}\partial_y^* \otimes \partial_y^*$$

and a straightforward computation shows that

$$\rho_1 = B_{xx} - \frac{1}{4}B_{yy}, \quad \rho_2 = \frac{5}{4}(\frac{1}{2}B_{yy} + B_{xy}), \quad \rho_3 = \frac{5}{4}(\frac{1}{2}B_{yy} - B_{xy}).$$

Using the canonical scalar product in $\mathbb{R}^4$, this can also be written

$$\rho_1 = \left\langle \begin{pmatrix} 1 \\ 0 \\ 0 \\ -1/4 \end{pmatrix}, \begin{pmatrix} B_{xx} \\ B_{xy} \\ B_{xy} \\ B_{yy} \end{pmatrix} \right\rangle, \quad \rho_2 = \left\langle \begin{pmatrix} 0 \\ 5/8 \\ 5/8 \\ 5/8 \end{pmatrix}, \begin{pmatrix} B_{xx} \\ B_{xy} \\ B_{xy} \\ B_{yy} \end{pmatrix} \right\rangle$$

$$\text{and} \quad \rho_3 = \left\langle \begin{pmatrix} 0 \\ -5/8 \\ -5/8 \\ 5/8 \end{pmatrix}, \begin{pmatrix} B_{xx} \\ B_{xy} \\ B_{xy} \\ B_{yy} \end{pmatrix} \right\rangle.$$

It then remains to apply Schwarz's inequality to obtain the desired result. □

3.2.2 First corrugation

Let

$$D_1 := g - f^*\langle ., . \rangle_{\mathbb{E}^3}.$$

From Assumption 2 of the Stage Theorem, we know that $D_1 \in C^\infty(\mathbb{T}^2, \mathcal{C})$. In other words, there exist three positive functions $\rho_1(D_1)$, $\rho_2(D_1)$, $\rho_3(D_1)$ $\in C^\infty(\mathbb{T}^2, \mathbb{R}_+^*)$ such that

$$D_1 = \rho_1(D_1)\ell_1 \otimes \ell_1 + \rho_2(D_1)\ell_2 \otimes \ell_2 + \rho_3(D_1)\ell_3 \otimes \ell_3.$$

We define an auxiliary metric μ_1 by

$$\mu_1 := f^*\langle \cdot, \cdot \rangle_{\mathbb{R}^3} + \rho_1(D_1)\ell_1 \otimes \ell_1.$$

Our goal is to apply the One Step Theorem of chapter 2 to build a new map that is almost isometric for μ_1. Note that

$$f : (\mathbb{T}^2, \mu_1) \to \mathbb{E}^3$$

fulfills the assumptions of the One Step Theorem. For every $N_1 \in \mathbb{N}^*$ there therefore exists an immersion

$$f_1 : (\mathbb{T}^2, \mu_1) \to \mathbb{E}^3$$

obtained by a convex integration process in the direction

$$W_1 := U(1) + \zeta_1 V(1) \text{ with } \zeta_1 := -\frac{\langle V(1)\cdot f, U(1)\cdot f\rangle_{\mathbb{R}^3}}{\langle V(1)\cdot f, V(1)\cdot f\rangle_{\mathbb{R}^3}}$$

such that

$$\|f_1 - f\|_\infty = O(\frac{1}{N_1}), \quad \|df_1 - df\|_\infty = O(\frac{1}{N_1}) + \sqrt{7}\|\rho_1(D_1)\|_\infty^{\frac{1}{2}}$$

and

$$\|\mu_1 - f_1^*\langle\cdot,\cdot\rangle_{\mathbb{R}^3}\|_\infty = O(\frac{1}{N_1}).$$

Let

$$Err_1 = \mu_1 - f_1^*\langle\cdot,\cdot\rangle_{\mathbb{R}^3} \quad \text{and} \quad err_1 := \|Err_1\|_\infty$$

be the isometric default of f_1 with respect to μ_1. We consider the bilinear form

$$\mu_2 := f_1^*\langle\cdot,\cdot\rangle_{\mathbb{R}^3} + \rho_2(D_2)\ell_2\otimes\ell_2$$

where

$$D_2 := g - f_1^*\langle\cdot,\cdot\rangle_{\mathbb{R}^3}$$

and $\rho_2(D_2)$ is the second coefficient in the decomposition

$$D_2 = \rho_1(D_2)\ell_1\otimes\ell_1 + \rho_2(D_2)\ell_2\otimes\ell_2 + \rho_3(D_2)\ell_3\otimes\ell_3.$$

Lemma 13. *Let* $\rho_{\min}(D_1) := \min_{p\in\mathbb{T}^2}\{\rho_1(D_1)(p),\ \rho_2(D_1)(p),\ \rho_3(D_1)(p)\}$. *If*

$$err_1 < \frac{8}{5\sqrt{3}}\ \rho_{\min}(D_1)$$

then $\rho_2(D_2) : \mathbb{T}^2 \longrightarrow \mathbb{R}_+^*$. *In particular* μ_2 *is a metric on* $\mathbb{T}^2$.

Proof. From the above definition of D_1, Err_1 and D_2 we easily get

$$Err_1 = \rho_1(D_1)\ell_1\otimes\ell_1 - D_1 + D_2.$$

Whence,

$$Err_1 = \rho_1(D_2)\ell_1\otimes\ell_1 + (\rho_2(D_2) - \rho_2(D_1))\ell_2\otimes\ell_2 + (\rho_3(D_2) - \rho_3(D_1))\ell_3\otimes\ell_3.$$

From our Preliminary Lemma we deduce that

$$\|\rho_2(D_2) - \rho_2(D_1)\|_\infty \le \frac{5\sqrt{3}}{8} err_1. \tag{3.2}$$

In particular,

$$\rho_2(D_2) \ge \rho_2(D_1) - \frac{5\sqrt{3}}{8} err_1$$

and from the trivial minoration

$$\rho_2(D_1) \geq \rho_{\min}(D_1)$$

we conclude

$$\rho_2(D_2) \geq \rho_{\min}(D_1) - \frac{5\sqrt{3}}{8} err_1 > 0.$$

□

We retain from the proof the following equality.

$$Err_1 = \rho_1(D_2)\ell_1\otimes\ell_1+(\rho_2(D_2)-\rho_2(D_1))\ell_2\otimes\ell_2+(\rho_3(D_2)-\rho_3(D_1))\ell_3\otimes\ell_3. \quad (3.3)$$

3.2.3 Second corrugation

Choosing N_1 large enough to fulfill the hypothesis of Lemma 13, the map $f_1 : (\mathbb{T}^2, \mu_2) \to \mathbb{E}^3$ satisfies the assumption of the One Step Theorem. Thus, for every $N_2 \in \mathbb{N}^*$, there exists

$$f_2 : (\mathbb{T}^2, \mu_2) \to \mathbb{E}^3$$

obtained by a convex integration process in the direction

$$W_2 := U(2) + \zeta_2 V(2) \text{ with } \zeta_2 := -\frac{\langle V(2)\cdot f, U(2)\cdot f\rangle_{\mathbb{R}^3}}{\langle V(2)\cdot f, V(2)\cdot f\rangle_{\mathbb{R}^3}}$$

such that

$$\|f_2 - f_1\|_\infty = O(\frac{1}{N_2}), \quad \|df_2 - df_1\|_\infty = O(\frac{1}{N_2}) + \sqrt{7}\|\rho_2(D_2)\|_\infty^{\frac{1}{2}}$$

and

$$\|\mu_2 - f_2^*\langle\cdot,\cdot\rangle_{\mathbb{R}^3}\|_\infty = O(\frac{1}{N_2}).$$

We now consider the bilinear form

$$\mu_3 = f_2^*\langle\cdot,\cdot\rangle_{\mathbb{R}^3} + \rho_3(D_3)\ell_3\otimes\ell_3 \quad (3.4)$$

where

$$D_3 := g - f_2^*\langle\cdot,\cdot\rangle_{\mathbb{R}^3} \quad (3.5)$$

and $\rho_3(D_3)$ is the third coefficient in the decomposition of D_3. Let us put

$$Err_2 = \mu_2 - f_2^*\langle\cdot\,,\cdot\rangle_{\mathbb{E}^3} \quad \text{and} \quad err_2 = \|Err_2\|_\infty.$$

Lemma 14. *If*

$$err_1 + err_2 < \frac{8}{5\sqrt{3}}\,\rho_{\min}(D_1)$$

then $\rho_3(D_3) : \mathbb{T}^2 \longrightarrow \mathbb{R}_+^*$, *so that* μ_3 *is a metric on* $\mathbb{T}^2$.

Proof. As for Err_1, we easily check that

$$Err_2 = \rho_2(D_2)\ell_2 \otimes \ell_2 - D_2 + D_3.$$

Equivalently,

$$Err_2 = (\rho_1(D_3)-\rho_1(D_2))\ell_1\otimes\ell_1+\rho_2(D_3)\ell_2\otimes\ell_2+(\rho_3(D_3)-\rho_3(D_2))\ell_3\otimes\ell_3. \quad (3.6)$$

From our Preliminary Lemma applied to (3.6) and (3.3) we deduce that

$$\|\rho_3(D_3) - \rho_3(D_2)\|_\infty \leq \frac{5\sqrt{3}}{8} err_2 \text{ and } \|\rho_3(D_2) - \rho_3(D_1)\|_\infty \leq \frac{5\sqrt{3}}{8} err_1$$

and by the triangle inequality we obtain

$$\|\rho_3(D_3) - \rho_3(D_1)\|_\infty \leq \frac{5\sqrt{3}}{8}(err_1 + err_2). \quad (3.7)$$

Whence

$$\rho_3(D_3) \geq \rho_{\min}(D_1) - \frac{5\sqrt{3}}{8}(err_1 + err_2) > 0.$$

□

3.2.4 Third corrugation

Once again we choose N_2 large enough to fulfill the hypothesis of Lemma 14 and apply the One Step Theorem to $f_2 : (\mathbb{T}^2, \mu_3) \to \mathbb{E}^3$: for every $N_3 \in \mathbb{N}^*$ there exists

$$\overline{f} = f_3 : (\mathbb{T}^2, \mu_3) \to \mathbb{E}^3$$

obtained by a convex integration process in the direction

$$W_3 := U(3) + \zeta_3 V(3) \text{ with } \zeta_3 := -\frac{\langle V(3)\cdot f, U(3)\cdot f\rangle_{\mathbb{R}^3}}{\langle V(3)\cdot f, V(3)\cdot f\rangle_{\mathbb{R}^3}}$$

such that

$$\|f_3 - f_2\|_\infty = O(\frac{1}{N_3}), \quad \|df_3 - df_2\|_\infty = O(\frac{1}{N_3}) + \sqrt{7}\|\rho_3(D_3)\|_\infty^{\frac{1}{2}}$$

and

$$\|\mu_3 - f_3^*\langle\cdot,\cdot\rangle_{\mathbb{R}^3}\|_\infty = O(\frac{1}{N_3}).$$

Let

$$Err_3 := \mu_3 - f_3\,{}^*\langle\cdot,\cdot\rangle_{\mathbb{R}^3} \quad \text{and} \quad err_3 = \|Err_3\|_\infty. \quad (3.8)$$

In the following, we are going to show that $\overline{f} = f_3$ satisfies the conclusions i to iv of the theorem.

3.2.5 Controling the error

Lemma 15. *We have*

$$\|g - f_3^*\langle\cdot,\cdot\rangle_{\mathbb{R}^3}\|_\infty \leq 4(err_1 + err_2 + err_3).$$

Proof. We set $D_4 = g - f_3^*\langle\cdot,\cdot\rangle_{\mathbb{R}^3}$. From (3.8), (3.4) and (3.5), we get $Err_3 = \rho_3(D_3)\ell_3 \otimes \ell_3 - D_3 + D_4$. Analogous relations where obtained for Err_1, Err_2 in Lemmas 13 and 14, so that for $i = 1, 2, 3$:

$$Err_i = \rho_i(D_i)\ell_i \otimes \ell_i - D_i + D_{i+1}.$$

By summation, we get

$$\sum_{i=1}^{3} Err_i = \sum_{i=1}^{3} \rho_i(D_i)\ell_i \otimes \ell_i - D_1 + D_4.$$

It follows that

$$D_4 = Err_1 + Err_2 + Err_3 - \rho_2(D_2 - D_1)\ell_2 \otimes \ell_2 + \rho_3(D_3 - D_1)\ell_3 \otimes \ell_3$$

We already get the bounds (3.2) and (3.7):

$$\|\rho_2(D_2) - \rho_2(D_1)\|_\infty \leq \frac{5\sqrt{3}}{8} err_1, \quad \|\rho_3(D_3) - \rho_3(D_1)\|_\infty \leq \frac{5\sqrt{3}}{8}(err_1 + err_2).$$

Since $\|\ell_2 \otimes \ell_2\| = \|\ell_3 \otimes \ell_3\| = 1$, we obtain by the triangle inequality:

$$\|D_4\| \leq (1 + \frac{5\sqrt{3}}{4})err_1 + (1 + \frac{5\sqrt{3}}{8})err_2 + err_3 \leq 4(err_1 + err_2 + err_3). \quad (3.9)$$

□

Lemma 16. *If*

$$err_1 + err_2 + err_3 < \frac{2}{5\sqrt{3}}\ \rho_{\min}(\overline{g} - g) \qquad (C_3)$$

then $\overline{g} - f_3^*\langle\cdot,\cdot\rangle_{\mathbb{R}^3} \in C^\infty(\mathbb{T}^2, \mathcal{C})$.

Proof. Let

$$\Delta := \overline{g} - g, \quad D_4 := g - f_3^*\langle\cdot,\cdot\rangle_{\mathbb{R}^3} \quad \text{and} \quad D := \overline{g} - f_3^*\langle\cdot,\cdot\rangle_{\mathbb{R}^3}.$$

We have $D = \Delta + D_4$ and for every $i \in \{1, 2, 3\}$

$$\begin{array}{rcl} \rho_i(D) & = & \rho_i(\Delta) + \rho_i(D_4) \\ & > & \rho_{\min}(\Delta) + \rho_i(D_4). \end{array}$$

Thus, for every $i \in \{1,2,3\}$, the condition $|\rho_i(D_4)| < \rho_{\min}(\Delta)$ implies $\rho_i(D) > 0$. From the Preliminary Lemma we know that

$$\max\{\|\rho_1(D_4)\|_\infty, \|\rho_2(D_4)\|_\infty, \|\rho_3(D_4)\|_\infty\} \leq \frac{5\sqrt{3}}{8} \|D_4\|_\infty$$

and from Lemma 15

$$\|D_4\|_\infty \leq 4(err_1 + err_2 + err_3).$$

Hence, the condition $err_1 + err_2 + err_3 < \frac{2}{5\sqrt{3}} \rho_{\min}(\Delta)$ implies that $\|\rho_i(D_4)\|_\infty < \rho_{\min}(\Delta)$ for $i = 1,2,3$, implying in turn that $D \in C^\infty(\mathbb{T}^2, \mathcal{C})$. □

3.2.6 End of proof and choice of the N_i

Loop conditions *Let $c > 0$ and let e_1, e_2 and e_3 be three positive numbers such that*

$$\begin{aligned} e_1 + e_2 &< \tfrac{8}{5\sqrt{3}} \rho_{\min}(D_1) \\ e_1 + e_2 + e_3 &< \tfrac{2}{5\sqrt{3}} \rho_{\min}(\overline{g} - g). \end{aligned}$$

We choose the number N_i of corrugations of the i-th convex integration large enough so that

$$err_i \leq e_i \quad \textit{and} \quad \|df_i - df_{i-1}\|_\infty \leq (c + \sqrt{7}) \|\rho_i(D_i)\|_\infty^{\frac{1}{2}}, \tag{3.10}$$

where $f_0 := f$.

Such a choice of the N_i's is always possible since, as we recalled in Sections 3.2.2, 3.2.3 and 3.2.4:

$$err_i = O(\frac{1}{N_i}) \quad \text{and} \quad \|df_i - df_{i-1}\|_\infty \leq O(\frac{1}{N_i}) + \sqrt{7} \|\rho_i(D_i)\|_\infty^{\frac{1}{2}},$$

and $\rho_i(D_i) > 0$. Assuming that $g - f_0^* \langle \cdot, \cdot \rangle_{\mathbb{R}^3}$ lies in the cone $\mathcal{C}$, the loop conditions imply by Lemmas 13 and 14 that we can apply the three consecutive corrugations of Sections 3.2.2, 3.2.3 and 3.2.4 to obtain f_3. Lemma 16 further implies that $\overline{g} - f_3^* \langle \cdot, \cdot \rangle_{\mathbb{R}^3}$ lies in $\mathcal{C}$, which is point ii) of the Stage Theorem. Moreover,

$$\begin{aligned} \|g - f_3^* \langle \cdot, \cdot \rangle_{\mathbb{R}^3}\| &\leq 4(err_1 + err_2 + err_3) && \text{(by Lemma 15)} \\ &\leq \frac{8}{5\sqrt{3}} \rho_{\min}(\overline{g} - g) && \text{(by the choice of the } N_i\text{'s)} \\ &\leq \|\overline{g} - g\|_\infty && \text{(by the Preliminary Lemma)} \end{aligned}$$

which shows point *iii*). Note that point *i*) trivially follows from the convex integration formulas (2.9) and (2.14). It remains to prove point *iv*). By the triangle inequality,

$$\begin{aligned}\|df_3 - df_0\| &\leq \|df_3 - df_2\| + \|df_2 - df_1\| + \|df_1 - df_0\| \\ &\leq (c+\sqrt{7})\sum_{i=1}^{3}\|\rho_i(D_i)\|_\infty^{\frac{1}{2}}.\end{aligned}$$

Let us bound the three terms $\|\rho_i(D_i)\|_\infty$. Recalling from (3.2) and (3.7) that

$$\|\rho_2(D_2) - \rho_2(D_1)\|_\infty \leq \frac{5\sqrt{3}}{8} err_1 \quad \text{and}$$

$$\|\rho_3(D_3) - \rho_3(D_1)\|_\infty \leq \frac{5\sqrt{3}}{8}(err_1 + err_2),$$

it follows that

$$\|\rho_2(D_2)\|_\infty \leq \|\rho_2(D_1)\|_\infty + \frac{5\sqrt{3}}{8} err_1 \quad \text{and}$$

$$\|\rho_3(D_3)\|_\infty \leq \|\rho_3(D_1)\|_\infty + \frac{5\sqrt{3}}{8}(err_1 + err_2)$$

whence, by the loop conditions:

$$\|\rho_2(D_2)\|_\infty \leq \|\rho_2(D_1)\|_\infty + \rho_{\min}(D_1) \leq 2\max_i \|\rho_i(D_1)\|_\infty.$$

Likewise $\|\rho_3(D_3)\|_\infty \leq 2\max_i \|\rho_i(D_1)\|_\infty$. Applying the Preliminary Lemma to the decomposition of D_1 gives

$$\begin{aligned}\|\rho_1(D_1)\|_\infty &\leq \tfrac{5\sqrt{3}}{8}\|D_1\|_\infty \\ \|\rho_2(D_2)\|_\infty &\leq \tfrac{5\sqrt{3}}{4}\|D_1\|_\infty \\ \|\rho_3(D_3)\|_\infty &\leq \tfrac{5\sqrt{3}}{4}\|D_1\|_\infty.\end{aligned} \tag{3.11}$$

We finally get

$$\|df_3 - df_0\| \leq (c+\sqrt{7})(2\sqrt{2}+1)\sqrt{\frac{5\sqrt{3}}{8}}\|g - f_0^*\langle\cdot,\cdot\rangle_{\mathbb{R}^3}\|_\infty^{\frac{1}{2}}.$$

Since

$$\sqrt{7}(2\sqrt{2}+1)\sqrt{\frac{5\sqrt{3}}{8}} < 11$$

this concludes the proof of point *iv*) by choosing c small enough.

Remark 3. To minimize the N_i's and for numerical purposes, it may be interesting to choose a large value of c. The constant 11 of the theorem should be changed accordingly.

3.3 A sequence converging to an isometric immersion

Let $\mathcal{F}_0 : \mathbb{T}^2 \to \mathbb{E}^3$ be an immersion[1] such that

$$\Delta := \langle \cdot, \cdot \rangle_{\mathbb{R}^2} - \mathcal{F}_0^* \langle \cdot, \cdot \rangle_{\mathbb{R}^3} \in C^\infty(\mathbb{T}^2, \mathcal{C}),$$

and let $(\delta_k)_{k \in \mathbb{N}^*}$ be an increasing sequence of positive numbers converging to 1. We consider the increasing sequence of metrics $(g_k)_{k \in \mathbb{N}^*}$ converging towards the Euclidean metric $\langle \cdot, \cdot \rangle_{\mathbb{R}^2}$ and given by

$$g_k := \mathcal{F}_0^* \langle \cdot, \cdot \rangle_{\mathbb{R}^3} + \delta_k \Delta.$$

We then build a sequence of immersions

$$\mathcal{F}_k = IC(\mathcal{F}_{k-1}, g_k, N_{k,1}, N_{k,2}, N_{k,3}).$$

by repeatedly applying the Stage Theorem. At stage $k \in \mathbb{N}^*$, the initial immersion is $f := \mathcal{F}_{k-1}$ and we set $\underline{g} := g_k$ and $\overline{g} := g_{k+1}$. The resulting immersion of the Stage Theorem is $\overline{f} := \mathcal{F}_k$. Note that

$$\overline{g} - g = (\delta_{k+1} - \delta_k)\Delta \in C^\infty(\mathbb{T}^2, \mathcal{C})$$

as required in hypothesis 1 of the theorem. Hypothesis 2 holds inductively from conclusion *ii*) of the theorem.

Theorem 17. *If*

$$\sum \sqrt{\delta_k - \delta_{k-1}} < +\infty,$$

the sequence $(\mathcal{F}_k)_{k \in \mathbb{N}^*}$ *is* C^1*-converging towards a* C^1 *isometric immersion* $\mathcal{F}_\infty : \mathbb{E}^2/\mathbb{Z}^2 \to \mathbb{E}^3$.

Proof. To prove that the sequence $(\mathcal{F}_k)_{k \in \mathbb{N}^*}$ is C^1-converging, we check that it satisfies the Cauchy condition. Conclusion *iv*) of the Stage Theorem states that

$$\|d\mathcal{F}_k - d\mathcal{F}_{k-1}\|_\infty \leq 11 \, \|g_k - \mathcal{F}_{k-1}^* \langle \cdot, \cdot \rangle_{\mathbb{R}^3}\|_\infty^{\frac{1}{2}}.$$

For $k > 1$, we have

$$\|d\mathcal{F}_k - d\mathcal{F}_{k-1}\|_\infty \leq 11 \, \|g_k - g_{k-1}\|_\infty^{\frac{1}{2}} + 11 \, \|g_{k-1} - \mathcal{F}_{k-1}^* \langle \cdot, \cdot \rangle_{\mathbb{R}^3}\|_\infty^{\frac{1}{2}}$$

and from conclusion *iii*) we deduce

$$\|g_{k-1} - \mathcal{F}_{k-1}^* \langle \cdot, \cdot \rangle_{\mathbb{R}^3}\|_\infty^{\frac{1}{2}} \leq \|g_k - g_{k-1}\|_\infty^{\frac{1}{2}}$$

[1] For instance, a standard parametrisation of a torus of revolution (with a suitable choice of minor radius and major radius) satisfies the above condition.

and therefore

$$\begin{aligned} \|d\mathcal{F}_k - d\mathcal{F}_{k-1}\|_\infty &\leq 22\ \|g_k - g_{k-1}\|_\infty^{\frac{1}{2}} \\ &\leq 22\ \sqrt{\delta_k - \delta_{k-1}}\|\Delta\|_\infty^{\frac{1}{2}}. \end{aligned}$$

Since the series

$$\sum \sqrt{\delta_k - \delta_{k-1}}$$

converges and $\mathcal{F}_k(0,0) = \mathcal{F}_0(0,0)$ for all $k \in \mathbb{N}^*$, the sequence $(\mathcal{F}_k)_{k\in\mathbb{N}^*}$ is C^1 converging towards a C^1-map $\mathcal{F}_\infty$. By taking the limit in both sides of inequality *iii*) of the Stage Theorem

$$\|g_k - \mathcal{F}_k^*\langle\cdot,\cdot\rangle_{\mathbb{R}^3}\|_\infty \leq \|g_{k+1} - g_k\|_\infty$$

we obtain

$$\|\langle\cdot,\cdot\rangle_{\mathbb{R}^2} - \mathcal{F}_\infty^*\langle\cdot,\cdot\rangle_{\mathbb{R}^3}\|_\infty = 0$$

i.e. $\mathcal{F}_\infty$ is a C^1-isometry. □

Remark 4. Suppose that the starting immersion $\mathcal{F}_0$ is an embedding. Since each corrugation is a normal deformation, the above process will produce a sequence of embeddings provided the $N_{k,i}$ are chosen sufficiently large. Unfortunately, we do not have any practical criterion to perform such a choice of the $N_{k,i}$. Nevertheless, as far as we can observe numerically, the maps resulting from our building process are embedded.

Chapter 4

Implementation

In this chapter, we provide details about our C++ implementation of the convex integration process. Our main goal is to produce a computer image or a 3D printing of the flat torus in the three dimensional space. As our flat torus is the result of a limit process, and since there is no closed formula for the limit, we actually compute an approximation of the limit. In practice, applying four successive corrugations to an initial (non-isometric) embedding of the torus seems to give visually satisfying results as discussed in Section 4.8. The first section describes the way continuous maps are encoded as discrete grids in the computer. In Section 4.2, we explain how to compute the flow of the vector field needed for each corrugation. The actual convex integration computation is described in Sections 4.3 and 4.4. We finally explain in Section 4.6 how to choose the main parameter of the process, i.e. the number of oscillations.

Here, we fix some notations. As described in Section 3.3, our flat torus isometric immersion is the limit of the sequence defined recursively by

$$\mathcal{F}_k = IC(\mathcal{F}_{k-1}, g_k, N_{k,1}, N_{k,2}, N_{k,3}).$$

The immersion $\mathcal{F}_k$ is itself obtained after three corrugations as discussed in Sections 3.2.2, 3.2.3 and 3.2.4. We denote by $f_{k,1}$, $f_{k,2}$, $f_{k,3}$ the corresponding three corrugated maps. In other words $f_{k,j}$ is the map at step k that is denoted f_j in Sections 3.2.2, 3.2.3 and 3.2.4. In particular, we have $f_{k,3} = \mathcal{F}_k$.

4.1 Immersion encoding

Our first concern is to represent the successive immersions in order to perform numerical computations. Since the convex integration process resorts to integrals and does not provide a closed formula for each immersion

$f := f_{k,j}$, we must discretize f in some way in order to obtain a finite representation. We choose to sample $\mathbb{T}^2$ with an $n \times n$ regular square grid whose boundaries are pairwise identified. The choice of the parameter n is discussed in Section 4.6. The grid node $p^{i,j} := (i/n, j/n)$, $0 \leq i, j < n$, thus points to the three coordinates of the sample $f^{i,j} := f(p^{i,j})$. On the one hand, we remark that the convex integration process relies on the computation of flows and integrals that only depend upon the map f and its first order derivatives. On the other hand, the best up to date numerical schemata for solving differential equations or for computing integrals need to evaluate the corresponding vector field or integrand at non grid points [25]. In order to provide those values at non grid points we interpolate the $n \times n$ grid representing f with a C^1 piecewise bicubic surface based on cubic Hermite splines[1]. This is a C^1 map $\hat{f} : \mathbb{T}^2 \to \mathbb{R}^3$ that is bicubic over each grid cell $P^{i,j} := [p^{i,j}, p^{i+1,j}, p^{i+1,j+1}, p^{i,j+1}]$ and such that $\hat{f}(p^{i,j}) = f^{i,j}$. We evaluate $\hat{f}$ at a non grid point inside $P^{i,j}$ as follows. We first estimate the partial derivatives $\frac{\partial f}{\partial x}(p^{i,j})$ and $\frac{\partial f}{\partial y}(p^{i,j})$ using finite differences of order 4. We respectively denote $f_x^{i,j}$ and $f_y^{i,j}$ these estimates up to the scaling factor n. Formally, we set

$$f_x^{i,j} := \frac{1}{12}(f^{i-2,j} - 8f^{i-1,j} + 8f^{i+1,j} - f^{i+2,j}) \tag{4.1}$$

$$f_y^{i,j} := \frac{1}{12}(f^{i,j-2} - 8f^{i,j-1} + 8f^{i,j+1} - f^{i,j+2}). \tag{4.2}$$

We also estimate the cross partial derivative $\frac{\partial^2 f}{\partial x \partial y}(p^{i,j})$ by applying finite differences of order 4 to the partial derivative estimates. We denote by $f_{xy}^{i,j} = f_{yx}^{i,j}$ the estimated cross partial derivative up to the scaling factor n^2:

$$f_{xy}^{i,j} := \frac{1}{12}(f_x^{i,j-2} - 8f_x^{i,j-1} + 8f_x^{i,j+1} - f_x^{i,j+2}) \tag{4.3}$$

$$:= \frac{1}{12}(f_y^{i-2,j} - 8f_y^{i-1,j} + 8f_y^{i+1,j} - f_y^{i+2,j}) = f_{yx}^{i,j}. \tag{4.4}$$

Let

$$h_0(t) := (1+2t)(1-t)^2, \quad h_1(t) := t^2(3-2t),$$
$$h_2(t) := t(1-t)^2, \quad h_3(t) := t^2(t-1)$$

be the Hermite basis functions. We finally define our interpolating bicubic surface at a parameter point (x, y) included in the grid cell $P^{i,j}$ by (see Fig. 4.1):

[1] We have also tried to use a bilinear interpolating surface. This only leads to a C^0 surface and appeared to be insufficient for the computation of the flow as the solver code was failing to integrate it correctly. Interpolating surfaces with C^2 or even higher degree of continuity can also be used but implies heavier computations and did not seem to be necessary for our purposes.

func F	$F(0)$	$F(1)$	$F'(0)$	$F'(1)$
h_0	1	0	0	0
h_1	0	1	0	0
h_2	0	0	1	0
h_3	0	0	0	1

Table 4.1: The following table lists the values and derivatives of the Hermite basis functions at the parameters 0 and 1. Here, F is a generic name for any of those functions.

$$\hat{f}(x,y) \quad := \quad \sum_{k=0}^{3}\sum_{\ell=0}^{3} q_{k\ell} h_k(x_i) h_\ell(y_j), \tag{4.5}$$

where $(x_i, y_j) := (nx - i, ny - j)$ are the *local* coordinates of (x, y) in $P^{i,j}$ and

$$q_{k\ell} = \begin{cases} f^{i+k,j+\ell}, & 0 \le k, \ell \le 1 \\ f_x^{i+k-2,j+\ell}, & 2 \le k \le 3, 0 \le \ell \le 1 \\ f_y^{i+k,j+\ell-2}, & 0 \le k \le 1, 2 \le \ell \le 3 \\ f_{xy}^{i+k-2,j+\ell-2}, & 2 \le k, \ell \le 3. \end{cases}$$

On the other hand, with the help of Table 4.1 we easily compute from (4.5):

$$q_{k\ell} = \begin{cases} \hat{f}(p^{i+k,j+\ell}), & 0 \le k, \ell \le 1 \\ \dfrac{1}{n}\dfrac{\partial \hat{f}}{\partial x}(p^{i+k-2,j+\ell}), & 2 \le k \le 3, 0 \le \ell \le 1 \\ \dfrac{1}{n}\dfrac{\partial \hat{f}}{\partial y}(p^{i+k,j+\ell-2}), & 0 \le k \le 1, 2 \le \ell \le 3 \\ \dfrac{1}{n^2}\dfrac{\partial^2 \hat{f}}{\partial x \partial y}(p^{i+k-2,j+\ell-2}), & 2 \le k, \ell \le 3. \end{cases}$$

Equating the two above expressions for the *control parameters* $q_{k\ell}$, the function $\hat{f}$ appears as the unique piecewise bicubic function whose values, partial and cross derivatives at the points p_{ij} are fixed by the estimates $f^{ij}, f_x^{ij}, f_y^{ij}$ and f_{xy}^{ij}. With the help of the above Table 4.1, the continuity of $\hat{f}$ and of its partial and cross derivatives $\frac{\partial \hat{f}}{\partial x}$, $\frac{\partial \hat{f}}{\partial y}$ and $\frac{\partial^2 \hat{f}}{\partial x \partial y}$ along grid edges can be checked easily.

For instance, let us denote by $q_{k\ell}$ and $q'_{k\ell}$ the control parameters of $\hat{f}$ on $P^{i,j}$ and $P^{i,j-1}$ respectively. For a parameter point $(x, j/n)$ on the edge $[p^{i,j}, p^{i+1,j}]$, we obtain

$$\hat{f}(x, j/n) = \sum_{0 \le k,\ell \le 3} q_{k\ell} h_k(x_i) h_\ell(0) = \sum_{0 \le k \le 3} q_{k0} h_k(x_i)$$

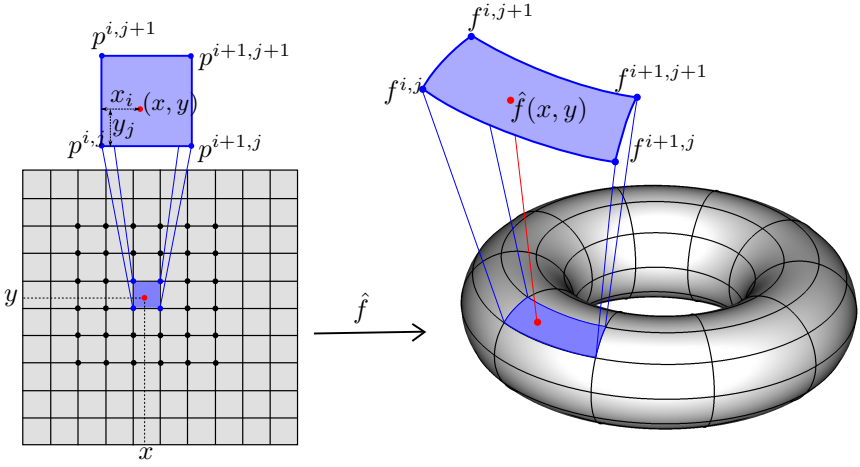

Figure 4.1: Interpolation of f at the (red) parameter point (x, y). The plain dots on the left grid indicate the samples involved in the computation of $\hat{f}(x, y)$.

considering that $(x, j/n)$ belongs to the bottom edge ($y_j = 0$) of the grid cell $P^{i,j}$, or

$$\hat{f}(x, j/n) = \sum_{0 \le k,\ell \le 3} q'_{k\ell} h_k(x_i) h_\ell(1) = \sum_{0 \le k \le 3} q'_{k1} h_k(x_i)$$

considering that $(x, j/n)$ belongs to the top edge ($y_j = 1$) of $P^{i,j-1}$. These two values indeed coincides because $q'_{k,1} = q_{k,0} = f^{i+k,j}$. The remaining continuity conditions can be checked in the same way. In particular $\hat{f}$ has continuous partial derivatives $\frac{\partial \hat{f}}{\partial x}$ and $\frac{\partial \hat{f}}{\partial y}$, whence $\hat{f}$ is of class C^1 over $\mathbb{T}^2$. We can now formally derive $\hat{f}$ to provide an estimate of the (first order) derivatives of f. In the computer program, $\hat{f}$ and its first order derivatives are indeed explicitly used in place of f and its first order derivatives. Figure 4.2 shows the effect of the interpolation on a sampled torus. Although the interpolating surface $\hat{f}$ is not C^2 in general, it is C^1 with continuous cross derivatives and appeared to be well suited for our computations.

4.2 Vector field and flow computation

At each substep (k, j), the quantities F, r, α, W, φ, ζ, μ of Section 2.3.2 are denoted $F_{k,j}$, $r_{k,j}$, $\alpha_{k,j}$, $W_{k,j}$, $\varphi_{k,j}$, $\zeta_{k,j}$ and $\mu_{k,j}$ respectively. We use the obvious circular convention $f_{k,0} := f_{k-1,3}$. Recall from Sections 2.3

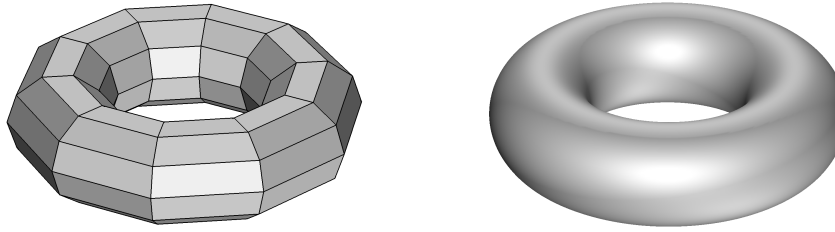

a **b**

Figure 4.2: **a,** The standard torus sampled with a 10×10 grid. **b,** Bicubic interpolation of the previous grid.

and 3.2 that the computation of $f_{k,j}$ from $f_{k,j-1}$ relies on the flow of the vector field

$$W_{k,j} = U(j) + \zeta_{k,j} V(j) \quad \text{with} \quad \zeta_{k,j} = -\frac{\langle U(j) \cdot f_{k,j-1}, V(j) \cdot f_{k,j-1} \rangle_{\mathbb{R}^3}}{\langle V(j) \cdot f_{k,j-1}, V(j) \cdot f_{k,j-1} \rangle_{\mathbb{R}^3}},$$

where $U(j)$ and $V(j)$ are the constant vector fields defined in Section 3.2:

$$U(1) := \partial_x, \quad U(2) := \frac{1}{5}(\partial_x + 2\partial_y), \quad U(3) := \frac{1}{5}(\partial_x - 2\partial_y)$$

and

$$V(1) := \partial_y, \quad V(2) := -2\partial_x + \partial_y, \quad V(3) := 2\partial_x + \partial_y.$$

The computation of $W_{k,j}$, in particular of $\zeta_{k,j}$, involves the first order derivatives of $f_{k,j-1}$, whose evaluation was described in Section 4.1. The next step is to compute the integral curves $\varphi_{k,j}(t, \cdot)$ of $W_{k,j}$ with initial condition $\varphi_{k,j}(t, 0) = O + tV(j)$. We use Hairer's solver based on DOPRI5 for non-stiff differential equations [25]. This is an explicit Runge-Kutta method of order 5 with adaptive step size. The non-stiffness of our ordinary differential equation relies on the eigenvalues 0 and $V(j) \cdot \zeta_{k,j}$ of the Jacobian matrix of $W_{k,j}$. Though we did not evaluate those eigenvalues, Hairer's code is able to detect when the equation becomes stiff, which did not happened in our case. For each $i = 0 \dots n-1$ we thus call Hairer's code to solve the first order ordinary differential equation:

$$\phi'(s) = W_{k,j}(\phi(s)) \quad \text{with} \quad \phi(0) = O + \frac{i}{n} V(j).$$

In practice, we use Hairer's solver to compute $\varphi_{k,j}(i/n, j/n) = \phi(j/n)$ for $0 \leq j < n$. These values are stored in a $n \times n$ table whose (i, j) entry contains $\varphi_{k,j}(i/n, j/n)$. Figure 4.3 shows the integral curves up to the fourth corrugation. Those were computed on a $10,000^2$ grid. Only 100 of the $10,000$ integral curves are shown at each step.

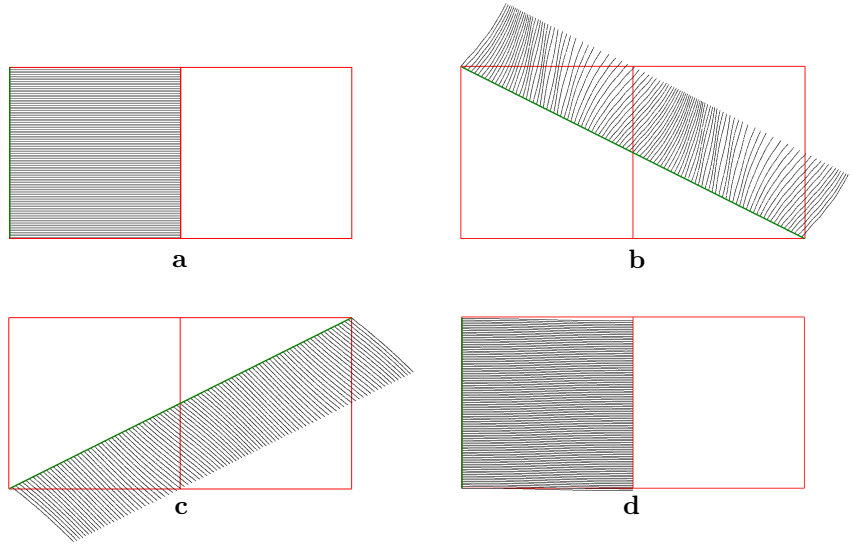

Figure 4.3: **Integral curves of $W_{k,j}$.** In each subfigure two squares of the integer grid are shown (in red). These are fundamental domains of the action of $\mathbb{Z}^2$ on $\mathbb{R}^2$. **a,** The usual parametrization of the standard torus exhibits orthogonal partial derivatives. The corresponding vector field $W_{11} = V(1)$ is thus constant and horizontal; its integral curves are horizontal lines. **b,** For the second corrugation, the initial point of each integral curve lies on the line with direction $V(2)$ through the origin. **c,** As we apply more corrugations, the embeddings get closer to an isometry. As a consequence, the vector field $W_{1,3}$ gets closer to the constant field $V(3)$ and its integral lines are straighter, though not yet orthogonal to $V(3)$. **d,** For the fourth corrugation, W_{11} is almost constant and horizontal.

4.3 Corrugation along flow curves

We are now ready to apply convex integration. From Equation (2.9) in Section 2.3, we start with the following map $F_{k,j}$ defined over the cylinder $\mathbb{R}/\mathbb{Z} \times [0,1]$:

$$F_{k,j} \circ \varphi_{k,j}(t,s) := f_{k,j-1}(O + tV(j)) + \int_{u=0}^{s} h(t,u,\{N_{k,j}u\})\mathrm{d}u, \quad (4.6)$$

with

$$\begin{aligned} h(t,s,u) &= \bar{h}(\varphi_{k,j}(t,s), \cos(2\pi u)), \quad \text{where} \\ \bar{h}(p,c) &= r_{k,j}(p)\big(\cos(\alpha_{k,j}(p)c)\mathbf{t}_{k,j-1}(p) + \sin(\alpha_{k,j}(p)c)\mathbf{n}_{k,j-1}(p)\big) \quad (4.7) \end{aligned}$$

and

$$r_{k,j} := \sqrt{\mu_{k,j}(W_{k,j}, W_{k,j})}, \qquad \mathbf{t}_{k,j-1} := \frac{W_{k,j}\cdot f_{k,j-1}}{\|W_{k,j}\cdot f_{k,j-1}\|},$$
$$\mathbf{n}_{k,j-1} := \frac{W_{k,j}\cdot f_{k,j-1}\wedge V(j)\cdot f_{k,j-1}}{\|W_{k,j}\cdot f_{k,j-1}\wedge V(j)\cdot f_{k,j-1}\|} \quad \text{and} \quad \alpha_{k,j} = J_0^{-1}(\frac{\|W_{k,j}\cdot f_{k,j-1}\|}{r_{k,j}}).$$

The metric $\mu_{k,j}$ corresponds to the auxiliary metric μ_j at step k as defined in Sections 3.2.2 and 3.2.3:

$$\mu_{k,j} = f_{k,j-1}^*\langle\cdot,\cdot\rangle_{\mathbb{R}^3} + \rho_j(D_{k,j})\ell_j \otimes \ell_j$$

where

$$\begin{aligned} D_{k,j} &:= g_k - f_{k,j-1}^*\langle\cdot,\cdot\rangle_{\mathbb{R}^3} \\ &= \rho_1(D_{k,j})\ell_1\otimes\ell_1 + \rho_2(D_{k,j})\ell_2\otimes\ell_2 + \rho_3(D_{k,j})\ell_3\otimes\ell_3, \end{aligned}$$

$$g_k := (1-\delta_k)\mathcal{F}_0^*\langle\cdot,\cdot\rangle_{\mathbb{R}^3} + \delta_k\langle\cdot,\cdot\rangle_{\mathbb{R}^2}$$

and

$$\delta_k = 1 - e^{-k/10}.$$

In practice, all the metrics are expressed as 2 by 2 matrices in the canonical basis. In particular, the coefficients of the pullback metric $f_{k,j-1}^*\langle\cdot,\cdot\rangle_{\mathbb{R}^3}$ are scalar products of the two partial derivatives of $f_{k,j-1}$. Note also that it is a matter of simple linear algebra to determine the coefficient $\rho_j(D_{k,j})$ in the decomposition of $D_{k,j}$. In order to compute the integral in (4.6) we use the same Hairer's code as for the flow computation. Indeed, for a fixed t, Equation (4.6) can be viewed as the solution of the differential equation

$$y'(u) = h(t, u, \{N_{k,j}u\}) \quad \text{with initial condition} \quad y(0) = f_{k,j-1}(O{+}tV(j)).$$

We solve this equation for the sampled values $t = i/n$, $0 \le i < n$. For each such t, we compute the solution $F_{k,j}\circ\varphi_{k,j}(t,u) = y(u)$ at the sampled values $u = j/n$, $0 \le j \le n$. We experienced a more accurate computation with Hairer's code than with the basic trapezoidal rule for calculating integrals. In the end we obtain a $n \times (n+1)$ table whose (i,j) entry contains $F_{k,j}\circ\varphi_{k,j}(i/n, j/n)$. It remains to glue the two boundaries of this immersion of the cylinder to get an immersion of the torus. As given by Equation (2.14) in the Section 2.3.2, we finally set

$$f_{k,j}\circ\varphi_{k,j}(\frac{i}{n},\frac{j}{n}) = F_{k,j}\circ\varphi_{k,j}(\frac{i}{n},\frac{j}{n}) - w(\frac{j}{n})\Big(F_{k,j}\circ\varphi_{k,j}(\frac{i}{n},1) - f_{k,j-1}\circ\varphi_{k,j}(\frac{i}{n},1)\Big)$$

where $w : [0,1] \to [0,1]$ is a smooth S-shaped function satisfying

$$w(0) = 0, \quad w(1) = 1, \quad \text{and} \quad \forall k \in \mathbb{N}^* : w^{(k)}(0) = w^{(k)}(1) = 0.$$

In practice, we have approximated w by the polynomial function

$$x^3(6x^2 - 15x + 10).$$

Though it only satisfies the above condition for $k = 1, 2$, we could not detect perceivable differences when considering higher degree polynomials. One reason is that we have performed only four convex integration steps. The other reason is that we have observed a very small gap $F_{k,j} \circ \varphi_{k,j}(\frac{i}{n}, 1) - f_{k,j-1} \circ \varphi_{k,j}(\frac{i}{n}, 1)$ in accordance with the C^0-density lemma 2 of the first part. In the next section we describe how to extract $f_{k,j}$ from $f_{k,j} \circ \varphi_{k,j}$.

4.4 Back to the Euclidean coordinates

The above computations yield a uniform sampling of $f_{k,j} \circ \varphi_{k,j}$. In order to iterate the process, that is to compute $f_{k,j+1}$ from $f_{k,j}$, we need to extract a uniform sampling of $f_{k,j}$. Said differently, knowing $f_{k,j}$ at the sample points $\varphi_{k,j}(i/n, j/n)$, $0 \leq i, j \leq n$, we want to evaluate $f_{k,j}$ at the grid points $p^{i,j} = (i/n, j/n)$. Since n is pretty large in practice we can hardly afford a superlinear time algorithm. Hopefully, the specificity of $\varphi_{k,j}$ allows us to design a linear time algorithm. As we observed in the first chapter, at Equation (2.6), we can write

$$\varphi_{k,j}(t, s) = O + sU(j) + \psi_{k,j}(t, s)V(j)$$

for some function $\psi_{k,j}$ such that $\psi_{k,j}(t, 0) = t$. It follows that for a fixed s, the set
$\{\varphi_{k,j}(t, s) \mid t \in \mathbb{R}/\mathbb{Z}\}$ is included in the line $L_s : x \to O + sU(j) + xV(j)$ that is parallel to $V(j)$. Since $V(j)$ has integer and relatively prime coordinates and since $|U(j) \times V(j)| = 1$, the lines $L_{u/n}$, for $u \in \mathbb{Z}$, sweep both the regular grid points and the points $(\varphi_{k,j}(u/n, v/n))_{u,v \in \mathbb{Z}}$ (see Fig 4.4). In order to evaluate $f_{k,j}$ at the regular grid points, for each integer $u \in [0, n-1]$, we sweep the set of sample points

$$\{q_v := \varphi_{k,j}(u/n, v/n) \mid v \in [0, n]\} \subset L_{u/n}.$$

Between any two consecutive points q_v and q_{v+1} in this set, we may encounter grid points $p^{i,j}$ of the form

$$p^{i,j} = (1 - t)q_v + tq_{v+1}$$

with $t \in [0, 1)$. We then approximate $f_{k,j}(p^{i,j})$ by the convex combination

$$(1 - t) \cdot f_{k,j} \circ \varphi_{k,j}(\frac{u}{n}, \frac{v}{n}) + t \cdot f_{k,j} \circ \varphi_{k,j}(\frac{u}{n}, \frac{v+1}{n}).$$

This simple one-dimensional interpolation appeared quite accurate in practice.

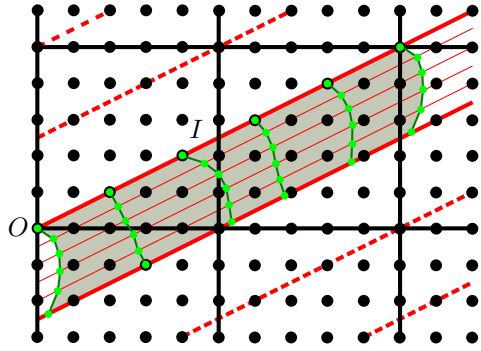

Figure 4.4: The flat torus is uniformly sampled by a regular 5×5 grid ($n = 5$). The gray shaded region is a fundamental domain bounded by two copies of the initial condition (thick red) line I and two copies of the integral curve $(\varphi_{k,j}(0,\cdot)$. Every point of the torus has a representative of its $\mathbb{Z}^2$-class in this domain. The integral curves are shown as (green) sampled curves. Every regular (black dot) sample of the domain lies in-between two (green) samples on the integral curves on some (red) line $L_{u/5}$.

4.5 The choice of $\mathcal{F}_0$

According to our convex integration process in Section 3.3, we must choose $\mathcal{F}_0$ such that $D_{1,1} := g_1 - \mathcal{F}_0^* \langle \cdot, \cdot \rangle_{\mathbb{R}^3}$ is interior to the positive cone $\mathcal{C}$ spanned by $\ell_1 \otimes \ell_1$, $\ell_2 \otimes \ell_2$ and $\ell_3 \otimes \ell_3$, where

$$\ell_1 := \mathrm{d}x, \quad \ell_2 := \frac{1}{\sqrt{5}}(\mathrm{d}x + 2\mathrm{d}y) \quad \text{and} \quad \ell_3 := \frac{1}{\sqrt{5}}(\mathrm{d}x - 2\mathrm{d}y).$$

Since $D_{1,1} = \delta_1(\langle \cdot, \cdot \rangle_{\mathbb{R}^2} - \mathcal{F}_0^* \langle \cdot, \cdot \rangle_{\mathbb{R}^3})$, this is equivalent to require that $\langle \cdot, \cdot \rangle_{\mathbb{R}^2} - \mathcal{F}_0^* \langle \cdot, \cdot \rangle_{\mathbb{R}^3}$ lies in this cone. (In particular, $\mathcal{F}_0 : (\mathbb{T}^2, \langle \cdot, \cdot \rangle_{\mathbb{R}^2}) \to \mathbb{E}^3$ should be a strictly short immersion.) We choose for $\mathcal{F}_0$ the standard torus

$$\begin{cases} X(x,y) = \dfrac{1}{2\pi}(r_2 + r_1 \cos 2\pi x) \cos 2\pi y \\ \\ Y(x,y) = \dfrac{1}{2\pi}(r_2 + r_1 \cos 2\pi x) \sin 2\pi y \\ \\ Z(x,y) = \dfrac{r_1}{2\pi} \sin 2\pi x \end{cases}$$

with minor and major radii r_1 and r_2 respectively. The matrix of $\mathcal{F}_0^* \langle \cdot, \cdot \rangle_{\mathbb{R}^3}$ in the canonical basis is given by

$$\begin{pmatrix} r_1^2 & 0 \\ 0 & (r_2 + r_1 \cos 2\pi x)^2 \end{pmatrix}.$$

It is easily checked that the above requirement is satisfied if and only if $r_1 + r_2 < 1$. In practice, we have chosen $r_1 = 1/5$ and $r_2 = 1/2$. Figure 4.5 shows the range of $\mathcal{F}_0^*\langle\cdot,\cdot\rangle_{\mathbb{R}^3}$ in the cone of metrics $Q_+ = \{\begin{pmatrix} E & F \\ F & G \end{pmatrix} \mid EG - F^2 > 0, E > 0, G > 0\}$ and in the cone $\mathcal{C}$.

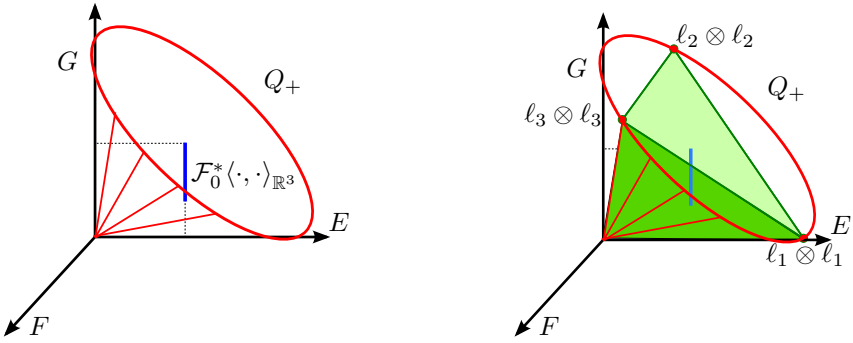

Figure 4.5: (Left) Range of $\mathcal{F}_0^*\langle\cdot,\cdot\rangle_{\mathbb{R}^3}$ in the cone Q_+. (Right) The cone $\mathcal{C}$ spanned by the primitive metrics $\ell_1 \otimes \ell_1$, $\ell_2 \otimes \ell_2$ and $\ell_3 \otimes \ell_3$.

4.6 The choice of the $N_{k,j}$'s and of the grid size

It remains to choose the appropriate oscillation number $N_{k,j}$ appearing in the formula (4.6). Here, appropriate means that the preliminary conditions of the Stage Theorem 11 should be satisfied by $f_{k,j}$ in order to apply the next convex integration. According to the Loop conditions of Section 3.2.6, in order to select an appropriate $N_{k,j}$, it suffices to satisfy the conditions:

$$\|\mu_{k,j} - f_{k,j}^*\langle\cdot,\cdot\rangle_{\mathbb{R}^3}\|_\infty \leq e_j \qquad (C_j)$$

where e_1, e_2, e_3 are positive numbers chosen so that

$$\begin{aligned} e_1 + e_2 &< \tfrac{8}{5\sqrt{3}}\,\rho_{\min}(g_k - f_{k-1,3}^*\langle\cdot,\cdot\rangle_{\mathbb{R}^3}) \\ e_1 + e_2 + e_3 &< \tfrac{2(1-e^{-\frac{1}{10}})}{5\sqrt{3}} e^{-\frac{k}{10}} \rho_{\min}(\langle\cdot,\cdot\rangle_{\mathbb{R}^2} - \mathcal{F}_0^*\langle\cdot,\cdot\rangle_{\mathbb{R}^3}), \end{aligned}$$

and the conditions

$$\|df_{k,j} - df_{k,j-1}\|_\infty \leq (c + \sqrt{7})\sqrt{\|\rho_j(D_{k,j})\|_\infty} \qquad (C'_j)$$

where $c > 0$ is a constant chosen arbitrarily. Here, $\mu_{k,j}$ and $\rho_j(D_{k,j})$ are defined as in Section 4.3 and $\rho_{\min}(\cdot)$ is the minimum over $\mathbb{T}^2$ of the

components of a bilinear form on the basis $(\ell_1 \otimes \ell_1, \ell_2 \otimes \ell_2, \ell_3 \otimes \ell_3)$, as defined in Lemma 13. In practice we can choose all the e_i equal to

$$0.99 \min\left(\frac{4}{5\sqrt{3}}\,\rho_{\min}(g_k - f^*_{k-1,3}\langle\cdot,\cdot\rangle_{\mathbb{R}^3}), \frac{2(1-e^{-\frac{1}{10}})}{15\sqrt{3}} e^{-\frac{k}{10}} \rho_{\min}(\langle\cdot,\cdot\rangle_{\mathbb{R}^2} - \mathcal{F}^*_0\langle\cdot,\cdot\rangle_{\mathbb{R}^3})\right.$$

Since we are computing a finite number of terms in the sequence $(f_{k,j})$ we can assume that c is large enough so that the Loop conditions (C'_j) are always satisfied for the computed $f_{k,j}$. We then select $N_{k,j}$ by an exponential search, starting from $N = 2N_{k,j-1}$. We plug this N into Equation (4.6) and check if the resulting $f_{k,j}$ satisfies the above conditions (C_j). If not, we simply double N until the conditions are satisfied. We finally obtain the least N satisfying the conditions by dichotomy and set $N_{k,j}$ to this N. Unfortunately, $N_{k,j}$ is increasing very fast with k and j so that it is practically impossible to implement this method. Indeed, the integral in (4.6) involves a function that oscillates $N_{k,j}$ times and it seems reasonable to require at least 10 samples per period. This implies that the regular grid that represents $f_{k,j}$ should contain approximately $n \times n$ samples with $n \geq 10N_{k,j}$. As explained below in the paragraph on the local computation, we experimentally found for the first four corrugations:

$$N_{1,1} = 611, \quad N_{1,2} = 69,311, \quad N_{1,3} = 20,914,595, \quad N_{2,1} = 6,572,411,478.$$

These values would imply that we use a grid with $(10 \times 6,572,411,478)^2 \approx 4.3\,10^{19}$ vertices! This is way above the capacity of the present computers. Since the Loop conditions are sufficient but not necessary, we have tried smaller values for the $N_{k,j}$'s. We also tried different values for the sequence δ_k. After several tentatives we could only perform three corrugations, starting from the initial standard embedding $\mathcal{F}_0$ of Section 4.5. However, it was desirable to apply four corrugations in order to give the feeling of a limit surface. We have overcome this technicality by first applying a corrugation to this $\mathcal{F}_0$ with $N_{1,1} = 12$ then *resetting* $\mathcal{F}_0$ to the resulting immersion. We were able this way to reduce the four first oscillation numbers to respectively

$$12, \quad 80, \quad 500, \quad 9000.$$

We have used a grid of size $10,000^2$ for the first three corrugations. For the last corrugation, we have refined the grid ten times in the direction ∂_y of integration and only twice in the direction ∂_x, leading to a grid with 2 billion samples. The following table summarizes the results.

k	j	$N_{k,j}$	$\sup \|I - f^*_{k,j}\langle\cdot,\cdot\rangle_{\mathbb{R}^3}\|$	ave$(\|I - f^*_{k,j}\langle\cdot,\cdot\rangle_{\mathbb{R}^3}\|)$	grid size
0	-	-	1.32	1.21	10^8
0	1	12	1.20	1.05	10^8
1	2	80	0.99	0.84	10^8
1	3	500	0.91	0.63	10^8
1	1	9000	0.75	0.25	2.10^9

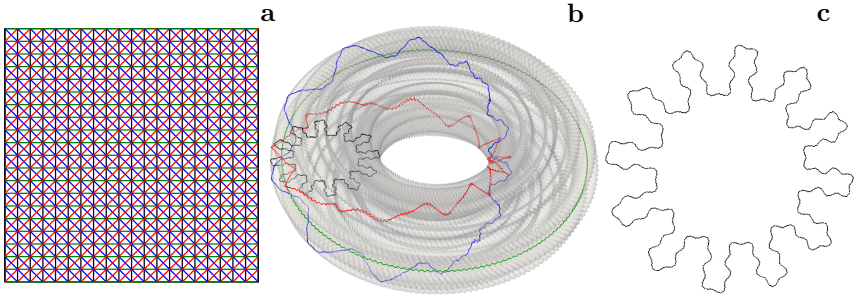

Figure 4.6: **Comparison of lengths in the parameter and image domain.** **a**, A fundamental domain of the flat torus with four nets of meridians, parallels, main diagonals and skew diagonals, each composed of 20 curves. **b**, The images by $f_{1,1}$ of four curves, one taken in each net. **c**, A closer look at the curves evinces a fractal geometry, though the limit curves are C^1 regular.

The first row corresponds to the standard embedding $\mathcal{F}_0$. The fourth and fifth columns indicate respectively the computed maximum and the average of the isometric default with respect to the Euclidean metric $I = \langle \cdot, \cdot \rangle_{\mathbb{R}^2}$. Keeping the index j to agree with the direction of integration, the sequence of computed immersions becomes

$$\mathcal{F}_0, \quad f_{0,1}, \quad f_{1,2}, \quad f_{1,3}, \quad f_{1,1}.$$

We also illustrate the metric improvement by comparing the lengths of a collection of curves on the flat torus (Fig. 4.6**a**) with the lengths of their images by the last immersion $f_{1,1}$. The length of any curve in the collection differs by at most 10.2% with the length of its $f_{1,1}$ image. By contrast, the deviation reaches 80% when the standard torus $\mathcal{F}_0$ is taken in place of $f_{1,1}$. The situation is even better, since we actually decreased the isometric default with respect to $g_1 = (1-\delta_1)\mathcal{F}_0^* \langle \cdot, \cdot \rangle_{\mathbb{R}^3} + \delta_1 \langle \cdot, \cdot \rangle_{\mathbb{R}^2}$ with $\delta_1 = 0.8$ rather than the Euclidean metric I. A simple computation shows that

$$0.217 < \|I - g_1\| < 0.244$$

to be compared with the average value 0.25 of $\|I - f_{1,1}^* \langle \cdot, \cdot \rangle_{\mathbb{R}^3}\|$). Figure 4.7 shows a local view of the successive corrugations.

Local computation. Independently of the production of images, it is interesting to evaluate the rate of growth of the $N_{k,j}$'s. A precise control of this rate could yield a lower bound on the Hölder exponent in the $C^{1,\alpha}$ continuity of the limit isometric embedding [12]. In order to compute a lower bound for the $N_{k,j}$'s we have implemented a local version of the

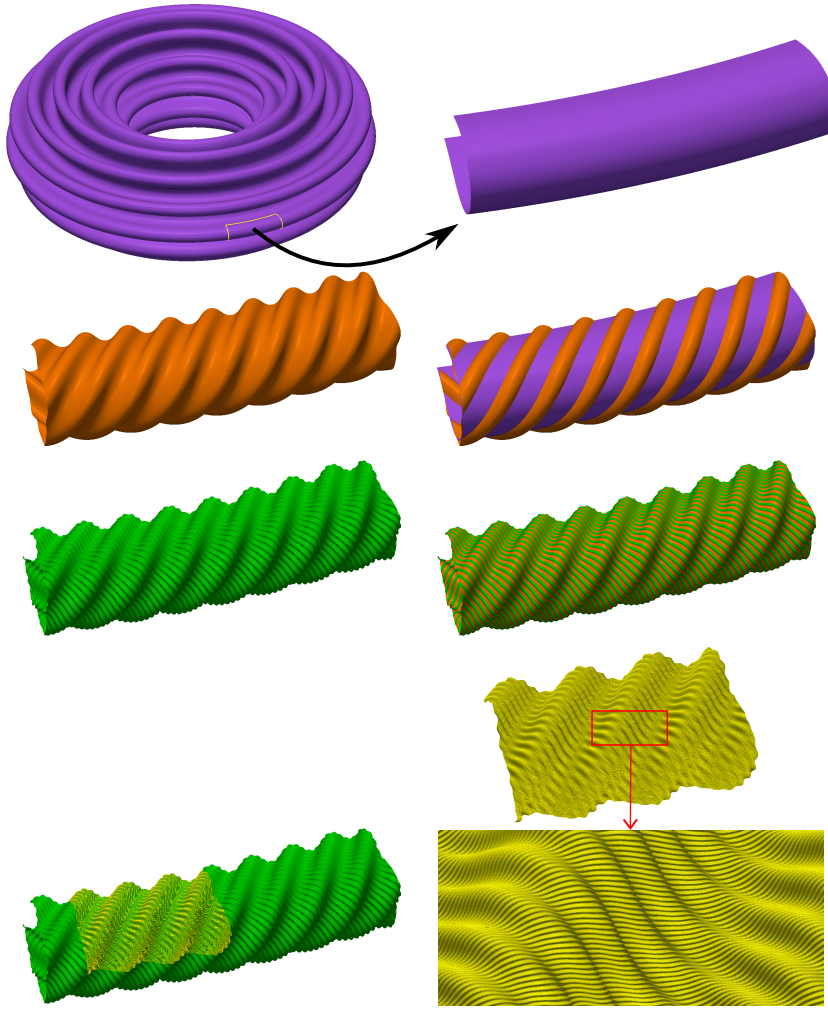

Figure 4.7: **Top**, Rendered view of $f_{0,1}$. **Second row**, Local view of $f_{1,2}$ and overlay with $f_{0,1}$. **Third row**, Local view of $f_{1,3}$ and overlay with $f_{1,2}$. **Bottom row**, Local view of $f_{1,1}$ overlaid with $f_{1,2}$ and zoom in of $f_{1,1}$.

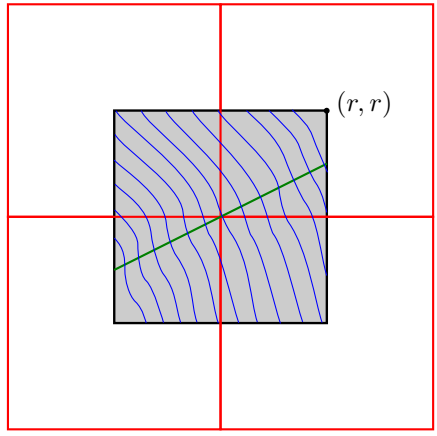

Figure 4.8: **Local computation of an isometric embedding.** Schematic view of the (blue) flow lines in the central neighborhood $\mathcal{N}_r$. The (green) slanted line represents the set of initial conditions for the flow lines. The outer (red) square represents four tiles of the integer grid. Each tile is a fundamental domain of $\mathbb{T}^2$.

isometric immersion program. In the local version of the program, the grid of sampled parameters represents a square neighborhood $\mathcal{N}_r = [-r, r]^2$ of the parameter point $(0, 0) \in \mathbb{T}^2$. The function $\mathcal{F}_0$ is now restricted to $\mathcal{N}_r$. We apply the convex integration process to this restriction. We have to slightly modify the process since the integral curves are restricted to a small domain and do not join back the initial condition line. In particular, there is no more gluing on the boundaries. We thus extend the flow lines on both sides of the initial conditions as on Figure 4.8. As we apply more corrugations we restrict the grid to a smaller neighborhood $\mathcal{N}_{r'<r}$ and resample it so as to keep always the same number of samples. We choose the half-width r' inversely proportional to $N_{k,j}$ in order to keep constant the number of samples per period of integration. We were able to apply more than 160 corrugations (See Fig. 4.9). In agreement with De Conti *et al.*[12], we observe that the oscillation numbers $N_{k,j}$ grow at least exponentially. It should be noted that the half-width r of the neighborhood decreases drastically; after 165 corrugations r drops to 10^{-300}. In order to preserve accuracy we apply an appropriate scaling of the domain *and* the codomain of $f_{k,j}$. In practice, we only take into account the condition (C_j) to select $N_{k,j}$. For this reason, and also because the domain is eventually shrinking to a point, the computed $N_{k,j}$ are probably much smaller than they should be. Computation were performed on a 64 bits processor using double precision (64-bit) binary floating-point numbers. Figure 4.10 shows

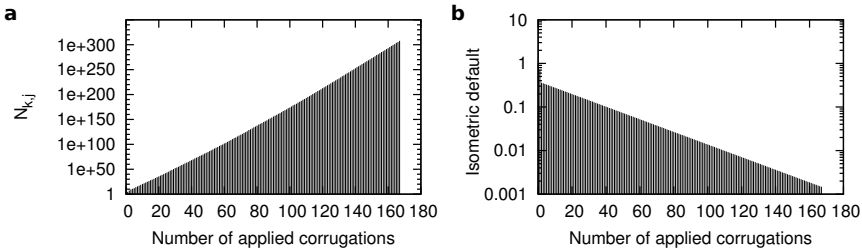

Figure 4.9: **Exponential growth of the oscillation numbers. a**, Numerical estimate of the corrugation frequencies plotted on a logarithmic scale. **b**, The isometric default of $f_{k,j}$ was measured as the maximum of the Frobenius norm of $\langle\cdot,\cdot\rangle_{\mathbb{R}^2} - f_{k,j}^*\langle\cdot,\cdot\rangle_{\mathbb{R}^3}$ over the appropriate square neighborhood.

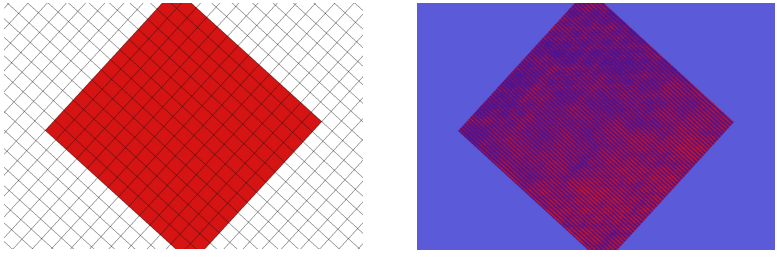

Figure 4.10: **Left**, The image of the grid mesh on $\mathbb{T}^2$ by $f_{36,3}$ looks virtually flat and isometric to the regular planar mesh at this scale. The half-width of the domain of $f_{36,3}$ is 9.34×10^{-219}. The (red) range of $f_{37,1}$ also looks flat. **Right**, The overlay of $f_{36,3}$ (blue) and $f_{37,1}$ (red) emphasizes the oscillations of $f_{37,1}$.

the overlay of $f_{36,3}$ after 118 corrugations with $f_{37,1}$. Since the domain of $f_{37,1}$ is (128 times) smaller than the domain of $f_{36,3}$, only a small part of this last domain is visible.

4.7 From Immersion to Embedding

It should be noted that the whole convex integration process applies to embeddings as well as to immersions. In theory we could thus claim to construct an isometric embedding rather than an isometric immersion. However, we do not have a numerical condition, similar to the Loop conditions, that would tell if $N_{k,j}$ is large enough to obtain an embedding $f_{k,j}$. In practice, checking that $f_{k,j}$ is an embedding would require a large

amount of computation for testing self-intersections. Although we did not perform such tests, our pictures clearly show that we did in effect obtain embeddings after four convex integrations. As further corrugations would not be visible, we can claim that our pictures show an isometric embedding of the flat torus. Indeed, we can assume to choose sufficiently big $N_{k,j}$'s for those remaining corrugations in order to get an embedding in the limit.

4.8 Rendering

We describe the final rendering stage to obtain the first images of an embedded flat torus. In the previous chapter, we have described the algorithm that produces the meshes associated to the immersions

$$\mathcal{F}_0, \quad f_{0,1}, \quad f_{1,2}, \quad f_{1,3}, \quad f_{1,1}.$$

For the first three corrugations, we found that a grid of size $10,000^2$ was enough to provide an accurate description of the immersions. However, for the fourth corrugation, the number of oscillations is very large (9000) and we had to use a grid of size 2 billions (20.10^8). Due to computer limitations, the most popular ray tracer softwares cannot deal with such a large grid. In fact, two problems arise:

- Ray tracer softwares require a large amount of memory (RAM). To give an example, the rendering of a surface parametrized over a grid of size $10,000^2$ consumes about 40 GB of RAM with the software Yafaray [4]. As the RAM needed by the software is roughly proportional to the number of vertices of the grid, the rendering of a grid of size 2 billions of points requires about 800 GB of RAM.

- The rendering computation is time consuming. For example, the software Sunflow [3] takes about one week to render a grid of size $10,000^2$ on a computer with 48 GB of RAM.

To cope with those limitations we had to cut the mesh into several small patches, and to produce an image for each patch separately. In a second step, we have combined the images of each patch to get an image of the whole surface.

There exist alternative methods to produce an image of the fourth corrugation directly from the mesh of the third corrugation. We can use the mesh of the third corrugation and render it by simulating the wrinkles of the fourth corrugation. This can be achieved by perturbing the normal vector to the third corrugation during lighting calculations. However, although those methods are much quicker, they have to be compared in any case to the rendering of the fourth corrugation. In practice, they work well if the fourth corrugation is small enough.

In Section 4.8.1, we recall the bases of ray-tracing. The merging step is described in Section 4.8.2. Section 4.8.3 provides some details on the computations.

4.8.1 Ray tracing and numerical images

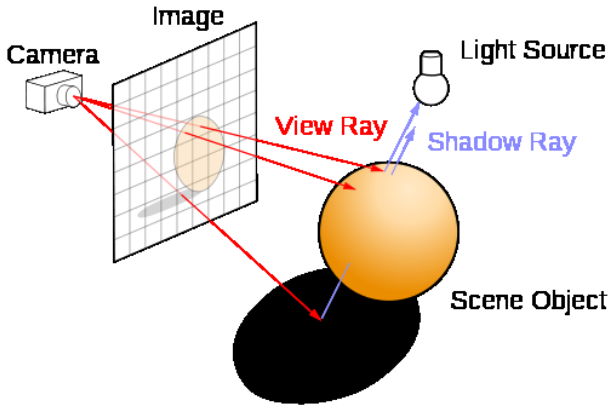

Figure 4.11: Ray-tracing. Image taken from wikipedia

A numerical image is composed of $n \times m$ pixels, where n is the width and m is the height of the image. A pixel is the smallest picture element and corresponds to a small monochromatic square or rectangle of the image. The ray-tracing is a technique that allows to create a numerical image from a scene that is composed of a camera, one or more objects, and one or more lights, as illustrated in Figure 4.11. It traces the reverse path of the light from the camera through any pixels of the image so as to calculate its color.

The ray from the camera to a pixel may encounter several objects. The *depth* of a pixel encodes how far is the first visible object along this ray. These depths are recorded into a bidimensional array called the *z-buffer*. If another object of the scene must be rendered in the same pixel, the graphics card compares the two depths and chooses the one closer to the observer. In Yafaray, the z-buffer is stored as a black and white image with 256 different values. In general, this z-buffer is not sufficiently accurate to compare pixels that have similar depths.

The aliasing refers to artifacts due to the discrete nature of the numerical image. For example, a slanted line will look like stairs if we just color the pixels intersecting this line. The anti-aliasing refers to techniques that allow to remove these artifacts, by slightly modifying the image. In Yafaray, the anti-aliasing essentially consists in a local averaging of the colors.

4.8.2 How to combine images

Our huge mesh is divided into long strip patches. We first render each strip as illustrated on Figure 4.13. The pixel width and height, the position of the camera, the lights, and all the rendering parameters are common to all the images. Once we have computed all these images, we need to combine them in order to create an image of the whole surface. The process is iterative. We explain how to combine two images A and B into an image C. We denote by $x_{i,j}$ the pixels of an image X. Again, we assume that A, B and C have the same dimensions (height and width). We denote by $\mathcal{M}_A$ and $\mathcal{M}_B$ the meshes associated to A and B respectively.

For each pixel $c_{i,j}$ of C, we need to select either the color of $a_{i,j}$ or the color of $b_{i,j}$. We choose the pixel that corresponds to an object which is closer to the camera. This choice relies on the z-buffer. We already noticed that the Yafaray z-buffer is not accurate for this purpose. There is in fact another issue. Although the anti-aliasing improves the rendering of the image, it creates artifacts on the boundary of the strips when we combine two images. More precisely, before any anti-aliasing, there is a color discontinuity in image A at the boundary of the rendered strip $\mathcal{M}_A$, passing from the interior of $\mathcal{M}_A$ to the background of the scene. The anti-aliasing will thus sensibly modify the pixel colors nearby this boundary. The same is true in image B for the boundary that is common to $\mathcal{M}_A$ and $\mathcal{M}_B$. The exact color of this boundary is lost in both images and a simple merge of A and B will not give the same result as rendering $\mathcal{M}_A \cup \mathcal{M}_B$. Unfortunately, we cannot simply remove the anti-aliasing process, as other numerous artifacts would appear. We bypass this anti-aliasing problem by considering larger strips that overlap. However, this creates another artifacts: for a pixel $c_{i,j}$ corresponding to the intersection of two strips, the two pixels $a_{i,j}$ and $b_{i,j}$ have the same depth and we don't know which pixel to select. If we choose randomly, we still have artifacts (see Figure 4.12) due to the fact that the light diffusion and shades are not the same in the two images. If we look more carefully at the images, we notice that the boundary of each strip is more exposed to the light. To overcome this problem, we pick the darker when two pixels have the same depth.

In practice, the previous tricks remove the local artifacts. However, we can still have global problems due to the shade. Suppose that the mesh $\mathcal{M}_A$ falls on the trajectory of the light between a light source and the mesh $\mathcal{M}_B$. In this case, the rendering of $\mathcal{M}_B$ alone in image B is lighter than it should be in a rendering of $\mathcal{M}_A \cup \mathcal{M}_B$. To overcome this problem, we put a large light above the center of the torus. Thanks to this choice, a triangle of a strip is in the shade of the global mesh if and only if it is in the shade of its strip. Therefore, there is no discontinuity of the light due to the global shade.

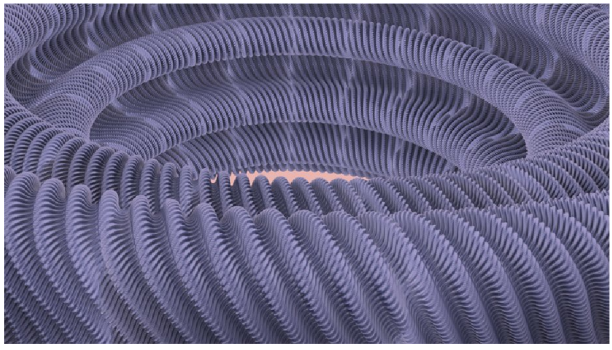

Figure 4.12: Combination of strip images: the pixels corresponding to two overlapping strips are chosen randomly among the two individually rendered strips. We notice many lighter pixels in each such overlapping region.

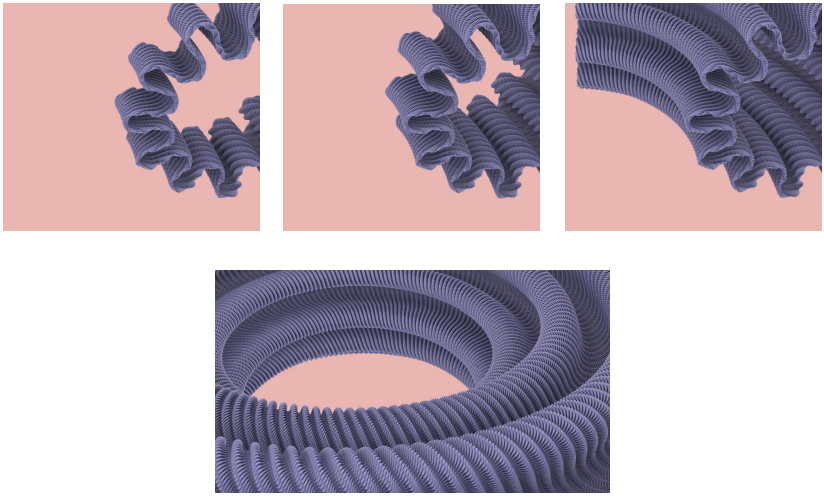

Figure 4.13: A rendered flat torus obtained by combining 33 different strip images. Each individual strip is rendered with Yafaray using a mesh with 10^8 vertices. Top raw, from left to right: the first strip alone, the combination of two strips and the combination of 8 strips.

4.8.3 Computer calculations

We have tested several popular ray-tracer softwares, such as PovRay [2], Sunflow [3] and Yafaray [4]. We opted for the β-version Yafaray.0.1.X (DarkTide-YafaRay-e45bb16) for the following reasons: we found its rendering quite aesthetic, the rendering time was reasonable, and most impor-

tantly, this β-version was the only one to provide the z-buffer information.

As already mentioned, the z-buffer computed by Yafaray is not accurate enough for our purpose. Moreover, the z-buffer computed by Yafaray is rescaled so that the range of depths of a rendered image fits to the interval $[0, 256]$. This scaling obviously depends on the maximal depth of the image and is different for each rendered strip. We thus had to modify the Yafaray software to take this scaling into account.

Furthermore, the images computed by this non stable version of Yafaray have many artifacts including pixels with wrong colors. Most of them are either white, or black. Some have a different color, but are hopefully very localised. The z-buffer exhibits similar artifacts. By smoothing simultaneously the z-buffer and the colors of the image, we were able to remove these artifacts. This smoothing was useful to get a nice image for each strip and also necessary for the combination of the strip images.

We used a $10,000^2$ grid mesh for the three first corrugations. For the fourth corrugation, we considered 33 grids of size $1,000 * 100,000$ with an overlap of size $400 * 100,000$ between consecutive strips. The rendering of each strip was performed on a 8-core CPU with 48 GB of RAM with the C++ parallelised Yafaray code and took about one hour and a half. Two hours were needed to generate the 33 strip meshes and the combination of their rendered images took a few minutes. Adding the time for the rendering of the 33 strips (33 times one hour and a half), the final rendering of the whole square flat torus thus took about two days. We could hardly apply more than four corrugations to the standard torus, but hopefully it appeared to be sufficient to get a good picture of the limit surface as further corrugations would not be visible to the naked eye.

4.8.4 3D printing

Since our embedding is encoded as a three dimensional mesh, it is possible to take advantage of the existing 3D printing devices to obtain a solid representation of an embedded flat torus. Due to the resolution of those devices (about 0.1 mm), we had to limit the printing to the first three corrugations. We used the printing facilities of an academic FABrication LABoratory [1] to get a torus with diameter 250 mm as shown on the following pictures.

Figure 4.14: 3D printing (left column) and computer renderings (right column) of the map $f_{1,3}$ output by our algorithm.

Chapter 5

Gauss map of the flat torus and convex integration

In chapter 3, we built a sequence of immersions that C^1-converges to a C^1-isometric immersion

$$\mathcal{F}_\infty : \mathbb{T}^2 \to \mathbb{E}^3,$$

where each element of the sequence is obtained by a convex integration process. In this chapter, we show that the Gauss map $\mathbf{n}_\infty$ of $\mathcal{F}_\infty$ can be approximated by an infinite product of rotation matrices. This behavior is reminiscent of a Riesz product that is known to have a fractal structure. The *Corrugation Theorem*, which captures the Riesz-like structure of the Gauss map, is stated in Section 5.2.

5.1 One dimensional case

In this section, we apply the iterative process of convex integrations as summarized in Section 3.3 for the case of a torus to the simpler case of a centrally symmetric immersion of the circle into the plane. Replacing the torus by a circle not only simplifies the computations, it actually allows to give an explicit formula for the limit immersion. Moreover, in this simple case the relationship of the normal map with a Riesz product is direct and manifest. A more thorough analysis of this special case can be found in [9].

5.1.1 Corrugation Theorem on $\mathbb{S}^1$

Similarly to the torus case, we thus build a sequence of immersions $f_k : \mathbb{S}^1 = \mathbb{E}/\mathbb{Z} \to \mathbb{E}^2$ that C^1-converges to a C^1-isometry $f_\infty : \mathbb{S}^1 \to \mathbb{E}^2$. Let $f_0 : \mathbb{S}^1 \to \mathbb{E}^2$ be a strictly short immersion of the circle, i.e., for every $x \in \mathbb{S}^1 : \|f_0'(x)\| < 1$. We further assume to simplify the calculations that f_0 is *radially symmetric*, i.e., satisfies:

$$\forall\, x \in \mathbb{S}^1, \quad f_0'(x + \frac{1}{2}) = -f_0'(x).$$

We consider a sequence $(\delta_k)_{k\in\mathbb{N}^*}$ of strictly positive numbers, strictly increasing towards 1. For every k, we then set the metric

$$g_k := f_0^* \langle \cdot, \cdot \rangle_{\mathbb{R}^2} + \delta_k \Delta,$$

where $\Delta := \langle \cdot, \cdot \rangle_{\mathbb{R}} - f_0^* \langle \cdot, \cdot \rangle_{\mathbb{R}^2}$. Trivially, $g_k \uparrow \langle \cdot, \cdot \rangle_{\mathbb{R}}$.

We define $f_k : [0, 1] \to \mathbb{E}^2 \simeq \mathbb{C}$ iteratively by:

$$f_k(x) := f_{k-1}(0) + \int_0^x r_k \left(c_k(s)\mathbf{t}_{k-1}(s) + s_k(s)\mathbf{n}_{k-1}(s) \right) \mathrm{d}s$$

where

$$\mathbf{t}_{k-1} := \frac{f_{k-1}'}{\|f_{k-1}'\|}, \quad \mathbf{n}_{k-1} := i\mathbf{t}_{k-1},$$

$$c_k(s) := \cos(\alpha_k(s) \cos 2\pi N_k s), \quad s_k(s) := \sin(\alpha_k(s) \cos 2\pi N_k s),$$

$$\alpha_k = J_0^{-1} \left(\frac{\|f_{k-1}'\|}{r_k} \right), \quad r_k = g_k(\partial_x, \partial_x)$$

and $(N_k)_{k\in\mathbb{N}^*}$ is a sequence of even numbers. Note that the functions r_k (and hence the functions α_k) are constant if $x \mapsto \|f_0'(x)\| < 1$ is constant. In any case, the limit of r_k is the constant function equal to 1. Since $0 < \frac{\|f_{k-1}'\|}{r_k} < 1$ we also have,

$$\forall x \in \mathbb{S}^1, \quad 0 < \alpha_k(x) < z$$

where $z \simeq 2.4$ is the first zero of J_0.

It is easy to check [9] that, for every $k \in \mathbb{N}^*$, the map f_k is well-defined on $\mathbb{S}^1$ and radially symmetric. Moreover, it can be shown that

$$\|f_k' - f_{k-1}'\|_\infty \leq C^{te} \sqrt{\delta_k - \delta_{k-1}}.$$

Hence, $(f_k)_{k\in\mathbb{N}}$ is C^1-converging if the increasing sequence $(\delta_k)_{k\in\mathbb{N}}$ is chosen so that
$\sum \sqrt{\delta_k - \delta_{k-1}} < +\infty$. Moreover, since

$$\forall\, x \in \mathbb{S}^1, \quad \|f_k'(x)\| = r_k(x)$$

the limit map f_∞ is parametrized by arc-length, and therefore is isometric.

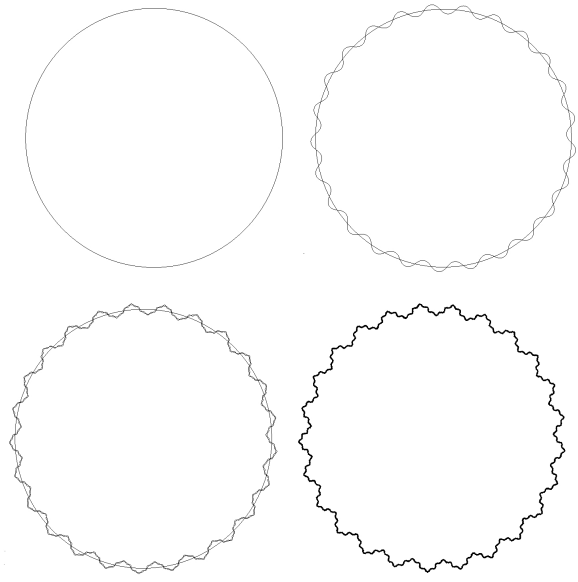

Figure 5.1: Example of a sequence of maps (f_0, f_1, f_2 and f_∞) with an exponential growth of the N_k's.

Theorem 18 (Corrugation Theorem on $\mathbb{S}^1$)**.** *The Gauss map* $\mathbf{n}_k$ *of* f_k *is given by*

$$\forall x \in \mathbb{S}^1, \quad \mathbf{n}_k(x) = \left(\prod_{j=1}^{k} e^{i\alpha_j(x)\cos 2\pi N_j x} \right) \mathbf{n}_0(x)$$

where $\mathbf{n}_0$ *is the Gauss map of* f_0*.*

Proof. We have

$$\mathbf{t}_k = c_k \mathbf{t}_{k-1} + s_k \mathbf{n}_{k-1}.$$

Therefore, by identifying $\mathbb{E}^2 \simeq \mathbb{C}$, we obtain

$$\mathbf{n}_k = i\mathbf{t}_k = i(c_k \mathbf{t}_{k-1} + s_k \mathbf{n}_{k-1}) = (c_k + is_k)\mathbf{n}_{k-1},$$

which allows to conclude. □

5.1.2 C^1 fractal structure

As an immediate application of the Corrugation Theorem on $\mathbb{S}^1$ we deduce a formal expression of the normal map of the limit map f_∞.

Corollary 19 (Riesz structure of the normal map)**.** *The normal map* $\mathbf{n}_\infty$ *of* f_∞ *is given by*

$$\forall x \in \mathbb{S}^1, \quad \mathbf{n}_\infty(x) = e^{iA_\infty(x)}\mathbf{n}_0(x) \quad \textit{with} \quad A_\infty(x) = \sum_{j=1}^{\infty} \alpha_j(x) \cos 2\pi N_j x.$$

This corollary puts into light some resemblance of $\mathbf{n}_\infty$ with a *Riesz product*, that is, an infinite product

$$p(x) := \prod_{j=1}^{\infty} (1 + \alpha_j \cos(2\pi N_j x)),$$

where $(\alpha_j)_{j\in\mathbb{N}}$ is a sequence of real numbers such that for every $j \in \mathbb{N}^*$, $|\alpha_j| \leq 1$, and

$$\forall j \in \mathbb{N}^*, \quad \frac{N_{j+1}}{N_j} \geq 3 + q$$

for some fixed $q > 0$. In particular, if

$$p(x) = 1 + \sum_{\nu=1}^{\infty} \gamma_\nu \cos(2\pi\nu x)$$

is the Fourier expansion of p, then $\gamma_{N_j} = \alpha_j$ and $\gamma_\nu = 0$ if ν is not of the form $N_{j_1} \pm N_{j_2} \pm ... \pm N_{j_k}$, $j_1 > j_2 > ... > j_k$ [33]. Riesz products are well known to have a fractal structure. Precisely, their Riesz measures $p(x)dx$ have a fractional Hausdorff dimension [32].

Informally, we say that the curve $f_\infty : \mathbb{S}^1 \longrightarrow \mathbb{E}^2$ has a C^1 *fractal structure* as it is both a primitive of $-i\mathbf{n}_\infty$ and of class C^1. An interesting case of a C^1 fractal structure occurs when

$$A_\infty(x) = \sum_j a^j \cos(2\pi b^j x)$$

for some positive numbers a, b with $a < 1$ and $ab > 1$. Indeed, in that case, A_∞ is the well-known Weierstrass function. Although its exact value is conjectural, the Hausdorff dimension of its graph is strictly larger than one [15]. It follows that the Hausdorff dimension of the graph of $\mathbf{n}_\infty$ is also strictly larger than one.

5.2 Riesz-like structure of the Gauss map of the flat torus

Recall that the C^1 isometric immersion of the flat torus $\mathcal{F}_\infty : \mathbb{T}^2 \to \mathbb{E}^3$ described in Part 3 is obtained as the limit of a sequence

$$\mathcal{F}_0; \quad f_{1,1}, f_{1,2}, f_{1,3}; \quad f_{2,1}, f_{2,2}, f_{2,3}; \quad f_{3,1}, f_{3,2}, f_{3,3}; \quad ...$$

In this section, we first show that there is a natural orthonormal basis $(v^{\perp}_{k,j+1}, v_{k,j+1}, \mathbf{n}_{k,j+1})$ that comes with each map $f_{k,j}$ of this sequence. We then state a theorem (the Corrugation Theorem) giving a description of the rotation matrix that maps $(v^{\perp}_{k,j}, v_{k,j}, \mathbf{n}_{k,j})$ to $(v^{\perp}_{k,j+1}, v_{k,j+1}, \mathbf{n}_{k,j+1})$. From this theorem, we deduce an expression of the Gauss map $\mathbf{n}_\infty$ of $\mathcal{F}_\infty$ showing its formal resemblance with a Riesz product.

5.2.1 The Corrugation Theorem

In this section, we use the notations of Sections 4.2 and 4.3. In particular, we set

$$\mathbf{t}_{k,j} := \frac{W_{k,j+1} \cdot f_{k,j}}{\|W_{k,j+1} \cdot f_{k,j}\|} \quad \text{and} \quad \mathbf{n}_{k,j} := \frac{W_{k,j+1} \cdot f_{k,j} \wedge V(j+1) \cdot f_{k,j}}{\|W_{k,j+1} \cdot f_{k,j} \wedge V(j+1) \cdot f_{k,j}\|}.$$

Let $p \in \mathbb{T}^2$. We consider the orthonormal basis $(v^{\perp}_{k,j}, v_{k,j}, \mathbf{n}_{k,j})(p)$ given by

$$v_{k,j} := \frac{V(j) \cdot f_{k,j}}{\|V(j) \cdot f_{k,j}\|} \quad \text{and} \quad v^{\perp}_{k,j} := v_{k,j} \wedge \mathbf{n}_{k,j}. \tag{5.1}$$

We also introduce the vector

$$v^{+}_{k,j} := \frac{V(j+1) \cdot f_{k,j}}{\|V(j+1) \cdot f_{k,j}\|}. \tag{5.2}$$

From the choice of $W_{k,j+1}$, the vectors $(\mathbf{t}_{k,j}, v^{+}_{k,j})$ form a direct orthonormal basis of the tangent plane of the embedding $f_{k,j}$ (see Lemma 24). In particular, $(\mathbf{t}_{k,j}, v^{+}_{k,j}, \mathbf{n}_{k,j})$ is a direct orthonormal basis in $\mathbb{E}^3$. We now, introduce the following definitions (see Figure 5.2).

Definition 1. Let $p \in \mathbb{T}^2$.

1. We denote by $\mathcal{R}_{k,j}(p)$ the rotation matrix that maps $(v^{\perp}_{k,j}, v_{k,j}, \mathbf{n}_{k,j})(p)$ to $(\mathbf{t}_{k,j}, v^{+}_{k,j}, \mathbf{n}_{k,j})(p)$. In other words

$$\begin{pmatrix} \mathbf{t}_{k,j} \\ v^{+}_{k,j} \\ \mathbf{n}_{k,j} \end{pmatrix}(p) = \mathcal{R}_{k,j}(p) \cdot \begin{pmatrix} v^{\perp}_{k,j} \\ v_{k,j} \\ \mathbf{n}_{k,j} \end{pmatrix}(p).$$

2. We denote by $\mathcal{L}_{k,j+1}(p, N_{k,j+1})$ the rotation matrix that maps $(\mathbf{t}_{k,j}, v^{+}_{k,j}, \mathbf{n}_{k,j})(p)$ to $(v^{\perp}_{k,j+1}, v_{k,j+1}, \mathbf{n}_{k,j+1})(p)$. In other words

$$\begin{pmatrix} v^{\perp}_{k,j+1} \\ v_{k,j+1} \\ \mathbf{n}_{k,j+1} \end{pmatrix}(p) = \mathcal{L}_{k,j+1}(p, N_{k,j+1}) \cdot \begin{pmatrix} \mathbf{t}_{k,j} \\ v^{+}_{k,j} \\ \mathbf{n}_{k,j} \end{pmatrix}(p).$$

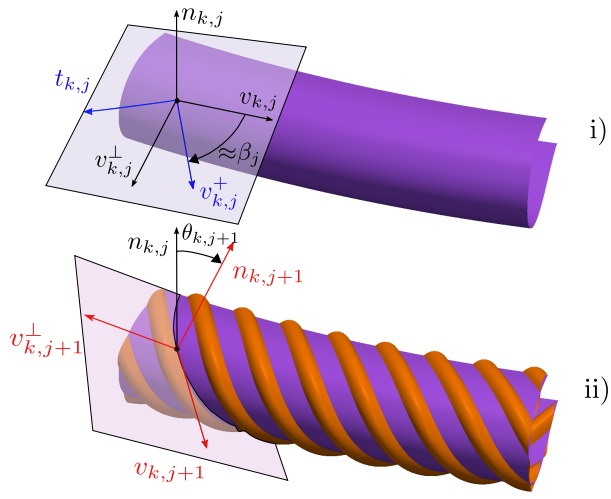

Figure 5.2: The rotation that maps the basis $(v^{\perp}_{k,j}, v_{k,j}, \mathbf{n}_{k,j})$ to $(v^{\perp}_{k,j+1}, v_{k,j+1}, \mathbf{n}_{k,j+1})$ is the composition of two rotations: i) Up to $O(\epsilon_{k,j})$, the rotation that maps $(v^{\perp}_{k,j}, v_{k,j}, \mathbf{n}_{k,j})$ to $(\mathbf{t}_{k,j}, v^{+}_{k,j}, \mathbf{n}_{k,j})$ is a rotation of angle β_j in the tangent plane to $f_{k,j}(\mathbb{T}^2)$ at $f_{k,j}(p)$. ii) Up to $O\left(\frac{1}{N_{k,j+1}}\right)$, the rotation that maps $(\mathbf{t}_{k,j}, v^{+}_{k,j}, \mathbf{n}_{k,j})$ to $(v^{\perp}_{k,j+1}, v_{k,j+1}, \mathbf{n}_{k,j+1})$ is a rotation about the axis spanned by $v_{k,j+1}$ of angle $\theta_{k,j+1}$.

3. We define the *corrugation matrix* $\mathcal{M}_{k,j+1}(p)$ as the rotation matrix that maps $(v^{\perp}_{k,j}, v_{k,j}, \mathbf{n}_{k,j})(p)$ to $(v^{\perp}_{k,j+1}, v_{k,j+1}, \mathbf{n}_{k,j+1})(p)$. In other words
$$\mathcal{M}_{k,j+1}(p) = \mathcal{L}_{k,j+1}(p, N_{k,j+1})\mathcal{R}_{k,j}(p).$$
Here the symbol "$\cdot$" denotes the natural action of 3×3 matrices on $(\mathbb{R}^3)^3$.

The corrugation matrix $\mathcal{M}_{k,j+1}(p, N_{k,j+1})$ has intricate coefficients with integro-differential expressions. The Corrugation Theorem provides, up to an error term, a simple expression for this matrix, which allows us to express the basis $(v^{\perp}_{k,j+1}, v_{k,j+1}, \mathbf{n}_{k,j+1})(p)$ in terms of the basis $(v^{\perp}_{k,j}, v_{k,j}, \mathbf{n}_{k,j})(p)$.

Lemma 20. *Let $p \in \mathbb{T}^2$. We have*

i)

$$\begin{aligned}\mathcal{L}_{k,j+1}(p, N_{k,j+1}) \quad &= \quad L_{k,j+1}(p, N_{k,j+1}) + O\Big(\|f_{k,j+1} - f_{k,j}\|_\infty \\ &\quad + \|V(j+1)\cdot f_{k,j+1} - V(j+1)\cdot f_{k,j}\|_\infty\Big),\end{aligned}$$

where

$$L_{k,j+1}(p,N_{k,j+1}) := \begin{pmatrix} \cos(\theta_{k,j+1}(p,N_{k,j+1})) & 0 & \sin(\theta_{k,j+1}(p,N_{k,j+1})) \\ 0 & 1 & 0 \\ -\sin(\theta_{k,j+1}(p,N_{k,j+1})) & 0 & \cos(\theta_{k,j+1}(p,N_{k,j+1})) \end{pmatrix},$$

$\theta_{k,j+1}(p,N_{k,j+1}) := \alpha_{k,j+1}(p)\cos(2\pi N_{k,j+1}s_{j+1}(p))$,
$\alpha_{k,j+1} = J_0^{-1}(\frac{\|W_{k,j+1}\cdot f_{k,j}\|}{r_{k,j+1}})$ *and* $s_{j+1}(p)$ *is the* $U(j+1)$ *coordinate of* p *in the frame* $(O,U(j+1),V(j+1))$.

ii)

$$\mathcal{R}_{k,j}(p) = R_j(p) + O(\epsilon_{k,j}),$$

where

$$R_j(p) = \begin{pmatrix} \cos\beta_j & \sin\beta_j & 0 \\ -\sin\beta_j & \cos\beta_j & 0 \\ 0 & 0 & 1 \end{pmatrix},$$

$\epsilon_{k,j} = \|\langle .,.\rangle_{\mathbb{E}^2} - f_{k,j}^*\langle .,.\rangle_{\mathbb{E}^3}\|$ *is the isometric default and* β_j *is the oriented angle between* $U(j)$ *and* $U(j+1)$.

We defer the proof of this lemma to the next section. From the One Step Theorem (Theorem 10), we get

$$\|f_{k,j+1} - f_{k,j}\|_\infty = O\left(\tfrac{1}{N_{k,j+1}}\right) \quad \text{and}$$
$$\|V(j+1)\cdot f_{k,j+1} - V(j+1)\cdot f_{k,j}\|_\infty = O\left(\tfrac{1}{N_{k,j+1}}\right),$$

which leads to the Corrugation Theorem.

Theorem 21 (Corrugation Theorem on $\mathbb{T}^2$)**.** *Let* $p \in \mathbb{T}^2$. *We have*

i)

$$\mathcal{L}_{k,j+1}(p,N_{k,j+1}) = L_{k,j+1}(p,N_{k,j+1}) + O\left(\frac{1}{N_{k,j+1}}\right),$$

ii)

$$\mathcal{R}_{k,j}(p) = R_j(p) + O(\epsilon_{k,j}).$$

Point *i)* states that, up to $O\left(\frac{1}{N_{k,j+1}}\right)$, the matrix $\mathcal{L}_{k,j+1}(p,N_{k,j+1})$ represents a rotation about an axis parallel to $v_{k,j+1}$. This rotation is related to the convex integration process in the direction $W_{k,j+1}$. The constant in $O\left(\frac{1}{N_{k,j+1}}\right)$ depends on k and j.

Point *ii)* states that, up to the isometric default $\epsilon_{k,j}$, the matrix $\mathcal{R}_{k,j}$ is a rotation of angle $\beta_j + \pi$ and thus only depends on the choice of the linear forms l_j and l_{j+1}.

5.2.2 Asymptotic behavior of the Gauss map

We denote by $\mathcal{M}_k$ and M_k the matrices corresponding to a stage k:

$$\mathcal{M}_k := \left(\prod_{j=1}^{3} \mathcal{M}_{k,j}\right) = \prod_{j=1}^{3} \mathcal{L}_{k,j}\mathcal{R}_{k,j-1} \quad \text{and} \quad M_k := \left(\prod_{j=1}^{3} L_{k,j}R_{j-1}\right).$$

Here and in the sequel, products of matrices such as $\prod_{j=p}^{q} N_j$ refer to left multiplications:

$$\prod_{j=p}^{q} N_j := N_q N_{q-1} \cdots N_p.$$

We have the following lemma

Lemma 22. *Let $p, q \in \mathbb{N}^*$, with $p < q$. Putting $d_k := \|\mathcal{M}_k - M_k\|_\infty$, we have*

i)

$$d_k = O\left(\sqrt{\delta_{k+1} - \delta_k} + (1 - \delta_k)\right),$$

ii)

$$\left\| \prod_{k=p}^{q} \mathcal{M}_k - \prod_{k=p}^{q} M_k \right\|_\infty \leq \prod_{k=p}^{q} (1 + d_k) \ - 1.$$

Proof. Let us bound the two terms involved in Lemma 20 i). We put $D_{k,1} := g_{k+1} - f_k^* \langle \cdot, \cdot \rangle_{\mathbb{R}^3}$. From Point 1 in the One Step Theorem 10, we have

$$\|f_{k,j+1} - f_{k,j}\|_\infty \leq 2\sqrt{7}\ \|U(j+1)\|\ \|\rho_{j+1}(D_{k,1})\|_\infty^{\frac{1}{2}}.$$

By the Loop condition (Equation (3.10)), we have:

$$\begin{aligned} \|V(j+1) \cdot f_{k,j+1} - V(j+1) \cdot f_{k,j}\|_\infty &\leq \|df_{k,j+1} - df_{k,j}\|_\infty \\ &\leq (c + \sqrt{7}) \|\rho_{j+1}(D_{k,1})\|_\infty^{\frac{1}{2}}. \end{aligned}$$

Now, by Equation (3.11), we have

$$\|\rho_{j+1}(D_{k,1})\|_\infty \leq \frac{5\sqrt{3}}{4} \|D_{k,1}\|_\infty.$$

By the triangle inequality and Conclusion *ii)* of the Stage Theorem, we have

$$\begin{aligned} \|D_{k,1}\|_\infty &= \|g_{k+1} - f_k^* \langle \cdot, \cdot \rangle_{\mathbb{R}^3}\|_\infty \\ &\leq \|g_{k+1} - g_k\|_\infty + \|g_k - f_k^* \langle \cdot, \cdot \rangle_{\mathbb{R}^3}\|_\infty \\ &\leq 2\ \|g_{k+1} - g_k\|_\infty. \end{aligned}$$

Combining these equations together, we get

$$\|f_{k,j+1}-f_{k,j}\|_\infty+\|V(j+1)\cdot f_{k,j+1}-V(j+1)\cdot f_{k,j}\|_\infty = O\Big(\|g_{k+1}-g_k\|_\infty^{\frac{1}{2}}\Big).$$

From Lemma 20, we then get

$$\|\mathcal{M}_k - M_k\|_\infty = O\left(\|g_{k+1}-g_k\|_\infty^{\frac{1}{2}} + \sum_{j=0}^{2}\epsilon_{k,j}\right).$$

By using that

$$\epsilon_{k,j} \le \|f_{k,j}^*\langle .,.\rangle - g_k\|_\infty + \|g_k - id\|_\infty \le \|g_{k+1}-g_k\|_\infty + \|g_k - id\|_\infty,$$

and since

$$\|g_{k+1}-g_k\|_\infty \le \|g_{k+1}-id\|_\infty + \|id-g_k\|_\infty = O(1-\delta_k),$$

we get

$$d_k = \|\mathcal{M}_k - M_k\|_\infty = O\left(\sqrt{\delta_{k+1}-\delta_k} + (1-\delta_k)\right).$$

We put $n = q-p+1$, and $A_k^0 = M_k$ and $A_k^1 = \mathcal{M}_k - M_k$ for $k \in \{p,...,q\}$. We have by the expansion of products in non-abelian rings

$$\prod_{k=p}^{q}(A_k^0+A_k^1) - \prod_{k=p}^{q}A_k^0 = \sum_{(\epsilon_p,\dots,\epsilon_q)\in\{0,1\}^n\setminus\{0\}^n}\prod_{k=p}^{q}A_k^{\epsilon_k}.$$

Whence, since the induced Euclidean norm $\|.\|$ is multiplicative and $\|A_k^0\| = 1$:

$$\begin{aligned}\left\|\prod_{k=p}^{q}(A_k^0+A_k^1) - \prod_{k=p}^{q}A_k^0\right\| &\le \sum_{(\epsilon_p,\dots,\epsilon_q)\in\{0,1\}^n\setminus\{0\}^n}\prod_{k=p}^{q}\|A_k^{\epsilon_k}\| \\ &= \prod_{k=p}^{q}(\|A_k^0\|+\|A_k^1\|) - 1 \\ &= \prod_{k=p}^{q}(1+\|A_k^1\|) - 1,\end{aligned}$$

which gives the point *ii)*. □

We then get the following theorem

Theorem 23 (Riesz Asymptotic Behavior)**.** *If the sequence* $(\delta_k)_{k\geq 0}$ *is chosen so that*

$$\sum_{k=1}^{\infty}(1-\delta_k) < +\infty \quad \textit{and} \quad \sum_{k=1}^{\infty}\sqrt{\delta_{k+1}-\delta_k} < +\infty,$$

then we have the following properties:

i) The product $\prod M_k$ *converges.*

ii) For every $\varepsilon > 0$*, there exists* $N > 0$ *such that for all* $n \geq N$*:*

$$\left\| \prod_{k=n}^{\infty} M_k - \prod_{k=n}^{\infty} \mathcal{M}_k \right\|_{\infty} \leq \varepsilon.$$

Remark 5. The behavior of the Gauss map has to be related to the regularity of the isometric embedding. It is well-known that every C^2 surface with zero Gaussian curvature is ruled, that is there is a straight-line (contained in the surface) passing through every point of the surface [28]. Moreover, the Gauss map is constant along each ruling.

Remark 6. In this theorem, the two convergence conditions $\sum_{k=1}^{\infty}(1-\delta_k) < +\infty$ and $\sum_{k=1}^{\infty}\sqrt{\delta_{k+1}-\delta_k} < +\infty$ are not equivalent and cannot be reduced one to the other. Tacking the Bertrand series $1-\delta_k = \frac{1}{k\log^{\beta} k}$ with $1 < \beta \leq 2$, we get the convergence of the first sum and the divergence of the second one. It is an exercise to define a sequence δ_k such that the first sum divergences and the second sum converges.

Proof. Let us show that $(\prod_{k=1}^{n} M_k)_{n\in\mathbb{N}^*}$ is a Cauchy sequence. Let $p, q \in \mathbb{N}^*$, with $p < q$. We have

$$\begin{aligned}
\| \prod_{k=1}^{q} M_k - \prod_{k=1}^{p-1} M_k \| &\leq \| \left(\prod_{k=p}^{q} M_k - Id \right) \left(\prod_{k=1}^{p-1} M_k \right) \| \\
&\leq \| \left(\prod_{k=p}^{q} M_k \right) - Id \| \\
&\leq \| \prod_{k=p}^{q} M_k - \prod_{k=p}^{q} \mathcal{M}_k + \prod_{k=p}^{q} \mathcal{M}_k - Id \| \\
&\leq \| \prod_{k=p}^{q} M_k - \prod_{k=p}^{q} \mathcal{M}_k \| + \| \prod_{k=p}^{q} \mathcal{M}_k - Id \|.
\end{aligned}$$

By Theorem 17, since

$$\sum \sqrt{\delta_{k+1} - \delta_k} < +\infty$$

the sequence $(f_k)_{k\in\mathbb{N}^*}$ is C^1 converging. It follows that $v_{k,0}$, $v^{\perp}_{k,0}$ and $n_{k,0}$ also converge. Let $\varepsilon > 0$. Since

$$\begin{pmatrix} v^{\perp}_{q+1,0} \\ v_{q+1,0} \\ \mathbf{n}_{q+1,0} \end{pmatrix} = \prod_{k=p}^{q} \mathcal{M}_k \cdot \begin{pmatrix} v^{\perp}_{p,0} \\ v_{p,0} \\ \mathbf{n}_{p,0} \end{pmatrix},$$

we have for p and q large enough

$$\| \prod_{k=p}^{q} \mathcal{M}_k - Id\| \leq \frac{\varepsilon}{2}.$$

By Lemma 22.i and the assumption on the δ_k, we have

$$\sum d_k < +\infty,$$

which implies if p and q are large enough that

$$\ln\left(\prod_{k=p}^{q}(1+d_k)\right) = \sum_{k=p}^{q}\ln(1+d_k) \leq \sum_{k=p}^{q} d_k \leq \ln\left(1+\frac{\varepsilon}{2}\right).$$

We finally have

$$\prod_{k=p}^{q}(1+d_k) \ -1 \leq \frac{\varepsilon}{2}.$$

By Lemma 22.ii we get that

$$\| \prod_{k=p}^{q} M_k - \prod_{k=p}^{q} \mathcal{M}_k\| \leq \frac{\varepsilon}{2},$$

which allows to show that $(\prod_{k=1}^{n} M_k)_{n\in\mathbb{N}^*}$ is a Cauchy sequence, hence point *i)*. Point *ii)* follows directly. □

5.2.3 C^1 fractal structure

Let us denote the limit bases

$$\begin{pmatrix} v^{\perp}_{\infty} \\ v_{\infty} \\ \mathbf{n}_{\infty} \end{pmatrix} = \prod_{k=N}^{\infty} \mathcal{M}_k \cdot \begin{pmatrix} v^{\perp}_{N,0} \\ v_{N,0} \\ \mathbf{n}_{N,0} \end{pmatrix},$$

and

$$\begin{pmatrix} v_\infty^\perp(N) \\ v_\infty(N) \\ \mathbf{n}_\infty(N) \end{pmatrix} = \prod_{k=N}^{\infty} M_k \cdot \begin{pmatrix} v_{N,0}^\perp \\ v_{N,0} \\ \mathbf{n}_{N,0} \end{pmatrix}.$$

Theorem 23 indicates that for any $\varepsilon > 0$, we can choose N so that

$$\|\mathbf{n}_\infty - \mathbf{n}_\infty(N)\| < \varepsilon.$$

In other words, the Gauss map $\mathbf{n}_\infty$ of the limit embedding $\mathcal{F}_\infty$ can be approximated by $\mathbf{n}_\infty(N)$.

The Corrugation Theorem together with theorem 23 show that the structure of the Gauss map $\mathbf{n}_\infty$ of $\mathcal{F}_\infty$ asymptotically resembles to a Riesz structure. By analogy with the one dimensional case (see Section 5.1) we call the corrugated torus $\mathcal{F}_\infty$ a C^1 *fractal*. This name suggests that the Hausdorff dimension of the graph of $\mathbf{n}_\infty$ is strictly larger than two. Although this is likely to be the case, we did not attempt to prove it.

5.3 Proof of Lemma 20

Lemma 24. *The family $(\mathbf{t}_{k,j}, v_{k,j}^+)$ is a direct orthonormal basis of the tangent plane of the embedding $f_{k,j}$. In particular, $(\mathbf{t}_{k,j}, v_{k,j}^+, \mathbf{n}_{k,j})$ is a direct orthonormal basis in $\mathbb{E}^3$.*

Proof. Since $W_{k,j+1} = U(j+1) + \zeta_{k,j+1} V(j+1)$, the basis $(W_{k,j+1}, V(j+1))$ is direct, thus $(\mathbf{t}_{k,j}, v_{k,j}^+)$ is also direct. Furthermore we recall that $W_{k,j+1}$ is chosen so that

$$f_{k,j}^* \langle \cdot, \cdot \rangle_{\mathbb{R}^3} (W_{k,j+1}, V(j+1)) = \mu_{k,j} (W_{k,j+1}, V(j+1)) = 0,$$

which implies that

$$\langle \mathbf{t}_{k,j}, v_{k,j}^+ \rangle = \langle W_{k,j+1} \cdot f_{k,j}, V(j+1) \cdot f_{k,j} \rangle = 0.$$

□

5.3.1 Proof of Lemma 20 i)

We use the following concise notations:

$$c_{k,j+1} = \cos(\theta_{k,j+1}(p, N_{k,j+1})) = \cos\left(\alpha_{k,j+1}(p) \cos(2\pi N_{k,j+1} s_{j+1}(p))\right).$$

$$s_{k,j+1} = \sin(\theta_{k,j+1}(p, N_{k,j+1})) = \sin\left(\alpha_{k,j+1}(p) \cos(2\pi N_{k,j+1} s_{j+1}(p))\right).$$

We also introduce the error vectors η_1, η_2 and η_3 given by:

$$\begin{pmatrix} \eta_1 \\ \eta_2 \\ \eta_3 \end{pmatrix} = \begin{pmatrix} v^{\perp}_{k,j+1} \\ v_{k,j+1} \\ \mathbf{n}_{k,j+1} \end{pmatrix} - \begin{pmatrix} c_{k,j+1} & 0 & s_{k,j+1} \\ 0 & 1 & 0 \\ -s_{k,j+1} & 0 & c_{k,j+1} \end{pmatrix} \cdot \begin{pmatrix} \mathbf{t}_{k,j} \\ v^{+}_{k,j} \\ \mathbf{n}_{k,j} \end{pmatrix}.$$

Lemma 26 is a technical preliminary lemma. Then Lemma 27 (respectively Lemmas 28 and 29) gives an upper bounds for η_1 (respectively η_2 and η_3).

Lemma 25. *For any vector a and b, one has:*

$$\left\| \frac{a}{\|a\|} - \frac{b}{\|b\|} \right\| \leq 2 \frac{\|b-a\|}{\|a\|}.$$

Proof. We have

$$\begin{aligned} \left\| \frac{a}{\|a\|} - \frac{b}{\|b\|} \right\| &= \left\| \frac{a}{\|a\|} - \frac{b}{\|a\|} + \frac{b}{\|a\|} - \frac{b}{\|b\|} \right\| \\ &\leq \tfrac{1}{\|a\|}\|a-b\| + \|b\| \left| \tfrac{1}{\|a\|} - \tfrac{1}{\|b\|} \right| \\ &\leq \frac{\|a-b\|}{\|a\|} + \frac{|\|b\| - \|a\||}{\|a\|}. \end{aligned}$$

We conclude by using the triangle inequality. □

Lemma 26. *We have the following properties*

i)

$$\|W_{k,j+1} \cdot f_{k,j+1} - r_{k,j+1} \left(c_{k,j+1}\mathbf{t}_{k,j} + s_{k,j+1}\mathbf{n}_{k,j}\right)\| \leq \|w'\|_\infty \ \|F_{k,j+1} - f_{k,j}\|_\infty.$$

ii)

$$\begin{aligned} |\langle W_{k,j+1} \cdot f_{k,j+1}, V(j+1) \cdot f_{k,j+1} \rangle| \ \leq \ & \|w'\|_\infty \ \|F_{k,j+1} - f_{k,j}\|_\infty \|V(j+1)\| \\ & + \|W_{k,j+1} \cdot f_{k,j+1}\| \|V(j+1) \cdot f_{k,j+1} \\ & - V(j+1) \cdot f_{k,j}\|. \end{aligned}$$

Remark 7. The two terms with a factor $\|w'\|_\infty$ in points i) and ii) would be zero without the smoothing operation (2.14). The other term depends on how the corrugation process rotates the image of $V(j+1)$.

Proof. By Equation 2.17, we have:

$$\begin{aligned} W_{k,j+1} \cdot f_{k,j+1}(p) = \ & W_{k,j+1} \cdot F_{k,j+1}(p) - w'(s_{j+1}(p)) \left(F \circ \Phi_{k,j+1}(p, 1 - s_{j+1}(p)) \right. \\ & \left. - f \circ \Phi_{k,j+1}(p, 1 - s_{j+1}(p))\right). \end{aligned}$$

Furthermore, from (2.8) and (2.9), one has:

$$W_{k,j+1}\cdot F_{k,j+1}(p) \quad = \quad r_{k,j+1}(p)\left(c_{k,j+1}\mathbf{t}_{k,j}(p)+s_{k,j+1}\mathbf{n}_{k,j}(p)\right).$$

We conclude the proof of point *i)* by using that

$$|F\circ\Phi_{k,j+1}(p,1-s_{j+1}(p))-f\circ\Phi_{k,j+1}(p,1-s_{j+1}(p))|\leq\|F_{k,j+1}-f_{k,j}\|_\infty.$$

For point *ii)*, we need to give an upper bound of $|\langle W_{k,j}\cdot f_{k,j}, V(j+1)\cdot f_{k,j+1}\rangle|$:

$$\begin{aligned}\langle W_{k,j+1}\cdot f_{k,j+1}, V(j+1)\cdot f_{k,j+1}\rangle \quad &= \quad \langle W_{k,j+1}\cdot f_{k,j+1}, V(j+1)\cdot f_{k,j}\rangle\\ &\quad + \langle W_{k,j+1}\cdot f_{k,j+1}, V(j+1)\cdot f_{k,j+1}\\ &\quad -V(j+1)\cdot f_{k,j}\rangle.\end{aligned}$$

By definition, $V(j+1)\cdot f_{k,j}$ is proportional to $v^+_{k,j}$, thus orthogonal to both $\mathbf{n}_{k,j}$ and $\mathbf{t}_{k,j}$ (by Lemma 24). Therefore

$$\begin{aligned}\langle W_{k,j+1}\cdot f_{k,j+1}, V(j+1)\cdot f_{k,j}\rangle \quad &= \quad \langle W_{k,j+1}\cdot f_{k,j+1}-r_{k,j+1}\left(c_{k,j+1}\mathbf{t}_{k,j}\right.\\ &\quad \left.+\, s_{k,j+1}\mathbf{n}_{k,j}\right), V(j+1)\cdot f_{k,j}\rangle.\end{aligned}$$

Thus, since $\|V(j+1)\cdot f_{k,j}\|<\|V(j+1)\|$, point *i)* of this lemma implies that

$$|\langle W_{k,j+1}\cdot f_{k,j+1}, V(j+1)\cdot f_{k,j}\rangle|\leq\|w'\|_\infty\|F_{k,j+1}-f_{k,j}\|_\infty\|V(j+1)\|.$$

Thus,

$$\begin{aligned}|\langle W_{k,j+1}\cdot f_{k,j+1}, V(j+1)\cdot f_{k,j+1}\rangle| \quad &\leq \quad \|w'\|_\infty\,\|F_{k,j+1}-f_{k,j}\|_\infty\|V(j+1)\|\\ &\quad +\|W_{k,j+1}\cdot f_{k,j+1}\|\|V(j+1)\cdot f_{k,j+1}\\ &\quad -V(j+1)\cdot f_{k,j}\|.\end{aligned}$$

□

Lemma 27.

$$\begin{aligned}\|\eta_1\| \quad &= \quad \|v^\perp_{k,j+1}-\left(c_{k,j+1}\mathbf{t}_{k,j}+s_{k,j+1}\mathbf{n}_{k,j}\right)\|\\ &\leq \quad C^1_{k,j}\|F_{k,j+1}-f_{k,j}\|_\infty+C^2_{k,j}\|V(j+1)\cdot f_{k,j+1}-V(j+1)\cdot f_{k,j}\|,\end{aligned}$$

where

$$C^1_{k,j}=\frac{\|w'\|_\infty}{\|W_{k,j+1}\cdot f_{k,j+1}\|}\left(1+\frac{2\|V(j+1)\|}{\|V(j+1)\cdot f_{k,j+1}\|}\right)$$

and

$$C^2_{k,j}=\frac{2}{\|V(j+1)\cdot f_{k,j+1}\|}.$$

PROOF. We introduce an intermediate vector

$$u_{k,j+1} := \frac{W_{k,j+1} \cdot f_{k,j+1}}{\|W_{k,j+1} \cdot f_{k,j+1}\|},$$

and we are going to show that $u_{k,j+1}$ is close to both $v^{\perp}_{k,j+1}$ and $(c_{k,j+1}\mathbf{t}_{k,j} + s_{k,j+1}\mathbf{n}_{k,j})$. Since $(W_{k,j+1}, V(j+1))$ is direct, the basis $(W_{k,j+1} \cdot f_{k,j+1}, v_{k,j+1})$ of the tangent plane is direct. We deduce, by using that $(v^{\perp}_{k,j+1}, v_{k,j+1})$ is also direct that

$$v^{\perp}_{k,j+1} = \frac{W_{k,j+1}{\cdot}f_{k,j+1} - \langle W_{k,j+1}{\cdot}f_{k,j+1}, v_{k,j+1}\rangle v_{k,j+1}}{\|W_{k,j+1}{\cdot}f_{k,j+1} - \langle W_{k,j+1}{\cdot}f_{k,j+1}, v_{k,j+1}\rangle v_{k,j+1}\|}.$$

We then have

$$\left\|u_{k,j+1} - v^{\perp}_{k,j+1}\right\| = \left\| \frac{W_{k,j+1} \cdot f_{k,j+1}}{\|W_{k,j+1} \cdot f_{k,j+1}\|} - \frac{W_{k,j+1}{\cdot}f_{k,j+1} - \langle W_{k,j+1}{\cdot}f_{k,j+1}, v_{k,j+1}\rangle v_{k,j+1}}{\|W_{k,j+1}{\cdot}f_{k,j+1} - \langle W_{k,j+1}{\cdot}f_{k,j+1}, v_{k,j+1}\rangle v_{k,j+1}\|} \right\|.$$

By using Lemma 25 with $a = W_{k,j+1}{\cdot}f_{k,j+1}$ and $b = W_{k,j+1}{\cdot}f_{k,j+1} - \langle W_{k,j+1}{\cdot}f_{k,j+1}, v_{k,j+1}\rangle v_{k,j+1}$, one has

$$\left\|u_{k,j+1} - v^{\perp}_{k,j+1}\right\| \leq 2\frac{\|\langle W_{k,j+1}{\cdot}f_{k,j+1}, v_{k,j+1}\rangle v_{k,j+1}\|}{\|W_{k,j+1}{\cdot}f_{k,j+1}\|} = 2\|\langle u_{k,j+1}, v_{k,j+1}\rangle\|.$$

However, by Lemma 26 *ii)* one has

$$\begin{aligned}\|\langle u_{k,j+1}, v_{k,j+1}\rangle\| \quad \leq \quad & \frac{\|w'\|_\infty \, \|V(j+1)\|}{\|W_{k,j+1} \cdot f_{k,j+1}\|\|V(j+1) \cdot f_{k,j+1}\|}.\|F_{k,j+1} - f_{k,j}\|_\infty \\ & + \frac{\|V(j+1) \cdot f_{k,j+1} - V(j+1) \cdot f_{k,j}\|}{\|V(j+1) \cdot f_{k,j+1}\|}.\end{aligned}$$

which leads to

$$\begin{aligned}\left\|u_{k,j+1} - v^{\perp}_{k,j+1}\right\| \quad \leq \quad & \frac{2 \, \|w'\|_\infty \, \|V(j+1)\|}{\|W_{k,j+1} \cdot f_{k,j+1}\|\|V(j+1) \cdot f_{k,j+1}\|}.\|F_{k,j+1} - f_{k,j}\|_\infty \\ & + \frac{2\|V(j+1) \cdot f_{k,j+1} - V(j+1) \cdot f_{k,j}\|}{\|V(j+1) \cdot f_{k,j+1}\|}.\end{aligned}$$

Recalling that $r_{k,j+1} = \|W_{k,j+1} \cdot f_{k,j+1}\|$, Lemma 26 *i)* directly implies that

$$\|u_{k,j+1} - (c_{k,j+1}\mathbf{t}_{k,j} + s_{k,j+1}\mathbf{n}_{k,j})\| \leq \frac{\|w'\|_\infty \, \|F_{k,j+1} - f_{k,j}\|_\infty}{\|W_{k,j+1} \cdot f_{k,j+1}\|}.$$

We get the result by combining the two last equations and the triangle inequality:

$$\begin{aligned}\left\|v^{\perp}_{k,j+1} - (c_{k,j+1}\mathbf{t}_{k,j} + s_{k,j+1}\mathbf{n}_{k,j})\right\| \quad \leq \quad & \left\|v^{\perp}_{k,j+1} - u_{k,j+1}\right\| + \\ & \|u_{k,j+1} - (c_{k,j+1}\mathbf{t}_{k,j} + s_{k,j+1}\mathbf{n}_{k,j})\|.\end{aligned}$$

□

Lemma 28.

$$\|\eta_2\| = \|v_{k,j+1} - v^+_{k,j}\| \leq C^3_{k,j}\|V(j+1)\cdot f_{k,j+1} - V(j+1)\cdot f_{k,j}\|,$$

where

$$C^3_{k,j} = \frac{2}{\|V(j+1)\cdot f_{k,j}\|}.$$

Proof of Lemma 28. By definition

$$v_{k,j+1} - v^+_{k,j} = \frac{V(j+1)\cdot f_{k,j+1}}{\|V(j+1)\cdot f_{k,j+1}\|} - \frac{V(j+1)\cdot f_{k,j}}{\|V(j+1)\cdot f_{k,j}\|}$$

Again by using Lemma 25, one has

$$\|v_{k,j+1} - v^+_{k,j}\| \quad \leq \quad 2\frac{\|V(j+1)\cdot f_{k,j+1} - V(j+1)\cdot f_{k,j}\|}{\|V(j+1)\cdot f_{k,j}\|}.$$

□

Lemma 29. *The error* $\eta_3 = \mathbf{n}_{k,j+1} - (-s_{k,j+1}\mathbf{t}_{k,j} + c_{k,j+1}\mathbf{n}_{k,j})$ *satisfies*

$$\|\eta_3\| \leq \|\eta_1\| + \|\eta_2\|.$$

Proof of Lemma 29. We put $a = c_{k,j+1}\mathbf{t}_{k,j} + s_{k,j+1}\mathbf{n}_{k,j}$. One has

$$\begin{array}{rcl} \eta_3 & = & n_{k,j+1} - n_{k,j} \\ & = & v^\perp_{k,j+1} \wedge v_{k,j+1} - a \wedge v^+_{k,j} \\ & = & v^\perp_{k,j+1} \wedge (v_{k,j+1} - v^+_{k,j}) - (a - v^\perp_{k,j+1}) \wedge v^+_{k,j}, \end{array}$$

whence

$$\|\eta_3\| \leq \|v_{k,j+1} - v^+_{k,j}\| + \|a - v^\perp_{k,j+1}\| \leq \|\eta_1\| + \|\eta_2\|.$$

□

End of Proof of Lemma 20 i).
We have

$$\begin{pmatrix} \eta_1 \\ \eta_2 \\ \eta_3 \end{pmatrix} = \begin{pmatrix} v^\perp_{k,j+1} \\ v_{k,j+1} \\ \mathbf{n}_{k,j+1} \end{pmatrix} - \begin{pmatrix} c_{k,j+1} & 0 & s_{k,j+1} \\ 0 & 1 & 0 \\ -s_{k,j+1} & 0 & c_{k,j+1} \end{pmatrix} \cdot \begin{pmatrix} \mathbf{t}_{k,j} \\ v^+_{k,j} \\ \mathbf{n}_{k,j} \end{pmatrix}$$

$$= \big(\mathcal{L}_{k,j+1}(p, N_{k,j+1}) - L_{k,j+1}(p, N_{k,j+1})\big) \begin{pmatrix} \mathbf{t}_{k,j} \\ v^+_{k,j} \\ \mathbf{n}_{k,j} \end{pmatrix}.$$

On the other hand, by applying Lemmas 27, 28 and 29, we get
$\max\{\|\eta_1\|, \|\eta_2\|, \|\eta_3\|\} = O(\|f_{k,j+1} - f_{k,j}\|_\infty + \|V(j+1)\cdot f_{k,j+1} - V(j+1)\cdot f_{k,j}\|_\infty)$,
which concludes point i).

5.3.2 Proof of Lemma 20 ii)

Since the two orthonormal basis $(v^{\perp}_{k,j}, v_{k,j}, \mathbf{n}_{k,j})(p)$ and $(t_{k,j}, v^{+}_{k,j}, \mathbf{n}_{k,j})(p)$ are direct, it is sufficient to show that error $\eta_{k,j}$ for the second line of the matrix satisfies

$$\eta_{k,j} := v^{+}_{k,j} - \left[-\sin\beta_j v^{\perp}_{k,j} + \cos\beta_j v_{k,j}\right] = O(\epsilon_{k,j}).$$

For convenience, we denote $\overline{U}(j) = U(j)/\|U(j)\|$ and $\overline{V}(j) = V(j)/\|V(j)\|$. From the equation

$$\overline{V}(j+1) = -\sin\beta_j\ \overline{U}(j) + \cos\beta_j\ \overline{V}(j),$$

we have

$$v^{+}_{k,j} = \frac{\overline{V}(j+1)\cdot f_{k,j}}{\|\overline{V}(j+1)\cdot f_{k,j}\|} = -\sin\beta_j \frac{\overline{U}(j)\cdot f_{k,j}}{\|\overline{V}(j+1)\cdot f_{k,j}\|} + \cos\beta_j \frac{\overline{V}(j)\cdot f_{k,j}}{\|\overline{V}(j+1)\cdot f_{k,j}\|}.$$

We denote by x and y the component of $\overline{U}(j)\cdot f_{k,j}/\|\overline{V}(j+1)\cdot f_{k,j}\|$ in the basis $(v^{\perp}_{k,j}, v_{k,j})$ of the tangent plane:

$$x = \langle \frac{\overline{U}(j)\cdot f_{k,j}}{\|\overline{V}(j+1)\cdot f_{k,j}\|}, v^{\perp}_{k,j}\rangle \quad \text{and} \quad y = \langle \frac{\overline{U}(j)\cdot f_{k,j}}{\|\overline{V}(j+1)\cdot f_{k,j}\|}, v_{k,j}\rangle.$$

We finally get

$$v^{+}_{k,j} = -\sin\beta_j\ x\ v^{\perp}_{k,j}\ +\ \left[\cos\beta_j\ \frac{\|\overline{V}(j)\cdot f_{k,j}\|}{\|\overline{V}(j+1)\cdot f_{k,j}\|}\ -\sin\beta_j\ y\right] v_{k,j}.$$

Finally, the error $\eta_{k,j}$ satisfies:

$$\|\eta_{k,j}\| \le |1-x| + \left|1 - \frac{\|\overline{V}(j)\cdot f_{k,j}\|}{\|\overline{V}(j+1)\cdot f_{k,j}\|}\right| + |y|. \tag{5.3}$$

The end of the proof consists in showing that each of the three terms in Equation (5.3) is bounded, up to a constant, by the isometric default $\epsilon_{k,j}$. We first need the following lemma:

Lemma 30. *Let (e_1, e_2) be a direct orthonormal basis of $T_p\mathbb{T}^2$. Then*

$$|1 - \|e_1\cdot f_{k,j}\|| \le \epsilon_{k,j} \qquad \textit{and} \quad |\langle e_1\cdot f_{k,j}, e_2\cdot f_{k,j}\rangle| \le \epsilon_{k,j}.$$

In particular, if V is any unit vector of $T_p\mathbb{T}^2$, one has :

$$\left|1 - \frac{\|e_1\cdot f_{k,j}\|}{\|V\cdot f_{k,j}\|}\right| \le \frac{2\ \epsilon_{k,j}}{(1-\epsilon_{k,j})} = O(\epsilon_{k,j}).$$

PROOF OF LEMMA 30. Denote by $M_{k,j}$ the matrix of the first fundamental form. By definition, the isometric default $\epsilon_{k,j}$ is the Frobenius norm $\|M_{k,j} - Id\|$ of the matrix $M_{k,j} - Id$. We have

$$|\|e_1 \cdot f_{k,j}\|^2 \ - 1| \ = \ |{}^t e_1 M_{k,j} e_1 - {}^t e_1 e_1| \ = \ |{}^t e_1 \ (M_{k,j} - Id) e_1|.$$

Now, by the Cauchy-Schwarz inequality and the fact that the Frobenius norm is submultiplicative, we have

$$|{}^t e_1 \ (M_{k,j} - Id) e_1| \leq \|{}^t e_1\| \|M_{k,j} - Id\| \|e_1\| \leq \epsilon_{k,j}.$$

We deduce

$$|1 - \|e_1 \cdot f_{k,j}\|| \leq \frac{\epsilon_{k,j}}{1 + \|e_1 \cdot f_{k,j}\|} \leq \epsilon_{k,j}.$$

Similarly, using that ${}^t e_1 e_2 = 0$, we also have

$$\begin{aligned} |\langle e_1 \cdot f_{k,j}, e_2 \cdot f_{k,j} \rangle| &= |{}^t e_1 M_{k,j} e_2| \\ &= |{}^t e_1 M_{k,j} e_2 - {}^t e_1 e_2| \\ &= |{}^t e_1 \ (M_{k,j} - Id) e_2| \\ &\leq \epsilon_{k,j}. \end{aligned}$$

□

Let us now bound $|y|$. By Lemma 30, since $\overline{U}(j)$ and $\overline{V}(j)$ are orthonormal, we have

$$\langle \overline{U}(j) \cdot f_{k,j}, \overline{V}(j) \cdot f_{k,j} \rangle \leq \epsilon_{k,j},$$

which leads to

$$|y| \leq \frac{\epsilon_{k,j}}{\|\overline{V}(j+1) \cdot f_{k,j}\| \|\overline{V}(j) \cdot f_{k,j}\|} \leq \frac{\epsilon_{k,j}}{(1 - \epsilon_{k,j})^2} = O(\epsilon_{k,j}).$$

Let us now bound $|1 - x|$. From

$$\begin{aligned} y^2 &= \left(\frac{\|\overline{U}(j) \cdot f_{k,j}\|}{\|\overline{V}(j+1) \cdot f_{k,j}\|} \right)^2 - x^2 \\ &= \left(\frac{\|\overline{U}(j) \cdot f_{k,j}\|}{\|\overline{V}(j+1) \cdot f_{k,j}\|} - x \right) \left(\frac{\|\overline{U}(j) \cdot f_{k,j}\|}{\|\overline{V}(j+1) \cdot f_{k,j}\|} + x \right), \end{aligned}$$

we get

$$\left| \frac{\|\overline{U}(j) \cdot f_{k,j}\|}{\|\overline{V}(j+1) \cdot f_{k,j}\|} - x \right| \leq y^2 \ \frac{\|\overline{V}(j+1) \cdot f_{k,j}\|}{\|\overline{U}(j) \cdot f_{k,j}\|} \leq \frac{\epsilon_{k,j}^2 \ (1 + \epsilon_{k,j})}{(1 - \epsilon_{k,j})^3}.$$

We then have by the triangle inequality and Lemma 30:

$$|1 - x| \leq \left| 1 - \frac{\|\overline{U}(j) \cdot f_{k,j}\|}{\|\overline{V}(j+1) \cdot f_{k,j}\|} \right| + \left| \frac{\|\overline{U}(j) \cdot f_{k,j}\|}{\|\overline{V}(j+1) \cdot f_{k,j}\|} - x \right| = O(\epsilon_{k,j}).$$

Again by Lemma 30:

$$\left|1 - \frac{\|\overline{V}(j)\cdot f_{k,j}\|}{\|\overline{V}(j+1)\cdot f_{k,j}\|}\right| \leq \frac{2\ \epsilon_{k,j}}{(1-\epsilon_{k,j})} = O(\epsilon_{k,j}).$$

We have proven that the three terms involved in Equation (5.3) are bounded, up to a constant, by $\epsilon_{k,j}$, thus

$$\eta_{k,j} = O(\epsilon_{k,j}).$$

Acknowledgments

The authors are indebted to the stimulating remarks, helpful advice and useful suggestions of Thierry Dumont, Jean-Pierre Kahane and Damien Rohmer. We are also thankful to the Grenoble University High Performance Computing Centre project and the Swiss National Supercomputing Centre for providing access to their computing platforms and to the Grenoble FabLab Gi-Nova for the 3D printing of the flat torus. This research was partially supported by Région Rhône-Alpes (Projet CIBLE) and Centre National de la Recherche Scientifique (Projet Exploratoire PEPS). The authors greatly thank the anonymous referee for many valuable comments and recommendations.

Bibliography

[1] *Gi-nova fab lab*, `http://www.aip-primeca-ds.net/-GI-Nova-.html`.

[2] *Povray*, `http://www.povray.org/`.

[3] *Sunflow*, `http://sunflow.sourceforge.net/`.

[4] *Yafaray,* Yet Another Free RAYtracer, `http://www.yafaray.org`.

[5] A. D. Aleksandrov and A. V. Pogorelov, *Uniqueness of convex surfaces of revolution*, Mat. Sb. **26** (1950), no. 2, 183–204.

[6] M. Berger, *Encounter with a geometer, part I*, Notices of the AMS **47** (2000), no. 2, 183–194.

[7] Y. Borisov, *Irregular $c^{1,\beta}$-surfaces with analytic metric*, Sib. Mat. Zh. **45** (2004), no. 1, 25–61.

[8] V. Borrelli, S. Jabrane, F. Lazarus, and B. Thibert, *Flat tori in three dimensional space and convex integration*, Proceedings of the National Academy of Sciences of the United States of America (PNAS) **109** (2012), no. 19, 7218–7223.

[9] V. Borrelli, S. Jabrane, F. Lazarus, and B. Thibert, *The Nash-Kuiper process for curves*, Actes du séminaire de théorie spectrale et géométrie, 2012.

[10] E. Cartan, *Sur la possibilité de plonger un espace riemannien donné dans un espace euclidien*, Ann. Soc. Pol. Math. **6** (1927), 1–7.

[11] S. E. Cohn-Vossen, *Die verbiegung von flachen im grossen*, Fortschr. Math. Wiss **1** (1936), 33–76.

[12] S. Conti, C. De Lellis, and L. Székelyhidi, *h-principle and rigidity for $c^{1,\alpha}$ isometric embeddings*, Nonlinear Partial Differential Equations (2012), 83–116.

[13] N. V. Efimov, *Appearance of singularities on surfaces of negative curvature*, A. M. S. Translations Series 2 **66** (1968), 154–190.

[14] Y. Eliashberg and N. Mishachev, *Introduction to the h-principle*, Graduate Studies in Mathematics, vol. 48, A.M.S., Providence, 2002.

[15] K. Falkoner, *Fractal geometry*, Wiley, 2003.

[16] S. D. Feit, *k-mersions of manifolds*, Acta Math. **122** (1969), 173–195.

[17] E. A. Feldman, *Deformations of closed space curves*, J. Diff. Geom. **2** (1968), 67–75.

[18] G. Francis, *A topological picturebook*, Springer, 1987.

[19] R. Greene, *Isometric embeddings of riemannian and pseudo-riemannian manifolds*, Mem. Amer. Math. Soc. **97** (1970).

[20] M. Gromov, *Convex integration of differential relations*, Math.USSR Izvestia **7** (1973), 329–343.

[21] ———, *Partial differential relations*, Springer-Verlag, 1986.

[22] M. Gromov and V. Rokhlin, *Embeddings and immersions in riemannian geometry*, Russian Math. Survey **5** (1970), 1–57.

[23] A. Haefliger, *Lectures on the theorem of gromov*, Lecture Notes in Math. **209** (1971), 128–141.

[24] A. Haefliger and V. Poénaru, *La classification des immersions combinatoires*, Inst. Hautes Etudes Sci. Publ. Math. **23** (1964), 75–91.

[25] E. Hairer, S. Paul Nørsett, and G. Wanner, *Solving ordinary differential equations i. nonstiff problems.*, second revised edition 1993 ed., Springer Series in Comput. Mathematic, vol. 8, Springer-Verlag, 1987.

[26] Q. Han and J.-X. Hong, *Isometric embedding of riemannian manifolds in euclidean spaces*, Mathematical Surveys and Monographs, vol. 130, AMS, 2006.

[27] A. Hanson, T. Munzner, and G. Francis, *Interactive methods for visualizable geometry*, Computer **27** (1994), no. 7, 73–83.

[28] P. Hartman and L. Nirenberg, *On spherical images whose jacobians do not change sign*, Amer. J. Math. **81** (1959), 901–920.

[29] M. Hirsch, *Immersions of manifolds*, Trans. Amer. Math. **93** (1959), 242–276.

[30] ———, *On imbedding differentiable manifolds in euclidean space*, Ann. of Math. **73** (1961), 566–571.

[31] M. Janet, *Sur la possibilité de plonger un espace riemannien donné dans un espace euclidien*, Ann. Soc. Pol. Math **5** (1926), 38–43.

[32] J.-P. Kahane, *Jacques Peyrière et les produits de Riesz*, 2010.

[33] F. R. Keogh, *Riesz products*, Proc. London Math. Soc. **14A** (1965), 174–182.

[34] N. Kuiper, *On C^1-isometric imbeddings*, Indag. Math. **17** (1955), 545–555.

[35] C. De Lellis and L. Székelyhidi, *The euler equations as a differential inclusion*, Ann. of Math. **170** (2009), 1417–1436.

[36] S. Levy, *Making waves: A guide to the ideas behind "outside in"*, AK Peters, 1995.

[37] S. Levy, D. Maxwell, and T. Munzner, *Outside in*, `http://www.geom.uiuc.edu/docs/outreach/oi/`.

[38] T. K. Milnor, *Efimov's theorem about complete immersed surfaces of negative curvature*, Adv. in Math. **8** (1972), 474–543.

[39] J. F. Nash, *C^1-isometric imbeddings*, Ann. of Math. **60** (1954), no. 3, 383–396.

[40] L. Nirenberg, *The weyl and minkowski problems in differential geometry in the large*, Comm. Pure Appl. Math. **6** (1953), 337–394.

[41] A. Phillips, *Submersions of open manifolds*, Topology **6** (1967), 171–206.

[42] V. Poénaru, *On regular homotopy in codimension 1*, Ann. of Math. **83** (1966), 257–265.

[43] A. V. Pogorelov, *Some results on surface theory in the large*, Advances in Math. **1** (1964), no. 2, 191–264.

[44] E. G. Poznyak, *Isometric embeddings of two-dimensional riemannian metrics in euclidean space*, Russian Math. Survey **28** (1973), no. 4, 47–77.

[45] L. Schlaefli, *Nota alla memoria del sig. beltrami, sugli spazii di curvatura constante*, Ann. di mat., 2nd série (1870-1873), no. 5, 170–193.

[46] S. Smale, *A classification of immersions of the two-sphere*, Trans. Amer. Math. Soc. **90** (1958), 281–290.

[47] ———, *The classification of immersions of spheres in euclidean spaces*, Ann. Math. **69** (1959), 327–344.

[48] D. Spring, *Note on the history of immersion theory*, pp. 114–116, Springer, 1993.

[49] ———, *Convex integration theory*, Monographs in Mathematics, vol. 92, Birkhäuser Verlag, 1998.

[50] ———, *The golden age of immersion theory in topology: 1959-1973. a mathematical survey from a historical perspective*, Bull. of the Amer. Math. Soc. **42** (2005), 163–180.

[51] J. Sullivan, *the optiverse and other sphere eversions*, `http://arxiv.org/pdf/math/9905020v2.pdf`, 1999.

[52] W. Thurston, *On proof and progress in mathematics*, Bull. of the Amer. Math. Soc. **30** (1994), no. 2, 161–177.

[53] C. Villani, *Paradoxe de Scheffer-Shnirelman revu sous l'angle de l'intégration convexe*, Séminaire Bourbaki, n. 1001, 2008-2009, 61 année.

[54] A. Zeghib, *Histoire des immersions isométriques*, `http://www.umpa.ens-lyon.fr/~zeghib/immersions.pdf`, 2002.

Vincent Borrelli
Institut Camille Jordan, Université Lyon I, France
borrelli@math.univ-lyon1.fr
http://math.univ-lyon1.fr/~borrelli

Saïd Jabrane
Institut Camille Jordan, Université Lyon I, France
jabrane@math.univ-lyon1.fr
http://math.univ-lyon1.fr/~jabrane

Francis Lazarus
GIPSA-Lab, CNRS, Grenoble, France
francis.lazarus@gipsa-lab.fr
http://www.gipsa-lab.fr/~francis.lazarus

Boris Thibert
Laboratoire Jean Kuntzmann, Université Joseph Fourier, Grenoble, France
Boris.Thibert@imag.fr
http://ljk.imag.fr/membres/Boris.Thibert